Testing the Hidden Local Symmetry Model

by Mark Prudden

Thesis submitted for the degree of Doctor of Philosophy

Department of Physics and Astronomy,

The University of Glasgow.

October 1988

ProQuest LLC.
789 East Eisenhower Parkway
P.O. Box 1346
Ann Arbor, MI 48106 – 1346

"...Well, I woke up this morning

Got myself a beer

Well, I woke up this morning

Got myself a beer

Well, the future's uncertain

The end is always near ..."

Roadhouse Blues, The Doors.

CONTENTS

Acknowledgements

I would like to thank David Sutherland very much for his supervision of this project and for contributing to my education in general.

My thanks also to Professor I.S.Hughes for the provision of facilities in the Department of Physics and Astronomy, University of Glasgow. Financial support for this research was provided by a University of Glasgow Postgraduate Scholarship.

I am most grateful to the following for their help and interest over the last few years: Tim Blackwell, Christine Davies, Alan McLachlan, David and Mirjam McMullan and Gordon Moorhouse. As well as all my other friends and aquaintances who have helped me.

I would also like to acknowledge the useful discussions I have had with Michael Feindt and Caroline Fraser.

I would like to thank the Department of Physics and Astronomy and the Institute of Physics for enabling me to attend the 8th International Workshop on $\gamma\gamma$-Interactions, Shoresh, Israel; at which this work was presented.

Finally, but by no means least, I would like to thank my parents for the essential support they have given over the past 3 years.

SUMMARY

The aim of this thesis is to test the recently proposed effective Lagrangian for π,ρ and γ physics, called the Hidden Local Symmetry (HLS) model, against experimental data on the process $\gamma\gamma\rightarrow\rho\rho$.

To this end Chapter 1 is a general introduction, motivating the interest in studying the HLS model in particular and pointing out its relation to composite models of Higgs and W/Z bosons. It is noted that there is a crucial sector of this model that has, until now, remained untested. It is observed that this untested sector can be probed by comparing the predictions of the model with the well established data on $\gamma\gamma\rightarrow\rho\rho$; which in itself is an interesting process and in need of better theoretical understanding.

Chapter 2 is an introduction to the HLS model and in section (i) the construction of the model Lagrangian is presented. The HLS model has an arbitrary parameter 'a', it is shown in section (ii) that so far the attempts to determine 'a' by some "underlying" symmetry principle fail when confronted with phenomenology. In section (iii) the pivotal role of the HLS model of vector mesons in the Skyrmion picture of baryon physics is explained. Section (iv) summarises the chapter and underlines the need to test the HLS model fully.

Chapter 3 is a summary of the current experimental and theoretical status of $\gamma\gamma\rightarrow V_1V_2$ physics ($V_{1,2}=\rho, \omega, k^*, \varphi$). It is emphasised that there is still room for a "conventional explanation" of the process $\gamma\gamma\rightarrow\rho\rho$.Thus the second strand of the thesis is testing the possibility of the HLS model explaining the data on $\gamma\gamma\rightarrow\rho\rho$.

Chapter 4 is the first order, or tree-level, calculation of $\gamma\gamma\rightarrow\rho\rho$ in the HLS model, it is found to be in disagreement with experimental data. Which leads us to consider in chapter 5 the motivation for a one loop calculation of $\gamma\gamma\rightarrow\rho\rho$; the approach taken in estimating the loop corrections, in the spirit of chiral perturbation theory, is outlined.

In chapter 6 the loop diagram calculation for $\gamma\gamma\rightarrow\rho^0\rho^0$ is presented, the

results indicate that the perturbative expansion fails. It is thus necessary to check this result before proceeding any further with the loop calculation.The $\rho^+\rho^-$ scattering amplitudes in the HLS model are shown to violate unitarity in chapter 7, this is an independent check on the loop diagram `calculation in chapter 6.

In chapter 8 it is concluded that the HLS model fails to describe $\gamma\gamma\rightarrow\rho\rho$ perturbatively. The discussion of the results of this thesis includes an outline of several interesting possibilities for future work.

Chapter 1 General Introduction

In attempting to construct models of the 'real world' a theoretical physicist generally aims to use a minimum number of physical principles. So that these physical principles can be tested by calculating consequences of the model to see whether or not they agree with experimental observation. The aim is to then generalise or expand upon those principles, which have been validated, in the hope of explaining experimental results previously without theoretical understanding and/or to make predictions as to what the experimentalist might measure in the future.

The generally accepted fundamental theory of the Strong Interactions is Quantum Chromodynamics (QCD), an $SU(3)_c$ (colour) gauge theory. QCD is a generalisation of Quantum Electrodynamics (QED), a U(1) gauge theory, the highly successful quantum field theory of electron and photon interactions.

The strongly interacting particles so far observed are colour singlet composites of quark-anti-quark (mesons) and three quark (baryons) states; the quarks being bound together by gluons, the gauge bosons of QCD.

However there is a major problem with QCD, how to construct from QCD a theory of Hadron Dynamics ? This many-bodied problem is made more difficult because QCD is asymptotically free, that is perturbation theory is only valid for processes at very high energies, whereas the observed strongly interacting particles $\pi,\rho,\ldots$, $p,n,\Delta,\ldots$ are, by comparison, low energy phenomena. Meson and baryon physics lies within the non-perturbative regime of QCD.

Consequently the hope is to derive an effective Lagrangian (L_{eff}) from QCD, in which the degrees of freedom are mesons and baryons, describing Hadron Dynamics. In general this is an extremely difficult task, the best that can be done at the moment is to construct various L_{eff}'s and to test them against experimental data.

A good example of an effective Lagrangian is

$$L = \frac{f_\pi^2}{4} \mathrm{Tr}(\partial_\alpha U(x) \partial^\alpha U(x)^\dagger) \quad , \quad U(x) = \exp\left(\frac{2\, i\, \pi^a(x)\, T^a}{f_\pi}\right) \qquad (1.1)$$

f_π = pion decay constant

the Weinberg Lagrangian [2],[3]. QCD has a $SU(3)_L \times SU(3)_R$ chiral symmetry, which is known to be broken to the vector subgroup $SU(3)_V$ with $3^2-1=8$ massless Goldstone bosons resulting from the spontaneously broken symmetry.

This spontaneously broken chiral symmetry is realised in non-linear form by equation (1.1), we have restricted ourselves to the case of $SU(2)_L \times SU(2)_R \rightarrow SU(2)_V$ with the pion being the Goldstone boson. Georgi [1] gives a particularly clear 'derivation' of equation (1.1). The exponential form of (1.1) is <u>not</u> a unique non-linear realization, Coleman et al [2] show that all non-linear realizations of broken chiral symmetry are equivalent in the sense of giving the same S-matrix elements.

Equation (1.1) is also frequently referred to as a (G/H) non-linear sigma model, where in this case $G = SU(2)_L \times SU(2)_R$ and $H = SU(2)_V$; not wishing to delve into the 'pure' mathematics of non-linear sigma models but basically the quantity U(x) takes values in the group manifold G/H ie $U(x) \in G/H$.

The Weinberg Lagrangian (1.1) is an effective Lagrangian for pion dynamics, describing low energy $\pi\pi$ scattering [4,5]. In fact a loop expansion using (1.1) can be performed [5], called chiral perturbation theory. Although originally (1.1) was simply a "mnemonic device" for reproducing the results of curent algebra [3].

The aim of this thesis is to study and test a particular effective Lagrangian, namely the Hidden Local Symmetry (HLS) model of vector mesons proposed by Bando et al [6].

The full details of the HLS model will be given in chapter 2. However roughly speaking the HLS model can be regarded as an 'extension' of the Weinberg

Lagrangian (1.1), in the sense that the G/H non-linear sigma model (1.1) is invariant under G_{global} whereas the HLS Lagrangian is constructed to be $G_{global} \times H_{local}$ invariant. The concept of such a hidden local symmetry first emerged in supergravity theories [7], where it was also shown [7]-[9]that the gauge fields of the HLS H_{local} ($=SU(2)_V$ in the Bando et al [6] model) are composite particles this was motivated by CP^{N-1} two dimensional models wherein meson+meson=vector.

Under the crucial assumption that the underlying dynamics (QCD) generate the kinetic term for the HLS gauge field Bando et al [6] argue that one should identify the ρ meson with the dynamical gauge bosons of the HLS.

By fixing the one parameter in the model to one unique value the HLS model successfully reproduces ρ meson phenomenology, namely the KSRF relation[10], universality of the ρ coupling $g_{\rho\pi\pi} = g_{\rho NN} = \ldots$[11] and when electromagnetism is included ρ dominance of the electromagnetic form factor [11]. In fact the HLS Lagrangian [6] is identical to the phenomenological Lagrangian due to Weinberg [12], in which the ρ meson is the gauge boson of a gauged chiral symmetry but with the ρ mass put in 'by-hand' instead of 'dynamically generated' as it is in the HLS model.

The HLS Lagrangian is an attractive model because not only does it reproduce well known ρ meson phenomenology, but also because of the 'neat' manner in which the chiral symmetries are used to generate the Lagrangian. Also the HLS model is very easily generalised to (i) include the axial-vector meson A_1 by taking $H_{local} = SU(2)_L \times SU(2)_R$ and (ii) include the other low lying vector mesons ω,k*,φ by enlarging the HLS to $H_{local} = U(3)_V$ (this also requires enlargment of G to $U(3)_L \times U(3)_R$).

One of the main reasons for wanting to study and fully test the HLS model of ρ mesons is the pivotal role it recently assumed in the construction of a unified effective Lagrangian of strong interactions.

It was originally found by Skyrme [13], over 25 years ago , that the Lagrangian (1.1) admitted soliton solutions, called Skyrmions; Skyrme suggested that these solitons be identified as baryons. The Skyrmion was only recently revived when Witten [14] showed that by add ing the Wess-Zumino term to the action, that the soliton solutions possessed the correct spin and statistics to be identified with baryons. Since this brealthrough there has been a great deal of interest in the possibility that the Skyrmion (soliton of the pion field) is an effective description for baryon physics. For a review of Skyrmion physics see, for example, Zahed and Brown [15].

What has not been mentioned so far is that the solitons arising from the Lagrangian (1.1) are energetically unstable and collapse unless a stabilization term

$$L_{Skyrme} = \frac{1}{32e^2}\ Tr\left[\partial_\alpha U.U^\dagger, \partial_\beta U.U^\dagger\right]^2$$

is added to (1.1). However ithas been claimed by Igarashi et al [16] that thep meson (and other vector mesons by extension of H_{local}), as a dynamical gauge boson of an HLS stabilises the Skyrmion. The details of this will be discussed in chapter 2(ii). The main point to be drawn from this is the construction of a unified effective Lagrangian for mesons and baryons, where mesons are described by a model based on an extension of chiral symmetry with the baryons emerging as solitons, of the meson field, stabilized by the vector meson.

The unified effective Lagrangian outlined above is made more interesting by the highly suggestive results of the large N_c-limit of QCD [17],[18]. For an $SU(N_c)$ colour gauge theory in the limit $N_c \to \infty$ 't Hooft showed that QCD becomes a theory of an infinite number of interacting mesons and glueballs, later Witten [14],[18] showed that baryons could emerge as chiral solitons of these meson fields. This fits in very well with the chiral symmetry/ Skyrmion picture of mesons and baryons, but it should be reiterated that the large N_c limit is only suggestive because in the'real

world' the number N_c=3 is generally well established.

Looking to the future, there is another interesting aspect to the HLS model, namely as a prototype for composite models. Because as the next generation of colliders start to produce data around the 1 TeV region it is hoped to begin to get indications as to whether or not the currently 'fundamental' particles quarks, leptons and weak gauge bosons are composite.

One possible theory of compositeness is Technicolour, basically an analogue of QCD, with all the inherent non-perturbative problems that has; the techni-fermions combine to make composite Goldstone bosons which are then responsible for the spontaneous breaking of the electroweak gauge symmetry.

So to calculate consequences of a Technicolour theory one would really like to work with an effective Lagrangian 'derived' from the Technicolour Lagrangian. The HLS Lagrangian is just such a prototype [chapter 8 of ref. 19] effective Lagrangian for Technicolour, with the dynamical gauge bosons being indentified with the techni-ρ meson.

A much more speculative possibility [chapter 8 of ref.19] is that of the HLS model being an effective Lagrangian for composite W/Z boson models, that is the W/Z bosons are 'fully' composite, as opposed to the Technicolour picture where just their longitudinal components are compo site.

However any possible connection between the HLS model and a composite W/Z boson picture is not at all clear because of the need to maintain massless (composite) fermions. Unlike the HLS model applied to QCD where the nucleon acquires a mass, due to the spontaneous symmetry breaking, which is physically acceptable. There is also a problem with the composite fermions destabilizing the dynamical gauge bosons through loop efffects, which were held responsible for the dynamical generation of the gauge bosons.

So given the pivotal role of the HLS model of vector mesons in constructing a unified effective theory of meson and baryon physics and its' importance as a prototype effective Lagrangian for testing the compositeness ideas of Technicolour (and the more "hazy" scenario of fully composite W and Z model), hopefully in the near future against experimental data, it is crucial that the HLS model is fully tested to see if it really is an effective description of ρ dynamics.

Although the HLS model of ρ mesons contains well established phenomenology there is one sector of the model that has so far remained untested, namely the non-abelian nature of the ρ meson in the model. The model would in fact not 'exist' if the ρ were not so, in the sense that the chiral structure 'forces' it to be an SU(2) (non-abelian) gauge theory.

The Skyrmion model builders have remained 'blissfully' unaware of the need to test this aspect of the HLS model, they simply take the HLS Lagrangian as it is and calculate Skyrmion properties.

Very much following the philosophy advocated by Ball [20] and Aitchison [21] of extrapolating effective chiral Lagrangians upwards in energy, from $\sqrt{s}\approx 300$MeV region of $\pi\pi$ scattering to $\sqrt{s}\approx 2$ GeV (max.) of Skyrmion physics, then the HLS Lagrangian should reasonably be expected to describe other processes in this energy range if it is truly "effective'.

Electromagnetism is easily incorporated by gauging U(1) , thus opening up the possibility of studying the process $\gamma\gamma\rightarrow\rho\rho$. It is precisely the non-abelian nature of the ρ that generates the ρ 'self-interaction' terms , arising from the ρ kinetic term, and thus gives rise to $\gamma\rho\rho$ and $\gamma\gamma\rho\rho$ vertices. Thus by studying $\gamma\gamma\rightarrow\rho\rho$ we will be testing the non-abelian nature of the ρ meson (in the HLS model) and with the $\rho\rho$ threshold $\sqrt{s}\approx 1.5$ GeV this might be hoped to be within the extrapolated energy range of the effective Lagrangian.

Two Photon Physics has been extensively studied at the electron-positron storage rings PETRA (DESY) and PEP (SLAC). For an overall review see, for example, Kolanoski [22] or Poppe [23].

Basically two-photon physics is studied via e^+e^- scattering, that is the photon-photon interactions occurring in the collisions of the 'photon clouds' surrounding the elctron and positron beam particles :

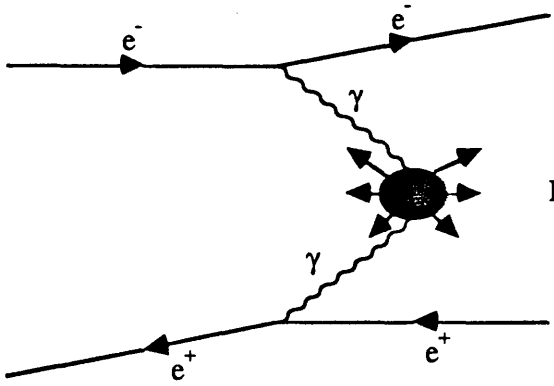

Figure 1.1

Among the many interesting aspects of particle physics that can be probed with two-photon physics we are specifically interested in those experiments which studied exclusive final states (eg $\rho\rho,\omega\rho,\omega\omega,\ldots$) produced by very nearly real photons, that is 'no-tag' data on exclusive final states; 'no-tag' means that neither of the scattered leptons are detected.

There has been a great deal of interest in the process $\gamma\gamma\rightarrow\rho\rho$ ever since the first data [24]-[26] (which has been confirmed by more recent analyses [27]-[29]) showed a massive cross-section at threshold, an order of magnitude larger than predicted. The data on $\gamma\gamma\rightarrow\rho^+\rho^-$ [30],[31] shows very different behaviour to the neutral channel, and this dismissed the possibility of a straightforward (or conventional) resonance mechanism interpretation.

The current experimental and theoretical status of $\gamma\gamma\rightarrow V_1V_2$ ($V_{1,2}=\rho,\omega,k^*,\varphi$) will be discussed in chapter 3. However there are two points that must be emphasised here:

(i) the data on $\gamma\gamma\rightarrow\rho\rho$ is well established and the charged and neutral channels are

highly distinctive in the size and shape of their cross-sections. Thus making $\sigma(\gamma\gamma\to\rho\rho)$ very good experimental data against which to test a model.

(ii) the current theoretical status of $\gamma\gamma\to V_1V_2$ (and $\gamma\gamma\to\rho\rho$ in particular) is such that there is still the possibility of a 'conventional' mechanism underlying the process, so it is necessary to test whether or not the HLS model of vector mesons is that possibility.

In summary, the philosophy of this thesis is to test an interesting (and important) model against experimental data; with the added interest that the data is in need of 'theoretical understanding'.

Chapter 2 The Hidden Local Symmetry Model

(i) Introduction to the Model

In this section the Hidden Local Symmetry (HLS) model of ρ mesons proposed by Bando et al [6] is described, basically following the original paper [6]. Although a more "sophisticated" approach can be taken [19] in considering HLS models, this does not really add any understanding to the basic idea of constructing an effective Lagrangian.

The HLS model was described in chapter 1 as being an "extension" of the chiral Lagrangian (1.1). In the sense that (1.1) is invariant under G_{global} whereas the HLS Lagrangian due to Bando et al [6] is constructed to be invariant under G_{global} and H_{local} , ie invariant under $G_{global} \times H_{local}$.

The Weinberg chiral Lagrangian (1.1), the non-linear realization of broken chiral symmetry for two flavour QCD, is an $SU(2)_L \times SU(2)_R / SU(2)_V$ non-linear sigma model. It is restated here for later convenience:

$$L = \frac{f_\pi^2}{4} \mathrm{Tr}\,(\partial_\alpha U(x)\, \partial^\alpha U^\dagger(x)) \qquad (2.1)$$

$$U(x) = \exp\left(\frac{2\,i\,\pi(x)}{f_\pi}\right) \;,\; \pi(x) = \pi^a(x)\, T^a$$

The pion decay constant f_π= 93MeV. The quantity U transforms under $G_{global}=SU(2)_L \times SU(2)_R$ as

$$U(x) \rightarrow g_L^\dagger\, U(x)\, g_R \;\;,\;\; g_{L(R)} \in G_{global} \qquad (2.2)$$

The model building, in outline, is as follows. To construct the HLS Lagrangian new variables are introduced, $\xi_{L(R)}$ and an $SU(2)_V$ valued gauge field $V_\mu(x)$, these are to realise the H_{local} symmetry. A 'minimal' Lagrangian invariant under $G_{global} \times H_{local}$ is constructed out of the covariant derivatives of the $\xi_{L(R)}$, the $\xi_{L(R)}$ are related to the U(x) of equation (2.1); this Lagrangian is then made

(classically) equivalent to the Weinberg Lagrangian (2.1) by taking a particular choice for the form of the $\xi_{L(R)}$ (the unitary gauge).

Then making the crucial assumption that the underlying dynamics generate the kinetic term for the H_{local} gauge field $V_\mu(x)$ and expanding the ξ in terms of the π field one obtains the HLS Lagrangian for π and V_μ , Bando et al [6] then argue that the V_μ field should be indentified with the ρ meson.

To realise the symmetry H_{local} new variables are introduced, $\xi_{L(R)}$ and an $SU(2)_V$ valued gauge field $V_\mu(x)$, such that

$$U(x) = \xi_L^\dagger(x)\, \xi_R(x) \tag{2.3}$$

$$V_\mu(x) = V_\mu^a(x)\, T^a \quad , \quad T^a \in SU(2)_V \tag{2.4}$$

and which transform as:

$$\xi_{L(R)}(x) \longrightarrow h(x)\, \xi_{L(R)}(x)\, g_{L(R)}^\dagger$$

$$V_\mu(x) \longrightarrow \frac{i}{f} h(x)\, \partial_\mu h^\dagger(x) + h(x)\, V_\mu(x)\, h^\dagger(x) \tag{2.5}$$

$$\text{under } h(x) \in H_{local} \ , \ g_{L(R)} \in SU(2)_{L(R)} \text{ global}$$

So U(x) is invariant under H_{local} , using equation (2.5):

$$U(x) = \xi_L^\dagger(x)\xi_R(x) \longrightarrow \xi_L^\dagger(x) h^\dagger(x)\, h(x)\xi_R(x) = U(x)$$

$$h(x) \in H_{local}$$

thus the local symmetry H_{local} is "hidden" in the U(x) basis.

The covariant derivative on $\xi_{L(R)}$ is defined as

$$D_\mu \xi_{L(R)}(x) := \partial_\mu \xi_{L(R)}(x) - i f V_\mu(x)\, \xi_{L(R)}(x) \tag{2.6}$$

where f is the H_{local} gauge field coupling constant.

Under $G_{global} \times H_{local}$ the covariant derivatives transform as

$$D_\mu \xi_{L(R)}(x) \longrightarrow h(x) \left(D_\mu \xi_{L(R)}(x) \right) g^\dagger_{L(R)} \qquad (2.7a)$$

$$D_\mu \xi_{L(R)}(x).\xi^\dagger_{L(R)}(x) \longrightarrow h(x)\, D_\mu \xi_{L(R)}(x).\xi^\dagger_{L(R)}(x)\, h^\dagger(x) \qquad (2.7b)$$

Notice that (2.7b) tells us that the object $D_\mu \xi_{L(R)} \xi^{\dagger}_{L(R)}$ is invariant under G_{global} and can thus be used to construct "currents" which are G_{global} invariants. Using a similar notation to Hung [32] for later convenience we define the following G_{global} invariant "currents":

$$j_\mu := \frac{if}{2} \left(D_\mu \xi_L . \xi^\dagger_L + D_\mu \xi_R . \xi^\dagger_R \right) \qquad (2.8a)$$

$$j_{5\mu} := \frac{if}{2} \left(D_\mu \xi_L . \xi^\dagger_L - D_\mu \xi_R . \xi^\dagger_R \right) \qquad (2.8b)$$

Noting that j_μ and $j_{5\mu}$ correspond to the Maurer-Cartan 1-forms $\alpha_{//}$ and $\alpha_\perp$ respectively, of reference [19].

The most general $G_{global} \times H_{local}$ invariant Lagrangian that can be constructed from the currents j_μ and $j_{5\mu}$ is :

$$L := L_A + a L_V \qquad (2.9)$$

$$L_A = Tr(j_{5\mu} j_5^\mu) \quad , \quad L_V = Tr(j_\mu j^\mu) \qquad (2.10\ a,b)$$

where a is an arbitary parameter.

Because no kinetic term for H_{local} is present in the Lagrangian (2.9) the field $V_\mu(x)$ obeys the Euler-Lagrange equation of motion

$$\frac{\partial L}{\partial V_\mu} = 0 \text{ which implies that}$$

$$V_\mu^{class} = \frac{1}{2if}(\partial_\mu \xi_L . \xi_L^\dagger + \partial_\mu \xi_R . \xi_R^\dagger) \qquad (2.11)$$

Then substituting V^{class} into equation (2.9) means that L_V vanishes.

There is a degree of arbitariness in the definition of the $\xi_{L(R)}$ given that the $\xi_{L(R)}$ must satisfy equuation (2.3). In fact

$$\xi_{L(R)}^\dagger = \exp(\frac{-i\varphi}{f_\pi}) \exp(\frac{\pm i\pi}{f_\pi}) \qquad (2.12)$$

where the φ are unphysical Nambu-Goldstone modes [6].

Bando et al [19] show that the Lagrangian (2.9) is equivalent to the Weinberg Lagrangian (2.1) when

(i) the classical equations of motion are used and V^{class} (2.11) is substituted into equation (2.9) and

(ii) the H_{local} "gauge" is fixed to the unitary gauge by taking φ=0. This means that

$$\xi_L^\dagger = \xi_R := \xi = \exp(\frac{i\pi}{f_\pi}) \qquad (2.13)$$

Procedures (i) and (ii) above result in the Lagrangian (2.9) reducing to the Weinberg Lagrangian (2.1), except that as it stands the gauge fixing condition (2.13) has violated the G_{global} symmetry. Since under G_{global} $\xi(x)$ transforms as

$$\xi(x) \rightarrow \xi'(x) = \xi(x)\, g^\dagger, \quad g \in G_{global}$$

$$\xi'(x) = \exp(\frac{i\varphi'(\pi(x),g)}{f_\pi}) \exp(\frac{i\pi'(x)}{f_\pi})$$

The G_{global} symmetry is restored by making a simultaneous H_{local} gauge transformation:

$$h(x) = \exp\left(\frac{-i\,\varphi'(\pi(x),g)}{f_\pi}\right) := h(\pi(x),g) \quad , \quad h(x) \in H_{local}$$

Denoting the combined transformation G , one now has that the ξ transform under G like

$$\xi(x) \rightarrow \xi'(x) = h(\pi(x),g)\, \xi(x)\, g^{\dagger} = \xi(\pi'(x))$$

Only under the above conditions do the Lagrangians (2.9) and (2.1) coincide.

The classical equivalence of the Lagrangians (2.9) and (2.1) outlined above, is referred to as the "gauge equivalence" of the $(G/H)_{global}$ non-linear sigma model to a 'linear' $G_{global} \times H_{local}$ model.

It is important to emphasise that the requirement of this gauge equivalence has forced us to work with the HLS model in the "unitary Gauge" only, we do not have the freedom to make some gauge choice as would be done in, say, the Standard Model to make calculations more tractable.

Further to this gauge equivalence, it has been shown [7]- [8], that the gauge bosons of H_{local} are composite. Which gives a great deal of motivation to the serious consideration of the HLS model as a possible dynamical model of the ρ meson as well as its possible role as a prototype model of composite W and Z bosons in the strongly interacting Higgs sector.

It is at this stage, having constructed the Lagrangian (2.9) to be gauge equivalent to the Weinberg Lagrangian (2.1), that Bando et al [6] make the crucial assumption that "...the kinetic terms of $V_\mu(x)$ are generated by the underlying

dynamics (QCD) or quantum effects at the composite level". Such dynamical generation of kinetic terms has been shown to occur in certain 2 and 3 dimensional models [8],[19] which encourages one to make the above assumption, however its occurrence in d=4 does remain a conjecture.

Thus the kinetic term $-1/2\ \mathrm{Tr}V_{\mu\nu}V^{\mu\nu}$ is added to (2.9), where

$$V_{\mu\nu} := \partial_\mu V_\nu - \partial_\nu V_\mu - i f [V_\mu, V_\nu] \qquad (2.14)$$

is the $SU(2)_V$ field strength, which transforms as:

$$V_{\mu\nu} \rightarrow h(x)\, V_{\mu\nu}\, h^\dagger(x)\ ,\ \ h(x) \in H_{local} \qquad (2.14)$$

External gauge fields are easily incorporated by extending the definition of the covariant derivative. For example electromagnetism couples to the charge Q

$$Q = I_3^L + I_3^R + \frac{Y}{2}\ ,\ I_3^{L(R)} = \text{global isospin and Y= hypercharge}$$

and Y=0 in this case. Denoting the $U(1)_Q$ gauge field by $B\mu$ with a coupling g', the covariant derivative becomes

$$D_\mu \xi_{L(R)}(x) := \partial_\mu \xi_{L(R)}(x) - i f V_\mu(x)\, \xi_{L(R)}(x) + i g' \xi_{L(R)}(x)\, B_\mu(x)\, T^3 \qquad (2.15)$$

The $\xi_{L(R)}$ and B_μ transform under U(1) as

$$\xi_{L(R)}(x) \rightarrow \xi_{L(R)}\, e^{i\alpha(x)\, T^3} \qquad (2.16a)$$

$$B_\mu(x) \rightarrow B_\mu(x) - \frac{1}{g'} \partial_\mu \alpha(x) \qquad (2.16b)$$

Equations (2.15) and (2.16) above imply that under U(1) the covariant

derivative transforms as

$$D_\mu \xi_{L(R)}(x) \rightarrow D_\mu \xi_{L(R)}(x)\, e^{i\,\alpha(x)\,T^3}$$

and consequently the currents j_μ and $j_{5\mu}$ are invariant under U(1).

Defining the U(1) field strength to be $B_{\mu\nu} = \partial_\mu B_\nu - \partial_\nu B_\mu$, then the total $G_{global} \times H_{local} \times U(1)$ invariant Lagrangian is

$$L = L_A + \alpha L_V - \frac{1}{4} B^2_{\mu\nu} - \frac{1}{2} \mathrm{Tr} V^2_{\mu\nu} \qquad (2.17)$$

To see why the ρ meson is identified with the dynamical gauge field $V_\mu(x)$ the Lagrangian (2.17) is written in terms of the fields π, V_μ and B_μ.

Expanding the exponential one obtains

$$\partial_\mu \xi^\dagger . \xi = \frac{i}{f_\pi} \partial_\mu \pi - \frac{1}{2f^2_\pi} [\pi , \partial_\mu \pi] + \ldots$$

$$\partial_\mu \xi . \xi^\dagger = \frac{i}{f_\pi} \partial_\mu \pi - \frac{1}{2f^2_\pi} [\pi , \partial_\mu \pi] + \ldots \qquad (2.18)$$

$$\xi^\dagger V_\mu \xi = V_\mu - \frac{i}{f_\pi} [\pi , V_\mu] + \ldots$$

$$\xi V_\mu \xi^\dagger = V_\mu + \frac{i}{f_\pi} [\pi , V_\mu] + \ldots \qquad (2.19)$$

So the currents j_μ and $j_{5\mu}$ become :

$$j_\mu = \frac{i f_\pi}{2}\left(\frac{1}{f_\pi^2}[\pi, \partial_\mu \pi] - 2 i f V_\mu + 2 i g' B_\mu T^3 + \ldots \right) \quad (2.20a)$$

$$j_{5\mu} = \frac{i f_\pi}{2}\left(- \frac{2i}{f_\pi} \partial_\mu \pi + \frac{2 g'}{f_\pi}[\pi, B_\mu T^3] + \ldots \right) \quad (2.20b)$$

Only keeping terms with up to two π fields gives the following

$$L_A = \frac{f_\pi^2}{4} Tr\left(\frac{4}{f_\pi^2} \partial_\mu \pi \, \partial^\mu \pi - \frac{8 i g'}{f_\pi} \partial_\mu \pi \, [\pi, B_\mu T^3] \right)$$

$$L_V = \frac{f_\pi^2}{4} Tr\left(\frac{4if}{f_\pi^2} V_\mu [\pi, \partial^\mu \pi] - \frac{4 i g'}{f_\pi^2} B_\mu T^3 [\pi, \partial^\mu \pi] - 4(-f V_\mu + g' B_\mu T^3)^2 \right)$$

and which finally yields

$$L = \frac{1}{2}(\partial_\mu \vec{\pi})^2 + \frac{a}{2} f \vec{V}_\mu . (\vec{\pi} \times \partial^\mu \vec{\pi}) + \frac{a}{2} f_\pi^2 f^2 \vec{V}_\mu^2 - \frac{1}{2} Tr V_{\mu\nu}^2$$

$$+ \frac{(2-a)}{2} g' B_\mu (\vec{\pi} \times \partial^\mu \vec{\pi})_3 - a f_\pi^2 f \, g' B_\mu V_3^\mu + \frac{a}{2} f_\pi^2 g'^2 B_\mu^2 - \frac{1}{4} B_{\mu\nu}^2 \quad (2.21)$$

Bando et al [6] argue that one should identify the ρ meson with the hidden local symmetry gauge field $V_\mu(x)$ on the following observations : consider the first line of equation (2.21), this is the Lagrangian L without the external U(1) gauge field B_μ, then identifying $V_\mu(x)$ with the ρ one obtains

$$(i) \quad f_{\rho\pi\pi} = \frac{a}{2} f \quad (2.22)$$

$$(ii) \quad m_\rho^2 = a f_\pi^2 f^2 \quad (2.23)$$

When a=2 then equation (2.22) gives 'universality' of the ρ coupling $f_{\rho\pi\pi} = f$ (2.24), and consequently the KSRF relation [10]

$$m_\rho^2 = 2 f_\pi^2 f_{\rho\pi\pi}^2 \quad (2.25)$$

The first line of equation (2.21) is identical with Weinberg's phenomological Lagrangian [12], based on gauged chiral symmetry and with the ρ mass put in 'by-hand'. So the HLS model has the attractive feature of building in with the Weinberg Lagrangian the "dynamical generation of mass" yielding universality of the ρ coupling and the KSRF relation when the special value a=2 is taken.

Considering all of equation (2.21) and setting a=2 one obtains the ργ mixing Lagrangian due to Sakurai [11], the vector meson dominance (VMD) model. Because when a=2 the parameter $g_{B\pi\pi}$ in (2.21) vanishes and the U(1) gauge field can only couple to the pion current ($\pi\times\partial\pi$) through the V_3B mixing term.

The Lagrangian (2.21) is easily diagonalized to give mass eigenstates, by defining the physical photon (A_μ) and ρ^0 fields as

$$B_\mu := \cos\theta\, A_\mu - \sin\theta\, \rho^0_\mu$$

$$V^3_\mu := \sin\theta\, A_\mu + \cos\theta\, \rho^0_\mu \qquad (2.26)$$

The full diagonalized Lagrangian, including kinetic terms, is given in appendix B, equation (B.3). The mixing angle θ is determined by requiring the physical photon field to be massless, this implies

$$\tan\theta := \frac{g'}{f} \qquad (2.27)$$

and the masses become

$$m^2_\gamma = 0 \ , \ m^2_{\rho^0} = a\,(f^2 + g'^2)\, f^2_\pi \ , \ m^2_{\rho^\pm} = a\, f^2 f^2_\pi \qquad (2.28)$$

In summary the HLS model is an extension, to include ρ mesons, of the broken chiral symmetry description of pions. There is an arbitary parameter (a), when a takes the special value a=2 the model simultaneously gives the KSRF mass relation, ρ universality and vector dominance. The only differences between the HLS model [6] and Weinberg's [12] model for the ρ meson is that the former takes on a particularly simple and attractive form and includes the "dynamical" generation of the ρ mass as opposed to simply putting this in 'by-hand'.

(ii) The Parameter 'a'

In the previous section it was shown that a=2 is consistent with ρ meson phenomenology. However Hung [32] claimed to have uniquely determined a=2 by embedding the electroweak gauge group $(SU(2)_L \times U(1)_Y)$ in the HLS Lagrangian and the Weinberg Lagrangian (2.1) and basically "equating" the two Lagrangians but ignoring the $V_\mu(x)$ field in the HLS Lagrangian. This follows much more in the spirit of constructing an effective Lagrangian from a few basic principles.

The result claimed by Hung [32] certainly offered the interesting possibility of extending the idea to an electroweak gauge group of the form $SU(2)_L \times SU(2)_R$ to see what sort of costraints on the effective Lagrangian emerged. This also offered the possibility of placing constraints on prototype strongly interacting Higgs models thought to be a possible theory of weak interactions in the 1TeV region.

Unfortunately there is a mistake in Hung's paper, there is a $-f\rho_\mu(\pi \times \partial_\mu \pi)$ term missing from his equation (21). The corrected equation (21) is a disaster because now $f_{\rho\pi\pi}=0$; although diagonalization of the mass matrix will generate a $\rho\pi\pi$ vertex the coupling will be $\approx g'\sin\theta$ (too small!). So phenomenologically equation (21) of reference [32] is useless.

The difference between the Bando et al [6] Lagrangian and that used by Hung is in the definition of the "currents" j_μ and $j_{5\mu}$. Hung [32] takes, using the same notation as in section (i),

$$j^H_\mu := \frac{i f_\pi}{2}\left(\xi_L^\dagger \overline{D}_\mu \xi_L + \xi_R^\dagger \overline{D}_\mu \xi_R\right)$$
$$j^H_{5\mu} := \frac{i f_\pi}{2}\left(\xi_L^\dagger \overline{D}_\mu \xi_L - \xi_R^\dagger \overline{D}_\mu \xi_R\right) \qquad (2.29)$$

With the covariant derivatives defined as follows

$$\bar{D}_\mu \xi_L := \partial_\mu \xi_L + i f V_\mu \xi_L - i g \xi_L W_\mu$$

$$\bar{D}_\mu \xi_R := \partial_\mu \xi_R + i f V_\mu \xi_R - i g' \xi_R B_\mu T^3 \qquad (2.30)$$

Where W_μ is the $SU(2)_L$ gauge field with coupling constant g.

The "Bando" currents are given by equation (2.8), but with the covariant derivatives modified so as to include the $SU(2)_L$ gauge field

$$D_\mu \xi_L := \partial_\mu \xi_L - i f V_\mu \xi_L + i g \xi_L W_\mu$$

$$D_\mu \xi_R := \partial_\mu \xi_R - i f V_\mu \xi_R + i g' \xi_R B_\mu T^3 \qquad (2.31)$$

The two sets of currents transform <u>differently</u> under H_{local}, the "Bando" currents are <u>covariant</u> under H_{local} that is

$$j_\mu \rightarrow h(x)\, j_\mu\, h^\dagger(x) \quad , \quad h(x) \in H_{local}$$

whereas the currents (2.29) used by Hung are <u>invariant</u> under H_{local}.

There would seem to be no a priori reason to choose one or other set of currents in constructing the Lagrangian. However if the currents are made to be <u>invariant</u> under H_{local} with gauge field V_μ (Hung's method) then taking a=2 implies that $f_{V\pi\pi}=0$ which is not allowed by the phenomenology. Whereas in the case of the Bando et al Lagrangian the currents are covariant under H_{local} but <u>invariant under the external gauge group</u>, for instance equation (2.21) constructed from currents invariant under U(1) with gauge field B_μ then taking a=2 implies $g_{B\pi\pi}=0$ and yet gives the correct $f_{\rho\pi\pi}$ coupling.

In fact the Bando currents (2.8) constructed from the covariant derivatives defined in equation (2.31) are invariant under $SU(2)_L \times U(1)_Y$. This is not true of the currents (2.29) constructed by Hung, they not transform covariantly under

$SU(2)_L \times U(1)_Y$ because the quantities used to construct the currents transform differently under a simultaneous $SU(2)_L \times U(1)_Y$ gauge transformation, ie

$$\xi_L^\dagger \overline{D}_\mu \xi_L \rightarrow g_L(x)\, \xi_L^\dagger \overline{D}_\mu \xi_L\, g_L^\dagger(x) \quad , \quad g_L(x) \in su(2)_L \text{ local}$$

$$\xi_R^\dagger \overline{D}_\mu \xi_R \rightarrow e^{-i\alpha(x)T^3}\, \xi_R^\dagger \overline{D}_\mu \xi_R\, e^{i\alpha(x)T^3} \quad , \quad e^{i\alpha(x)T^3} \in U(1)_Y \text{ local}$$

(see Hung[32] equation (4)).

So taking the trace to obtain L_A and L_V (equation 2.10) does not ensure invariance of the Lagrangian $L_A + aL_V$ under $SU(2)_L \times U(1)_Y$. Although if the external gauge group were only $U(1)_Y$, then the currents (2.29) would be covariant and thus taking the trace would ensure invariance under $U(1)_Y$.

However the above analysis leads us to understand an even stronger reason for the failure of Hung's Lagrangian.This is because the Lagrangian he constructs is not invariant under global $SU(2)_L \times SU(2)_R$ for precisely the same reasons that it was'nt invariant under $SU(2)_L \times U(1)_Y$ gauge transformations; except it can be seen that the cross terms in $L_A + aL_V$,which cannot be made invariant by taking the trace, can cancel if one selects a=1. This is unsatisfactory.

Hung fails to determine a=2 by embedding the electroweak gauge group in the theory due to a 'mistake' in his calculation which meant that he was 'unaware' of the phenonmenological failing $f_{\rho\pi\pi}=0$ of his construction, but worse than that his construction would appear to be not strictly correct since it is not invariant under global $SU(2)_L \times SU(2)_R$.

Yamawaki [33] has shown that it is possible to determine the parameter a=2 by extending the HLS model to $H_{local}=SU(2)_L \times SU(2)_R$ so that the ρ and A_1 are gauge bosons of the HLS. Yamawaki then assumes that $m_A \gg m_\rho$and so eliminates

the A_1 field by its (classical) equation of motion which gives (eventually) the Bando Lagrangian [6] with a=2. This is a nice result, but completely unphysical because m_ρ=770 MeV and m_A=1270 MeV so the assumption of the A_1 mass being infinite by comparison with the ρ mass is untenable.

So both attempts to determine the parameter a, by some sort of "underlying" gauge symmetry principle, fail when confronted with phenomenology.

(iii) Skyrmion Physics

As described in chapter 1 the revival of the Skyrmion picture of baryon physics has led to the vector mesons ρ,ω,...(as described by the HLS model [6] or Weinberg's gauged chiral symmetry approach [12]) attaining something of a pivotal role in constructing a 'unified picture' of hadronic physics for $\sqrt{s} \leq 2$ GeV.

Originally Skyrme [13] showed that the Lagrangian (2.1) admitted soliton solutions, these solutions were energetically unstable unless an extra term contining four derivatives, L_{Skyrme}, was added

$$L = \frac{f_\pi^2}{4} Tr(\partial_\alpha U\, \partial^\alpha U^\dagger) + L_{Skyrme} \qquad (2.32)$$

$$L_{Skyrme} = \frac{1}{32e^2} Tr\left[\partial_\alpha U.U^\dagger, \partial_\beta U.U^\dagger\right]^2 \qquad (2.33)$$

Where e is a parameter to be fixed and not the electromagnetic charge!

However it has been claimed [16] that ρ mesons as described by the HLS model [6] will give the Skyrmion stability against collapse.

The HLS Lagrangian (2.17) constructed in section (i) is rewritten here ignoring the U(1) field B_μ :

$$L = \frac{f_\pi^2}{4} Tr(\partial_\alpha U \partial^\alpha U^\dagger) - \frac{a f_\pi^2}{4} Tr(\partial_\alpha \xi_L . \xi_L^\dagger + \partial_\alpha \xi_R . \xi_R^\dagger - 2i f V_\alpha)^2 - \frac{1}{2} Tr V_{\mu\nu}^2 \qquad (2.34)$$

Igarashi et al [16] claim that the Lagrangian (2.34) above gives stable soliton solutions. To see the connection between this and the Lagrangian (2.32) consider the classical limit of (2.34) by taking the limit $a \to \infty$ (with f fixed), also noting that the gauge (2.13) is taken. In this limit the gauge bosons decouple from the physical sector so that V is replaced V^{class} (equation 2.11) in (2.34), it can then be shown that:

$$-\frac{1}{2} Tr V_{\mu\nu}^2 = \frac{1}{32 f^2} Tr\left[\partial_\alpha U.U^\dagger, \partial_\beta U.U^\dagger\right]^2 \qquad (2.35)$$

The middle term of equation (2.34) vanishes and identifying f=e , the resulting Lagrangian is seen to be the same as (2.32).

Stable soliton solutions are then obtained [16] for finite values of a (a=2 in particular) by using what is known as the "hedgehog" ansatz for the π field

$$U(x) = \exp(i \hat{x}^a T_a F(r)) \ , \ \hat{x}^a := \frac{x^a}{r}$$

and the Wu-Yang-'t Hooft -Polyakov ansatz for the ρ field

$$f V_0^a(x) = 0 \ , \ f V_i^a(x) = \varepsilon_{ija} \hat{x}^a \frac{G(r)}{r}$$

F(r) and G(r) are then given as solutions to the (classical) Euler-Lagrange equations of motion; they are then used to calculate the properties of the Skyrmion such as mass, mean square radius,... .

It should be emphasised that in the above the fields are treated classically, as a result of using the Euler-Lagrange equations of motion as derived from equation (2.34) without quantum corrections. That is to say, as pointed out by both Ball [20] and Aitchison [21] , there are no "meson loops" in any of the current Skyrmion

calculations.

The Skyrmion model stabilized by the ρ meson is moderately successful, the obvious way to extend this is to include the other low-lying vector mesons ω,φ,k*,... and axial-vector mesons such as the A_1. Unfortunately Igarashi et al [16] find that coupling the ω to the baryonic current leads to a saddle point solution, that is the Skyrmion is not properly stabilized. In fact Kunz and Masak [34] claim that the same problem besets the model with the ρ mesons alone and 'satisfactory' stabilization is only achieved when explicit stabilization terms like L_{Skyrme} are added (and fitted to the data). The same is true when the A_1 is included [35].

However if the ρ and ω are described by an HLS model [36] with $H_{local}=U(2)_V$ and the Wess-Zumino term (which accounts for anomalous decays such as $\omega\rightarrow\pi^0\gamma$, $\omega\rightarrow 3\pi$) is included then the Skyrmion is stabilized, without any problem regarding saddle-point solutions, and gives baryon properties to ≈30% of the experimental data. Extending this to an $U(3)_V$ HLS model (ρ,ω,k*,φ) [37]then the results obtained are not so good, for instance the proton mass≈2GeV.

In general it would seem that the more complete the prescription for including vector (and axial-vector) mesons, so the Skyrmion picture iterates towards a more satisfactory level. Although the iteration would appear to be rather "unstable" in the sense that progressing from ρ and ω to ρ,ω,k*,φ somewhat worse results.The process is not yet finished.

In summary the above makes a particularly appealing unified theoretical approach to low energy strong interactions, starting from the minimum of assumptions one constructs an effective pion Lagrangian, equation (2.1), which is well tested. This is then extended, making seemingly reasonable assumption [19] concerning the dynamical generation of kinetic terms by an underlying theory such as QCD, to give an effective Lagrangian for π,ρ mesons. This effective Lagrangian admits soliton solutions which have the correct spin-statistics to be interpreted as baryons, giving baryon properties to ≈30%.

(iv) Testing the HLS Model

Given the pivotal role of the HLS model of vector mesons, as described in the previous section, in constructing effective chiral Lagrangians for hadrons it is important that the model be fully tested. Preferably this test should be in a different sector of physics to that in which it has already been used; a test independent of parameter choice would be even stronger.

The notions of vector dominance (VMD), ρ universality and KSRF relation have long been established. However the core of the HLS model is that the ρ mesons are non-abelian gauge bosons. This is manifested in the 'self-interaction' vertices that are generated from the V_μ field kinetic term (see appendix B rules 3 to 8).

In fact the non-abelian nature of the ρ meson in this model does not seem to have been considered at all in the literature. The model has simply been found to be very useful in one sector of physics and any other sectors of physics that it might describe have been ignored.

Data on the process $\gamma\gamma\rightarrow\rho\rho$ is an ideal testing ground for the model; the experimental data [24]-[31] on $\gamma\gamma\rightarrow\rho\rho$ is very well established and there is a distinctive difference in the magnitude and shape of the cross section between the charged and neutral channels. There is also the added attraction that this data is still open to a 'conventional type' explanation, more details of this in chapter 3.

The couplings for $\gamma\gamma\rightarrow\rho\rho$ are fixed by the gauge nature of the interaction, so there is no 'fine tuning' required. In fact at the tree level $\gamma\gamma\rightarrow\rho\rho$ is purely a consequence of the ρ being a non-abelian gauge boson.

It might seem that with the ρρ threshold at $\sqrt{s}\approx1.54$ GeV that the process is at too high an energy scale, given that the chiral (pion) Lagrangian are used at $\sqrt{s}$ the order of a few hundred MeV. However in the Skyrmion picture the energy range has already been exteneded up to $\sqrt{s}\approx2$GeV, calculating nucleon masses and so on although it is not necessarily clear what fraction of the proton mass is generated by

the model in this high energy range. Extending the energy range upwards being very much the approach advocated by Ball [20]. So if the HLS model <u>really</u> is to be an <u>effective</u> theory then it would be reasonable to expect it to describe the process $\gamma\gamma\rightarrow\rho\rho$ (perhaps to ≈30% ,the sort of accuracy achieved in Skyrmion physics).

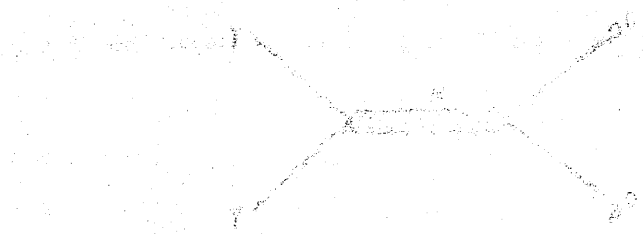

(i) Introduction

The two photon production of vector mesons

$$\gamma\gamma \rightarrow V_1V_2 \qquad V_{1,2}= \rho,\omega,k^*,\varphi$$

is a process that has aroused a great deal of interest since the observation [24]-[29] of a very large cross-section for the process $\gamma\gamma \rightarrow \rho^0\rho^0$ near threshold, see graph (3.1). This was because the data turned out to be about an order of magnitude larger than the "VDM prediction" [22] and was consequently an interesting process because theory appeared to be (drastically) wrong.

The large $\rho^0\rho^0$ cross-section is frequently referred to in the literature as an 'enhancement', however Poppe [23] stresses that the term enhancement arose "... a discrepancy by a factor of 10 between the first data [24],[27] and a "VDM" prediction [22]. This "VDM" prediction is a simple pomeron exchange amplitude and hence, the prediction is only valid in the limit $W \rightarrow \infty$. The large discrepancy on the other hand occurred right at the $\rho^0\rho^0$ threshold". So a suspect argument fails to describe $\gamma\gamma \rightarrow \rho^0\rho^0$.

The large cross-section at threshold suggests that the mechanism underlying the reaction could be resonance (R) formation

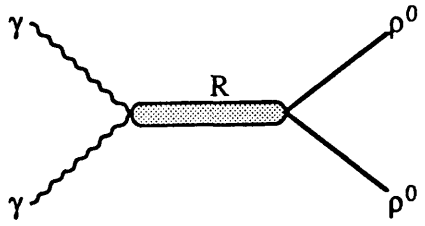

Fig. 3.1

Where R is a 0^+ $q\bar{q}$ resonance (q=quark) with I=0,1 . The ratios of the the various cross-sections $\sigma(\gamma\gamma \rightarrow V_1V_2)$ are calculated in appendix F according to such a possible resonance interpretation, basically the different channels are related by the

SU(3) Clebsch-Gordon coefficients.

In the case of $\gamma\gamma\rightarrow\rho\rho$ it is found that

$$\sigma(\gamma\gamma\rightarrow'R'\rightarrow\rho^+\rho^-) = 2\,\sigma(\gamma\gamma\rightarrow'R'\rightarrow\rho^0\rho^0) \qquad (3.1)$$

The upper limits on $\gamma\gamma\rightarrow\rho^+\rho^-$ have been given by the JADE Collaboration [30] and more recently a more detailed analysis by the ARGUS Collaboration [31], $\gamma\gamma\rightarrow\rho^+\rho^-$ has a completely different shape to $\gamma\gamma\rightarrow\rho^0\rho^0$. The cross-section rises to a peak of $\approx$40 nb at around $\sqrt{s}\approx$1.9GeV and then tails off at higher energies. So in summary

$$\frac{\sigma(\gamma\gamma\rightarrow\rho^0\rho^0)}{\sigma(\gamma\gamma\rightarrow\rho^+\rho^-)} \begin{cases} = \frac{1}{2} & \text{I=0 } 'q\bar{q}' \text{ resonance} \\ > 1 \ (\approx 4) & \text{experiment} \end{cases} \qquad (3.2)$$

The simple SU(3) resonance model is in serious disagreement with the data,in fact giving the ratio (3.2) completely the wrong way around.

Thus the data on $\gamma\gamma\rightarrow\rho\rho$ cannot be "explained" by I=0,1 $q\bar{q}$ resonance formation alone. However it is quite instructive to compare the above with the rest of the SU(3) resonance predictions for the other channels. The reactions $\gamma\gamma\rightarrow\omega\rho^0$[38], $\gamma\gamma\rightarrow\omega\omega$[39], $\gamma\gamma\rightarrow k^{*o}\overline{k^{*o}}$[40], $\gamma\gamma\rightarrow k^{*+}k^{*-}$ [41] see graphs (3.2), (3.3), (3.4) and (3.5) (and $\gamma\gamma\rightarrow\rho^+\rho^-$ [30]) all have a definite 'bump' at around $\sqrt{s}\approx$1.9GeV. It is obviously tempting to interpret this as being the same effect, ie same resonance, for all these channels.

Expressing the cross-sections as multiples of $\sigma(\gamma\gamma\rightarrow\omega\rho^0)$ one has the following results:

TABLE 3.1	Multiple of $\sigma(\gamma\gamma\rightarrow\omega\rho^0)$	Predicted cross-section at $\sqrt{s}\approx1.9$GeV (nb)	Experimental Data (nb)
$\sigma(\gamma\gamma\rightarrow\omega\rho^0)$	1	Input	30±8
$\sigma(\gamma\gamma\rightarrow\omega\omega)$	25/18	41.6±11.1	20
$\sigma(\gamma\gamma\rightarrow\rho^+\rho^-)$	25/9	83.3±22.2	40±10
$\sigma(\gamma\gamma\rightarrow\rho^0\rho^0)$	25/18	41.6±11.1	≈40
with 's'			
$\sigma(\gamma\gamma\rightarrow k^{*+}k^{*-})$	25/9	83.3±22.2	54±18
$\sigma(\gamma\gamma\rightarrow k^{*o}\overline{k^{*o}})$	4/9	13.3±3.6	6±2
without 's'			
$\sigma(\gamma\gamma\rightarrow k^{*+}k^{*-})$	16/9	53.3±14.2	54±18
$\sigma(\gamma\gamma\rightarrow k^{*o}\overline{k^{*o}})$	1/9	3.3±0.9	6±2
$\sigma(\gamma\gamma\rightarrow\omega\varphi)$	0	0	<1.7
$\sigma(\gamma\gamma\rightarrow\varphi\varphi)$	2/9	6.6±1.8	<7.1

TABLE 3.1 SU(3) predictions at $\sqrt{s}\approx1.9$GeV

Firstly note that the $\rho^+\rho^-$ cross-section is a factor of 2 too large, that for $\omega\omega$ is not much better, but given the error in $\sigma(\omega\rho^0)$ the result is that the discrepancy between the SU(3) prediction and experiment is for these two channels is only about two standard deviationswhich is not too bad given the accuracy of the data. And, of course, the fit is better than the factor of 8 difference (nearly an order of magnitude) of equation (3.2). The mass of the $s\bar{s}$ resonance 's' is not expected to be degenerate with m_σ and m_v, so it is not clear that the amplitudes due to 's' exchange should be added coherently to the other amplitudes. Thus cross-sections for the k*k* system have been quoted for both "with" and "without" the 's' exchange part, although it would be perhaps better to try to estimate this degree of coherence quantitatively. In

fact the results "with' seem to be in pretty good agreement with the data. The predictions for the K*K*, $\omega\varphi$ and $\varphi\varphi$ systems are much better and certainly not differing by an order of magnitude. In fact the recently presented data on $\gamma\gamma\rightarrow k^{*+}k^{*-}$ [41] gives

$$\frac{\langle \sigma(\gamma\gamma\rightarrow k^{*+}k^{*-}) \rangle}{\langle \sigma(\gamma\gamma\rightarrow k^{*0}\bar{k}^{*0}) \rangle} = 7.8 \pm 3.7 \qquad (3.3)$$

which should be compared with the prediction from Table 3.1 of 6.25 with the 's' intermediate resonance and a ratio of 16 "without" 's'.

(ii) Models for $\gamma\gamma\rightarrow VV$

The I=0,1 intermediate resonance picture would seem to work quite well around the bump at $\sqrt{s}$=1.9GeV for the K*K*, $\omega\varphi$ and $\varphi\varphi$ final states, but the large threshold cross-section for $\gamma\gamma\rightarrow\rho^0\rho^0$ cannot be explained by a straightforward I=0 resonance mechanism.

There are several contrasting approaches to a theory for $\gamma\gamma\rightarrow\rho\rho$, born as a result of the so far apparent failure of any "conventional" explanation.

Four-Quark Models

If one assumes that $\gamma\gamma\rightarrow\rho\rho$ proceeds via an I=2 resonance (R), then Clebsch-Gordon coefficients give

$$\sigma(\gamma\gamma\rightarrow\rho^+\rho^-) = \frac{1}{2}\,\sigma(\gamma\gamma\rightarrow\rho^0\rho^0) \qquad (3.4)$$

which at least gives the ratio (3.2) the right way around. However it is still not enough to reproduce the experimental data assumming that the mechanism in $\gamma\gamma\rightarrow\rho\rho$ was entirely due to an I=2 resonance.

If one considers a model consisting of I=0 and I=2 resonances which interfere constructively in the neutral channel and destructively in the charged channel then a 'resonance mechanism' interpretation for $\gamma\gamma \rightarrow \rho\rho$ is tenable. This requires the introduction of 'exotic' four-quark states ($Q^2\bar{Q}^2$) with I=2.

There are two groups [45]-[50] working on the four-quark model of two photon production of vector mesons. Although their approaches differ in detail, the basic idea is the same.

The proposed mechanism, Fig.3.2, is that the incoming photons 'change into' vector mesons via the vector dominance model (VDM), these mesons then interact to form four-quark states which then decay ("fall apart mode") into two vector mesons.

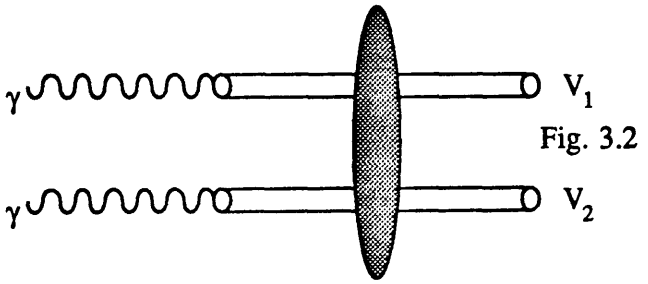

Fig. 3.2

Four quark states with $J^{PC}(I^G) = 0^{++}(0^+, 2^+)$ and $2^{++}(0^+, 2^+)$ have been considered by Johnson and Jaffe [43],[44]. Jaffe [44] has calculated the $Q^2\bar{Q}^2$ masses in the MIT bag model, yielding the following states which are very close to the $\rho^0\rho^0$ peak at $\sqrt{s} \approx 1.6$ GeV

masses : 1.65 GeV (2^{++}) , 1.45 GeV (0^{++}) , 1.80 GeV (0^{++})

The amplitudes $Q^2\bar{Q}^2 \rightarrow V_1V_2$ (and consequently $Q^2\bar{Q}^2 \rightarrow \gamma\gamma$ by VDM) are calculated using the MIT bag model results [43], [44] and are then combined to give the S-matrix element $\langle V_1V_2 \mid S \mid \gamma\gamma \rangle$.

Thus the S-matrix element , say, $\langle \rho^0\rho^0 \mid S \mid \gamma\gamma \rangle$ can be calculated according to the bag model for whichever intermediate resonances (given the restrictions of

spin and parity) the model builder decides to input. Both Li&Liu [45]-[47] and Achasov et al [48]-[50] use the 3 $Q^2\bar{Q}^2$ states (one I=2 and two I=0 states) whose masses were given above and lie in the region of the $\rho^0\rho^0$ peak . Taking the I=0 and the I=2 amplitudes for the process $\gamma\gamma\rightarrow\rho\rho$ to be A_0 and A_2 respectively then the Clebsch-Gordon coefficients conspire to give

$$A(\gamma\gamma\rightarrow\rho^0\rho^0) = A_0 + 2A_2$$
$$A(\gamma\gamma\rightarrow\rho^+\rho^-) = \sqrt{2}\,A_0 - \sqrt{2}A_2 \qquad (3.5)$$

In the first approximation $A_0 \approx A_2$, resulting in a suppression of the $\rho^+\rho^-$ final state; this was predicted by Achasov et al [48] before the upper limits on $\sigma(\gamma\gamma\rightarrow\rho^+\rho^-)$ were available from JADE [30] and was "post-dicted" by Li&Liu [45].

Both groups fit the model to the data by tuning the parameter 'a' [45],[47],[48] and [49] (nothing to do with the parameter'a'discussed in chapter 2!) and parameters 'a_i' in the case of Achasov et al [50]. A good fit to $\gamma\gamma\rightarrow\rho^0\rho^0$ is achieved, but the cross-section for $\gamma\gamma\rightarrow\rho^+\rho^-$ is well below the upper limits set by JADE [30]. The bulk of the effect is due to the interference between the 2^{++}(I=0,2) states with a small contribution from the 0^{++}(I=0,2) states.

Although the four quark model makes a definite prediction that near threshold the states coupling to vector mesons have spin-parity $J^P=2^+$. The early J^P analysis by the TASSO Collaboration [25] found that the $\rho^0\rho^0$ cross section basically consists of positive parity states, in particular that the 0^+ state dominates at threshold which is in disagreement with the four quark model. However recent analysis from the PLUTO Collaboration [29] again finds that positive parity states are definitely favoured and specifically the 2^+ state in the wide range $1.2\text{GeV}<\sqrt{s}<1.8\text{GeV}$, but the 0^+ state is not necessarily excluded at low $\sqrt{s}$. In fact Feindt [51] has stressed that there is no evidence for a single J^P state dominating.

Unfortunately the four quark model is unsuccessful in the predictions it makes

for other V_1V_2 channels.

The ARGUS Collaboration [38] data on $\gamma\gamma\rightarrow\omega\rho$ shows a definite bump of $\approx$30nb at $\sqrt{s}\approx$1.9GeV whereas the four quark model [45] and [50] predict a bump at $\sqrt{s}\approx$1.6GeV and cross-section of $\approx$25nb. The data [38] also has a bump indicating $a_2(1320)$ formation. The predictions [45]-[50] for $\gamma\gamma\rightarrow\omega\omega$ and $\gamma\gamma\rightarrow k^*k^*$ (charged and neutral channels) are too small by an order of magnitude, again with the bump at the wrong energy. Although the ratio of the two k*k* channels predicted by the four quark model is in agreement with the data [41]

$$\frac{\langle \sigma(\gamma\gamma\rightarrow k^{*+}k^{*-}) \rangle}{\langle \sigma(\gamma\gamma\rightarrow k^{*o}\bar{k}^{*o}) \rangle} = \begin{cases} 7.8\pm3.7 & \text{experiment} \\ 4.0 - 8.0 & \text{4 quark model} \end{cases}$$

The only other channels, other than $\rho\rho$ which was fitted to the data anyway, that are still compatible with the four quark model predictions are the upper limits on $\gamma\gamma\rightarrow\omega\varphi$ and $\gamma\gamma\rightarrow\varphi\varphi$ [42].

It should be noted that the parameter(s) 'a' are completely free and in reality may take different values for different channels. In this way, as stressed by Maor [52], the different channels are in fact somewhat unrelated within the context of the four quark model.

t-Channel Factorization

The t-channel factorization model for $\gamma\gamma\rightarrow\rho^0\rho^0$ by Alexander et al [53] is a more conservative approach, by comparison with the 'exotic' four quark resonance models, to the problem of the large $\sigma(\gamma\gamma\rightarrow\rho^0\rho^0)$ at threshold.

The model relates the $\gamma\gamma\rightarrow V_1V_2$ cross-section to photo-production and nucleon-nucleon scattering cross-sections; the basic assumption is that:

$$\sigma(\gamma\gamma\rightarrow V_1V_2) = \sum_i \frac{\sigma^i(\gamma N\rightarrow V_1 N)\,\sigma^i(\gamma N\rightarrow V_2 N)\,F^2_{\gamma N}}{\sigma^i(NN\rightarrow NN)\,F_{NN}\,F_{\gamma\gamma}} \qquad (3.6)$$

The above factorization relates matrix elements for different processes and so corrective flux factors F_{ij} have to be included to account for the different masses involved.

The sum in (3.6) is over different exchanges, Pomeron, pion,.... Factorization is a high energy property relating matrix elements, so it is clearly a major assumption that the factorization can be extrapolated down from high to low energies, the $\rho\rho$ threshold.

Assuming the process $\gamma\gamma\rightarrow\rho^0\rho^0$ to be dominated by pomeron exchange and taking experimental data for $\gamma N\rightarrow\rho^0 N$ and $pp\rightarrow pp$ Alexander et al [53] reproduce the large cross-section at threshold and the general shape of the observed $\sigma(\gamma\gamma\rightarrow\rho^0\rho^0)$. However the model is unable to give any results for $\gamma\gamma\rightarrow\rho^+\rho^-$, as this is a non-diffractive process; and factorization for this channel is unreliable [53].

Thus if the t-channel factorization is correct, it would 'explain' why the $\rho^+\rho^-$ and $\rho^0\rho^0$ cross-sections are so different, as they would be proceeding via different mechanisms.

However the t-channel factorization model has recently come in for quite extensive criticism. Kolanoski [54] claims that the large $\sigma(\gamma\gamma\rightarrow\rho^0\rho^0)$ at threshold cannot be accounted for by a pomeron exchange mechanism, whilst Achasov and Shestakov [55] claim that there is no theoretical justification for using the factorization of amplitudes at $\rho\rho$ threshold.

The t-channel factorization prediction [53] for $\gamma\gamma\rightarrow\omega\rho$ is incompatible with the data [38]; the model gives a peak of $\approx$18nb at $\sqrt{s}\approx$1.6GeV and then levels off to $\approx$5nb at energies >1.8GeV whereas the data [38] has a definite bump , as previously mentioned, at $\sqrt{s}\approx$1.9GeV with a maximum cross-section of$\approx$30nb. The model prediction for $\gamma\gamma\rightarrow\omega\omega$ is also incompatible with the data [39] the shape of the curve

is different , although it is explicitly stated in [53] that the t-channel model predictions for $\gamma\gamma\rightarrow\omega\omega$ are "unreliable". There are no predictions for $\gamma\gamma\rightarrow k^*k^*$ because there is no input data, finally though the prediction for $\varphi\rho^0$ is within experimental limits [40]. But the processes $\gamma\gamma\rightarrow\omega\rho,\rho^+\rho^-,k^*k^*$ are not diffractively dominated in the 'pure' t-channel view, so it is not only the $\omega\omega$ final state that is badly predicted from this point of view.

Hatzis and Paschalis [56] have caculated $\sigma(\gamma\gamma\rightarrow\rho^0\rho^0)$ in a theory with tree diagrams involving pseudoscalar meson (π,η,η') exchange.They have obtained a reasonable fit to the data putting in, 'by-hand', vertex form factors, although their model gives a cross-section which is less steep after threshold than experiment. They do not calculate $\sigma(\gamma\gamma\rightarrow\rho^+\rho^-)$. However more serious to their approach is that experiment [24]-[29] has ruled out the 0^- state, the angular analysis indicating that the $\rho^0\rho^0$ final state is dominated by 2^+ with a sizeable contribution from 0^+.

QCD

Brodsky et al [57] have calculated cross-sections for the non-diffractive processes $\gamma\gamma\rightarrow\rho^+\rho^-$, $k^{*+}k^{*-}$, $k^{*0}\overline{k^{*0}}$ in perturbative QCD. USing a dual picture between perturbative QCD and resonance production to calculate amplitudes for the process $\gamma\gamma\rightarrow q\bar{q}Q\bar{Q}$, where the mesons are $q\bar{Q}$ and $\bar{q}Q$. The main assumption is that the picture remains valid as the model is extended downwards in energy, down from the high p_T region where perturbative QCD is generally valid to the'$\rho\rho$' threshold region of $\sqrt{s}\approx1.0$ - 2.5 GeV.

The calculation of $\gamma\gamma\rightarrow\rho^+\rho^-$ [57] appears to be quite successful, less than the upper limits set by JADE [30] but the shape of the QCD curve is in agreement with the data. Unfortunately the recent data on the k^*k^* final states [40] and [41] is in

serious disagreement with the QCD predictions [57]. The prediction for $\gamma\gamma\rightarrow k^{*o}\overline{k^{*o}}$ is smoothly varying with a maximum of ≈1nb at $\sqrt{s}\approx 2.5$GeV whereas the data [40] has a peak of ≈6nb at $\sqrt{s}\approx 2$GeV and drops sharply to ≈1nb at $\sqrt{s}\approx 2.6$GeV; so the shape and magnitude of the prediction is in contradiction with the data. For the charged channel $\gamma\gamma\rightarrow k^{*+}k^{*-}$ the QCD prediction is nearly an order of magnitude out, the data shows a peak of ≈54nb at $\sqrt{s}\approx 2$GeV whereas 'QCD' predicts a peak of ≈7nb at $\sqrt{s}\approx 2.4$GeV. Although it is interesting to note that in [57] they give the ratio of the charged to neutral channel cross-sections to be ≈8, which is certainly in agreement with the data equation (3.3). However this is a rather specious result because examining the graphs in reference [57] it can be seen that this ratio is only true at $\sqrt{s}\approx 2.4$ GeV, whereas the ARGUS Collaboration [31] and [41] take the ratio of the averaged values.

One Kaon Exchange Model

Recently Achasov and Shestakov [55] proposed that the observed 'bump' in the $k^{*o}\overline{k^{*o}}$ system, at $\sqrt{s}\approx 1.9$GeV, could be described by a reggeised one-kaon-exchange(OKE) model. By fitting their parameter 'B' they obtain quite good agreement with the data on $\gamma\gamma\rightarrow k^{*o}\overline{k^{*o}}$ [40]. A prediction for the ratio of the charged to neutral channel cross-sections was made using this model [55]; this prediction was soon shown to be in serious disagreement with data [31] and [41].

$$\frac{\langle \sigma(\gamma\gamma\rightarrow k^{*+}k^{*-})\rangle}{\langle \sigma(\gamma\gamma\rightarrow k^{*o}\overline{k}^{*o})\rangle} = \begin{cases} \frac{1}{5.3} & \text{OKE model} \\ 7.8\pm 3.7 & \text{experiment} \end{cases}$$

(iii) Conclusions

A large cross-section for $\gamma\gamma\rightarrow\rho^0\rho^0$ has been observed at the threshold, the data on $\gamma\gamma\rightarrow\rho^+\rho^-$ is a factor of 4 smaller and has a different shape. This is surprising, and a single I=0 resonance mechanism for the process is untenable.

The four quark model explains the large ratio

$$\frac{\sigma(\gamma\gamma\rightarrow\rho^0\rho^0)}{\sigma(\gamma\gamma\rightarrow\rho^+\rho^-)} \approx 4$$

as an interference effect, which arises naturally, between 'exotic' four quark states (which are not necessarily 'natural') with I=0 and I=2. Unfortunately the four quark model predictions for the other channels are in complete disagreement with data (except for the $\omega\varphi$ and $\varphi\varphi$ final states for which the upper bounds are still in agreement with the model but this could change with better data), the indications being that another resonance structure is required at $\sqrt{s}\approx 1.9$ GeV.

The t-channel factorization model successfully gives $\gamma\gamma\rightarrow\rho^0\rho^0$ (ignoring Kolanoski's claim [54]), but predictions for other channels eithe do not exist or are in disagreement with experimental data.

The QCD predictions for channels other than $\gamma\gamma\rightarrow\rho^+\rho^-$ either do not exist or are in serious disagreement with the experimental data, although the calculation for $\gamma\gamma\rightarrow\rho^+\rho^-$ is in very good agreement with data.

The possibility of a conventional explanation for $\gamma\gamma\rightarrow\rho\rho$ cannot be discounted [23] and [55]. It remains unclear whether or not the channel $\rho\rho$ is related to the other V_1V_2 channels, ie do they proceed via the same mechanism?

Given that ρ dynamics are supposedly described by the HLS model of vector mesons, as used in Skyrmion physics, then the model should be tested to see whether or not it correctly describes the experimental data on $\gamma\gamma\rightarrow\rho\rho$. The HLS model includes a $\gamma\rho^+\rho^-$ vertex, giving a Born term for $\gamma\gamma\rightarrow\rho^+\rho^-$ analogous to $\gamma\gamma\rightarrow\pi^+\pi^-$, which Poppe [23] regards as a serious omission from the current 'exotic' models.

The HLS model certainly has a number of attractive features to recommend it

as a candidate 'conventional' explanation for $\gamma\gamma \rightarrow V_1V_2$. For instance the model is based on an extension of a well established chiral (effective) Lagrangian, the ρ field enters as a gauge field in a covariant derivative. The model is also easily extended to the other vector mesons simply by enlarging the hidden symmetry H_{local}, to $U(3)_V$ in order to include the ω, k* and φ (this also requires the chiral group G to be enlarged to $U(3)_L \times U(3)_R$).

In a sense the HLS model is complimentary to the QCD approach of Brodsky et al [57] (and the t-channel factorization approach of Alexander et al [53]) because the chiral model well known to be good up to $\sqrt{s} \approx 300$MeV is being extrapolated upwards in energy. This is very much in line with the approach advocated by Ball [20] for constructing effective Lagrangians for mesons and baryons.

Finally the data on $\gamma\gamma \rightarrow \rho\rho$ is a particularly attractive process against which to test a model because of the highly distinctive nature of the charged and neutral channels.

(i) Introduction

Having motivated in chapters 2 and 3 the need to consider the process $\gamma\gamma\to\rho\rho$ in the context of the HLS model of ρ mesons, the model is used to calculate $\sigma(\gamma\gamma\to\rho\rho)$ in first order perturbation theory.

At the tree level the process $\gamma\gamma\to\rho^+\rho^-$ is given by, using Feynman rules 3&6 in appendix B, the following three diagrams:

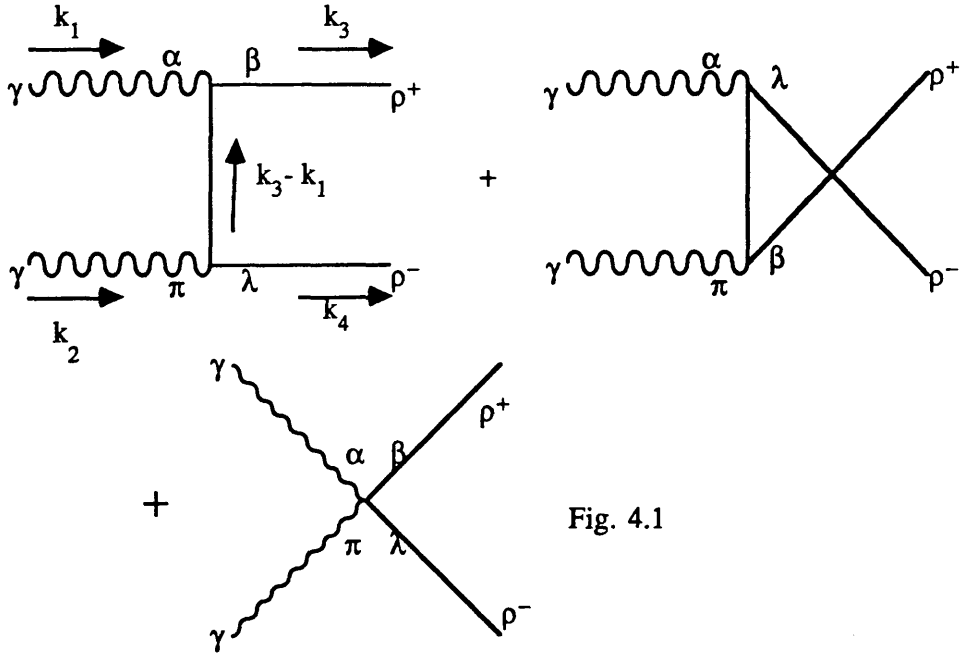

Fig. 4.1

The Feynman amplitude corresponding to Fig.4.1 is of the order e^2. However the process $\gamma\gamma\to\rho^0\rho^0$ is exactly zero at the tree level. Thus the model at the tree-level is in contradiction with the experimental data which gives

$$\frac{\sigma(\gamma\gamma\to\rho^0\rho^0)}{\sigma(\gamma\gamma\to\rho^+\rho^-)} > 1 \ (\simeq 4) \qquad (3.2)$$

This has been observed by myself [58] as well as Moussallam [59] and

Achasov Sheshtakov[55]; Moussallam has also calculated $\sigma(\gamma\gamma\rightarrow\rho^+\rho^-)$ at the tree level but the latter only note the tree level failure and do not actually calculate $\sigma(\gamma\gamma\rightarrow\rho^+\rho^-)$ to see how close it is to the experimental value.

(ii) Calculation

The four momenta k_i (i=1,2,3,4) in the centre of mass frame and the Mandelstam variables s,t,u for the process $\gamma\gamma\rightarrow\rho\rho$ are given in appendix A.

Using Feynman rules 3&6 the diagrams in Fig. 4.1 yield the following Feynman amplitude :

$$M^{\alpha\pi\beta\lambda} = (-i)\Big\{ i e \big(g^{\alpha\beta}(k_1+k_3)^{\mu} + g^{\beta\mu}(k_1-2k_3)^{\alpha} + g^{\alpha\mu}(k_3-2k_1)^{\beta}\big)$$

$$\times i \frac{\big(-g_{\mu\nu} + (k_3-k_1)_{\mu}(k_3-k_1)_{\nu}/m^2\big)}{(k_3-k_1)^2 - m^2}$$

$$\times i e \big(g^{\pi\lambda}(k_2+k_4)^{\nu} + g^{\lambda\nu}(k_2-2k_4)^{\pi} + g^{\pi\nu}(k_4-2k_2)^{\lambda}\big)$$

$$+ \big(\text{the above term with } k_1 \leftrightarrow k_2 \text{ and } \alpha \leftrightarrow \pi \text{ interchanged}\big)$$

$$+ i e^2\big(g^{\alpha\beta}g^{\pi\lambda} + g^{\alpha\lambda}g^{\pi\beta} - 2g^{\alpha\pi}g^{\beta\lambda}\big) \Big\} \quad (4.1)$$

From now on m will be taken to be the ρ mass , unless otherwise stated. Each of the external particles has associated polarization vectors (given in appendix C), which project out definite helicity states. Given a particle of four-momentum k^{α} and polarization vector $\varepsilon_{\alpha}(k)$, then $\varepsilon_{\alpha}(k)$ must satisfy the 'subsidiary condition' $k^{\alpha}\varepsilon_{\alpha}(k)=0$ (4.2).

Appling the subsidiary condition (4.2) to each of the external particles in $\gamma\gamma\rightarrow\rho^+\rho^-$ means setting

$$k_1^{\alpha} = k_2^{\pi} = k_3^{\beta} = k_4^{\lambda} = 0 \qquad (4.3)$$

which considerably simplifies equation (4.1). The Feynman amplitude with (4.3)

applied will be denoted $\mathcal{M}^{\alpha\pi\beta\lambda}$, thus:

$$\mathcal{M}^{\alpha\pi\beta\lambda} = -2e^2\Big\{ g^{\alpha\pi}g^{\beta\lambda} + \frac{s}{t-m^2} g^{\alpha\beta}g^{\pi\lambda} + \frac{s}{u-m^2} g^{\alpha\lambda}g^{\pi\beta}$$

$$- \frac{2}{t-m^2}\Big(g^{\alpha\beta}(k_1^{\pi}k_2^{\lambda} + k_4^{\pi}k_1^{\lambda}) + g^{\pi\lambda}(k_2^{\alpha}k_1^{\beta} + k_3^{\alpha}k_2^{\beta})$$

$$- g^{\pi\beta}k_3^{\alpha}k_2^{\lambda} - g^{\alpha\lambda}k_4^{\pi}k_1^{\beta} - g^{\beta\lambda}k_3^{\alpha}k_4^{\pi} - g^{\alpha\pi}k_1^{\beta}k_2^{\lambda}\Big)$$

$$- \frac{2}{u-m^2}\Big(g^{\pi\beta}(k_2^{\alpha}k_1^{\lambda} + k_4^{\alpha}k_2^{\lambda}) + g^{\alpha\lambda}(k_1^{\pi}k_2^{\beta} + k_3^{\pi}k_1^{\beta})$$

$$- g^{\alpha\beta}k_3^{\pi}k_1^{\lambda} - g^{\pi\lambda}k_4^{\alpha}k_2^{\beta} - g^{\beta\lambda}k_3^{\pi}k_4^{\alpha} - g^{\alpha\pi}k_1^{\lambda}k_2^{\beta}\Big)\Big\} \quad (4.4)$$

The total unpolarized cross-section is given by averaging over intial photon polarizations and summing over the final ρ meson polarizations, hence

$$\sigma(\gamma\gamma\rightarrow\rho^+\rho^-) = \frac{1}{64\,\pi^2\,s}\sqrt{1-\frac{4m^2}{s}}\int d\Omega\ |\mathcal{M}|^2 \qquad (4.5)$$

$$|\mathcal{M}|^2 := \frac{1}{4}\sum_{\text{polarizations}} \varepsilon_{1\alpha}\varepsilon_{2\pi}\varepsilon_{3\beta}\varepsilon_{4\lambda}\varepsilon_{1\alpha'}\varepsilon_{2\pi'}\varepsilon_{3\beta'}\varepsilon_{4\lambda'}\,\mathcal{M}^{\alpha\pi\beta\lambda}\,\mathcal{M}^{*\alpha'\pi'\beta'\lambda'} \qquad (4.6)$$

For a photon of four momentum k the polarization sum in general is :

$$\sum_{\text{pol}} \varepsilon_{\alpha}(k)\,\varepsilon_{\beta}(k) = -g_{\alpha\beta} - \frac{1}{(kn)^2}\left[k_{\alpha}k_{\beta} - (kn)(k_{\alpha}n_{\beta} + k_{\beta}n_{\alpha})\right] \qquad (4.7)$$

Where n_{α}= (1,0) and for a ρ meson of four momentum k the polarization sum is

$$\sum_{pol} \varepsilon_\alpha(k)\, \varepsilon_\beta(k) = - g_{\alpha\beta} + \frac{k_\alpha k_\beta}{m^2} \qquad (4.8)$$

A problem, as first noted by Pesic[60], arises when the subsidiary condition (4.2) is applied to amplitudes involving two or more photons. First of all consider a $U(1)_{em}$ invariant amplitude M, with one external photon with polarization vector $\varepsilon_\alpha(k)$ so that $M = \varepsilon_\alpha(k)\, M^\alpha$; as a consequence of the $U(1)_{em}$ gauge invariance one has the result $k_\alpha M^\alpha = 0$ (4.9). As a result when M is 'squared' and the sum over polarizations is made equation (4.9) means that only the $-g_{\alpha\beta}$ term in equation (4.7) contributes, all the others give zero. Thus

$$\sum_{pol} \varepsilon_\alpha \varepsilon^*_\beta\, M^\alpha M^{*\beta} = - g_{\alpha\beta} M^\alpha M^{*\beta} \qquad (4.10)$$

The amplitude $M^{\alpha\pi\beta\lambda}$ (4.1) is $U(1)_{em}$ gauge invariant, ie

$$k_{1\alpha} M^{\alpha\pi\beta\lambda} = 0 = k_{2\pi} M^{\alpha\pi\beta\lambda} \qquad (4.11)$$

However the problem, alluded to earlier, is that the amplitude with the subsidiary conditions applied for both photons ($\mathcal{M}^{\alpha\pi\beta\lambda}$) is not $U(1)_{em}$ gauge invariant. In fact

$$k_{1\alpha} \mathcal{M}^{\alpha\pi\beta\lambda} = 2 e^2 k_2^\pi g^{\beta\lambda}$$

$$k_{2\pi} \mathcal{M}^{\alpha\pi\beta\lambda} = 2 e^2 k_1^\alpha g^{\beta\lambda} \qquad (4.12)$$

So the "trick" used to obtain the simple polarization sum (4.10) cannot be used in the case of calculating $|\mathcal{M}|^2$ (equation 4.6). It has been shown [60] and [61] that the correct formmula for the polarization sum is

$$|\mathcal{M}|^2 = \frac{1}{4} \left(g_{\alpha\alpha'} g_{\pi\pi'} \mathcal{M}^{\alpha\pi\beta\lambda} \mathcal{M}^{\alpha'\pi'\beta'\lambda'} - 8 e^4 g^{\beta\lambda} g^{\beta'\lambda'} \right)$$
$$\times \left(-g_{\beta\beta'} + \frac{k_{3\beta} k_{3\beta'}}{m^2}\right) \left(-g_{\lambda\lambda'} + \frac{k_{4\lambda} k_{4\lambda'}}{m^2}\right) \qquad (4.12')$$

This is easily shown by substituting equation (4.7) into (4.6) for each of the two photons and using equation (4.12) (where it is essential that the photons are 'on-shell'); and the ρ meson polarization sums are given by equation (4.8). This is the method employed by Pesic[60], who proves a similar formula for the related process $\gamma\gamma \rightarrow ss$ (s=scalar) and quotes the result for $\gamma\gamma \rightarrow vv$ (v=vector). Whereas Tupper and Samuel [61] prove a more general result, which is then specialised to $\gamma\gamma \rightarrow vv$, it is not clear if this generalised result gives any further understanding.

Finally it should be noted that (i) no such problem occurs for massive vector fields and (ii) if only one of the subsidiary conditions is applied for the photons then equation (4.10) can be used for both photons.

Putting equation (4.4) into equation (4.12) gives, after some work (& without the need to resort to the use of REDUCE),

$$|\mathcal{M}|^2 = \frac{e^4}{(\alpha_1^2 - z^2)^2} \left\{ \frac{1}{2} x(1-x) z^4 + \frac{1}{4}\alpha_1^2 (4x^2 - 4x + 8 + \frac{3}{x}) z^2 \right.$$
$$+ \frac{1}{4}\alpha_1^4 (-2x^2 + 2x + 8 - \frac{3}{x} + \frac{3}{x^2})$$
$$\left. + 2 (3x + 4x^2 - 4x) (\alpha_1^2 - z^2)^2 \right\} \qquad (4.13)$$

Where $\alpha_1 = \sqrt{\frac{s}{s - 4m^2}}$ and z is the cosine of the scattering angle, as defined in appendix A ; and $x = \frac{s}{4m^2}$

Putting the equation for $|\mathcal{M}|^2$ (equation 4.13) into the formula for the unpolarized cross-section (equation4.5) and performing the solid angle integration gives:

$$\sigma(\gamma\gamma\to\rho^+\rho^-) = \frac{4\pi\alpha^2}{s}\sqrt{1-\frac{4m^2}{s}}\left\{\left(\frac{12m^4}{s^2}-\frac{6m^2}{s}\right)2\alpha_1 Q_0(\alpha_1) + \frac{s}{m^2}\left(2+\frac{3m^2}{2s}+\frac{6m^4}{s^2}\right)\right\} \qquad (4.14)$$

Where $Q_n(z) = \frac{1}{2}\ln\left(\frac{z+1}{z-1}\right)$, as defined in appendix A.

Where $Q_0(z) = \frac{1}{2}\ln\left(\frac{z+1}{z-1}\right)$, as defined in appendix A.

$\alpha \equiv e^2/4\pi \approx 1/137$ is the fine structure constant.

Note that as $s\to\infty$, so $\alpha_1\to 1$, and equation (4.14) has the following limit:

$$\underset{s\to\infty}{\sigma(\gamma\gamma\to\rho^+\rho^-)} = \frac{8\pi\alpha^2}{m^2} \qquad (4.15)$$

It is interesting to note that $\gamma\gamma\to W^+W^-$ has already been calculated [60]-[62], basically the same calculation as the one above, but in the Standard Model; this was for the purpose of calculating the production cross section for W^+W^- via two photons at e^+e^- machines ie $e^+e^-\to e^+e^- W^+W^-$ .The cross-section for $\gamma\gamma\to W^+W^-$ is found to be very sensitive to the magnetic moment (κ) of the W. Thus measurements of $\gamma\gamma\to W^+W^-$ at future machines are hoped to give indications of possible deviations from the Standard Model. It is also worth recalling that part of the motivation for testing the HLS model at ≈1GeV is that the model is also considered a prototype effective Lagrangian for Technicolour theories ≈1TeV.

(iii) Results

The HLS model calculation of $\sigma(\gamma\gamma\rightarrow\rho^+\rho^-)$ in first order perturbation theory is now compared with the experimental data [30] and [31]. Working with $\sqrt{s}$ and m in GeV, then equation 4.14 will give the cross-section in nanobarns (nb) when 4.14 is multiplied by 389390, using the fact that $(1GeV)^{-2} \equiv 389390$ nb.

The cross-section is evaluated around the maximum of the experimental data on $\sigma(\gamma\gamma\rightarrow\rho^+\rho^-)$, ie at $\sqrt{s} = 1.96$GeV, and around the peak of the experimental data on $\sigma(\gamma\gamma\rightarrow\rho^0\rho^0)$ at $\sqrt{s} = 1.66$GeV.

	Experimental	HLS model
$\sqrt{s}$ GeV	$\sigma(\gamma\gamma\rightarrow\rho^+\rho^-)$ nb	$\sigma(\gamma\gamma\rightarrow\rho^+\rho^-)$ nb
1.96	42	583
1.655	25	367

The HLS model gives a cross-section generally an order of magnitude larger than the experimental data. Comparison of the plot of (4.14), graph (4.1), with the experimental data [30] in graph (3.1) shows a very large discrepency, not only is the model an order of magnitude too large but also the shape of the curve is quite different to that observed; ie the model tends to a large constant value, whereas the experimental data tends to zero.

Although, of course, since the HLS model is supposedly an 'effective theory' there is a value of s (s_{cutoff}) above which the model would not be believed anyway. Unfortunately even below $\sqrt{s_{cutoff}} \approx 2.0$ GeV the model gives a cross-section for $\gamma\gamma\rightarrow\rho^+\rho^-$ which cannot be reconciled with the data; at the tree-level at least.

By expressing the helicity amplitudes as partial wave amplitudes the cross-section σ can be written as

$$\sigma = \sum_J (2J+1)\,\sigma_J \qquad (4.17)$$

Where $J=|\lambda_a - \lambda_b|$ and $\lambda_a - \lambda_b$= the total angular momentum of the $\gamma\gamma$ system projected onto the z-axis. So J=0 or 2,as J=1 is not allowed.

To a very good approximation a helicity amplitude M^{abcd} for $\gamma\gamma \rightarrow \rho^+\rho^-$ is given by the first non-zero wave in its' partial wave expansion, higher waves being ignored. Using the result

$$\int d\Omega \, |M^{abcd}|^2 = 4\pi \sum_J (2J+1) \, |T_J^{abcd}|^2 \qquad (4.18)$$

and the relations between the various T^{abcd} amplitudes (see appendix C) one obtains:

$$\sigma_0 = \frac{1}{32\pi s}\sqrt{1-\frac{4m^2}{s}}\left(|T_0^{+\,+\,+\,+}|^2 + |T_0^{+\,+\,-\,-}|^2 + |T_0^{+\,+\,0\,0}|^2 \right) \qquad (4.19a)$$

$$\sigma_1 = 0 \qquad (4.19b)$$

$$\sigma_2 = \frac{1}{32\pi s}\sqrt{1-\frac{4m^2}{s}}\left(|T_2^{+\,-\,0\,0}|^2 + |T_2^{+\,-\,+\,-}|^2 + |T_2^{+\,-\,-\,+}|^2 + 2|T_2^{+\,-\,+\,0}|^2 + 2|T_2^{+\,-\,-\,0}|^2 + 2|T_2^{+\,-\,+\,+}|^2 \right) \qquad (4.19c)$$

The cross sections σ_0, σ_2 and $\sigma_0 + 5\sigma_2$ are plotted in graph (4.2) for $4m^2 \leq s \leq 5m^2$, the J=2 component is substantially larger than the J=0 part near threshold. This should be compared with the recently presented analysis of $\gamma\gamma \rightarrow \rho^+\rho^-$ by the ARGUS Collaboration [31] who find that the J^P states 0^+ and 2^+ dominate about equally, with a peak at $\sqrt{s} \approx 1.9$GeV. Interestingly the J=0 and the J=2 contributions in graph (4.2) actually coincide at $s \approx 6.0m^2$ ie at $\sqrt{s} \approx 1.9$ GeV. However it should be remembered that the magnitude of the HLS model cross section for the charged channel at tree level is too large by an order of magnitude, as well as the shape of the cross section being in disagreement with the data.

(iv) Conclusions

The HLS model fails at the tree-level to describe the process $\gamma\gamma\rightarrow\rho\rho$. With $\gamma\gamma\rightarrow\rho^0\rho^0$ exactly zero at the first order indicates a problem for the model, but then calculating $\sigma(\gamma\gamma\rightarrow\rho^+\rho^-)$ and comparing with the experimental data shows the tree-level failure to be even worse than indicated by simply noting that $\sigma(\gamma\gamma\rightarrow\rho^0\rho^0)= 0$, as was done by Achasov & Shestakov [55].

(i) Introduction

The tree level calculation fails, giving

$$\frac{\sigma(\gamma\gamma\rightarrow\rho^0\rho^0)}{\sigma(\gamma\gamma\rightarrow\rho^+\rho^-)} = 0 \qquad (5.1)$$

in contradiction to the experimental data which gives the ratio to be >1.

The KSRF relation (equation 2.23) can be used to determine the HLS ($SU(2)_v$) coupling constant f. Taking as input m_ρ=770 MeV and the pion decay constant f_π=93 MeV gives f=5.85, this is a large coupling constant.In the spirit of chiral perturbation theory [5] and [63] one can make an estimate of the one loop effects, consider the simplest loop diagram for $\gamma\gamma\rightarrow\rho\rho$, with intermediate ρ's.

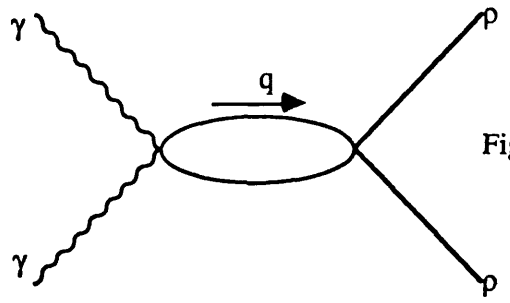

Fig. 5.1

Neglecting the spin complications of the ρ and ignoring the external momentum dependence of the loop, the diagram in figure 5.1 is written as

$$M_{loop} \approx \frac{f^2}{16\pi^4}\int \frac{d^4q}{(q^2-m^2)^2} M_{tree} \qquad (5.2)$$

So M_{loop} looks like a modified seagull diagram, the f^2 coupling arises from the RHS of figure 5.1. Assuming that the loop integral has a cut off Λ equation 5.2 becomes

$$M_{loop} \approx \frac{f^2}{16\pi^2} \ln\left(\frac{\Lambda^2}{m^2}\right) M_{tree} \qquad (5.3)$$

Taking $\Lambda \approx 1.3\text{-}1.4$ GeV indicates that the loop amplitudes could be at least 25% of the tree-level amplitudes and possibly larger since equation 5.3 is a rather crude estimate ignoring s dependence, particle spin etc .

The loop corrections, in the light of the above estimate, to $\gamma\gamma \rightarrow \rho\rho$ should be calculated to check whether or not there is a conspiracy between helicity amplitudes such that the loop corrections for $\gamma\gamma \rightarrow \rho^+\rho^-$ are large enough, and of the correct relative sign, to decrease $\sigma(\gamma\gamma \rightarrow \rho^+\rho^-)_{tree}$ by an order of magnitude and increase $\sigma(\gamma\gamma \rightarrow \rho^0\rho^0)_{tree}$ from zero to $\approx$100nb.

Given the estimated size of the loop corrections it is very important to be sure that the non-abelian nature of the ρ meson in the HLS model really has been tested and from the $\gamma\gamma$ physics standpoint any model which might offer the possibility of a 'conventional' explanation $\gamma\gamma \rightarrow \rho\rho$ should be thoroughly investigated (or perhaps more realistically to show that extrapolating a chiral model upwards in energy is not whole story with regard to $\gamma\gamma \rightarrow \rho\rho$). Although it would be a most unsatisfactory "effective" theory if all the important processes entered at the loop level.

Moussallam's attempt [59] to generate a non-zero $\sigma(\gamma\gamma \rightarrow \rho^0\rho^0)$in the gauged chiral model is based on a 'k-matrix' approach of unitarizing the amplitudes generated by his particular version of the model. In the preprint form of reference [59] the k-matrix method was applied to amplitudes generated by the tree and one loop diagrams, with this he was able to generate reasonable results but under the rather questionable assumption that the real parts of the loop amplitudes are negligible. Thus further motivating a one-loop calculation of $\gamma\gamma \rightarrow \rho^0\rho^0$ in which one calculates both real and imaginary parts and so tests the HLS model at face value with no further input other than a cut off in the chiral loop expansion.However in the version that has recently appeared in print [59] it would seem that Moussallam has taken only the tree-level amplitudes for the k-matrix, which is probably less accurate

than including the loop effects.

It is interesting to note that an analogous calculation by Bijnens and Cornet [64] and Donoghue et al [65] of $\gamma\gamma\rightarrow\pi\pi$ in chiral perturbation theory [5] and [63] has yielded reasonable results. Using a $U(1)_{em}$ gauged chiral lagrangian it is found that whilst $\gamma\gamma\rightarrow\pi^+\pi^-$ is non-zero at the tree level the neutral channel $\gamma\gamma\rightarrow\pi^0\pi^0$ is exactly zero, just the same situation found for the process $\gamma\gamma\rightarrow\rho\rho$ in the HLS model. Calculating the one loop corrections to $\gamma\gamma\rightarrow\pi\pi$ in chiral perturbation theory gives reasonable agreement with the experimental data, although they have the distinct advantage that there are no "box diagrams" in their approach. This encourages us to examine the one loop corrections to $\gamma\gamma\rightarrow\rho\rho$ in the HLS model.

(ii) Method

The usual method for calculating loop diagrams is through the Feynman parameterization of the loop, leading to multi-dimensional scalar integrals. The degree of difficulty of the integrals increases with the number of internal lines in the loop, the powers of loop momentum in the numerator of the loop integral; this is as well as the possibility of the particle masses conspiring to produce anomalous thresholds. In principle these integrals can be performed analytically [66], although the Spence functions resulting from this approach quite often have to be evaluated numerically [67]. For $\gamma\gamma\rightarrow\rho\rho$ the analytic approach [66] this would be an extensive task and inexpedient since only an estimate ($\approx$20-30% cf Skyrmion physics accuracy) of the integrals is required.

The obvious approach is to thus to perform a numerical integration over the Feynman parameters. Unfortunately the loop diagrams with intermediate ρ's (and π,k,...) develop singularities in the s-channel; extracting the real and imaginary parts from numerical multi-dimensional integration is unfeasible.

Motivated by the above problems it was decided to take a dispersive approach in the evaluation of the loop integrals. It is relatively straightforward to evaluate the

imaginary part of the integrals by using the Cutkosky rule [68], the real part is then reconstructed from the imaginary part using a dispersive integral derived from Cauchy's Theorem. Consider a simple example of exactly how this is expected to work.

The simplest one loop diagram for $\gamma\gamma \rightarrow \rho\rho$ is the bubble diagram, constructed from Feynman rules 6 and 5/8 (appendix B)

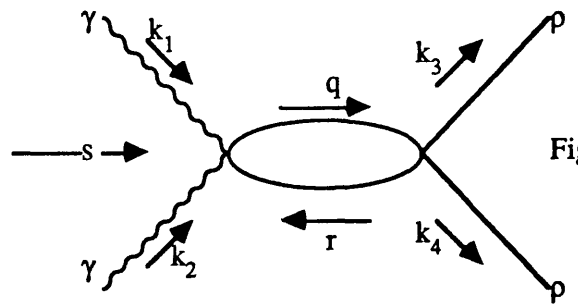

Fig. 5.2

The basic loop integration for this diagram is

$$\int \frac{d^4q}{(q^2-m^2+i\varepsilon)(r^2-m^2+i\varepsilon)} = 2\pi^2 i\, I_1(s) \qquad (5.4)$$

It is shown in appendix D (equation D10) that the Cutkosky rule yields

$$\text{Im}\, I_1(s) = \frac{\pi}{2}\sqrt{1-\frac{4m^2}{s}} \qquad (5.5)$$

The dispersion relation D.14, derived from Cauchy's Theorem in appendix D, is applied to equation (5.5) to reconstruct the real part of $I_1(s)$ giving

$$I_1(s) = \frac{1}{2}\int_{4m^2}^{\infty} \frac{ds'}{s'-s-i\varepsilon}\sqrt{1-\frac{4m^2}{s'}} \qquad (5.6)$$

The HLS model is supposed to be an effective theory and as such is only expected to be valid for $s<s_c$, where s_c is the cut off ($2\Lambda\approx\sqrt{s_c}$). Where a reasonable cutoff is in the range 2.0 GeV $< \sqrt{s_c} <$ 2.5 GeV, above the $\rho^0\rho^0$ threshold peak.

So the model is not believed for $s>s_c$ and any effects above s_c are ignored since any attempt at incorporating the region $s>s_c$ is outside the scope of the calculation, recalling that an estimate (to ≈30%) of the loop corrections is required.Thus the function Im $I_1(s)$ is modified to

$$\text{Im } I_1(s) = \begin{cases} \frac{\pi}{2}\sqrt{1-\frac{4m^2}{s}} & s<s_c \\ 0 & s>s_c \end{cases} \qquad (5.7)$$

that is to say we only believe the integrand up to s_c so that the dispersive integral equation 5.6 becomes

$$I_1(s) = \frac{1}{2}\int_{4m^2}^{s_c} \frac{ds'}{s'- s - i\varepsilon}\sqrt{1-\frac{4m^2}{s'}} \qquad (5.8)$$

It is interesting to note that the use of dispersive integrals to calculate scattering amplitudes (at the one loop level) is reminiscent of the "Analytic S-Matrix" approach to the strong interactions, but instead of 'postulating' the imaginary parts to have some simple 'pole-like' form the HLS model explicitly gives the imaginary part through applying the Cutkosky rule to the loop diagrams.

The integral 5.4 is logarithmically divergent but in the dispersive approach being adopted here the integral (equation 5.8) is finite, since the integral is simply cut-off above that point at which the model is expected to fail. One covariant way in which the integral 5.4 can be regulated (made finite) is the Pauli-Villars (PV) method, whereby the replacement

$$\frac{1}{q^2 - m^2} \rightarrow \frac{1}{q^2 - m^2} - \frac{1}{q^2 - \Lambda^2} \qquad (5.9)$$

is made in 5.4 and it is assumed that $\Lambda \gg m$. This corresponds to putting in a very heavy particle exchange term, and basically "subtracts out" the bad high energy behaviour of 5.4.However in the case under consideration $\Lambda \approx 2m$, so the PV method introduces an unphysical pole very close to the origin of the $\angle s$ plane and since, in a sense, it is the singularity structure that is controlling the physics it can be seen that the PV method has the most undesirable effect of introducing extra "physics" which is not really part of the model. The PV method of cut-off is unviable. Closely related to the PV method is that of Dimensional Regularization but again that is unviable, because the "extra" singularity is still present it simply has been shifted to the dimension (D) of the integral, where $D=4-\eta$,and one gets terms like $1/\eta$ from an integration which obviously diverges as $\eta \rightarrow 0$.

Alternatively to the PV method in the usual dispersive approach, where the integration is over the interval $[4m^2,\infty)$, the integral 5.4 is made finite by means of the subtraction constants. For example $\gamma\gamma$ scattering amplitudes[69] are taken to be zero when s=t=0, in which case 5.6 would be rewritten

$$\bar{I}_1(s) = \frac{1}{2}\int_{4m^2}^{\infty} ds' \{ \frac{1}{s'-s-i\varepsilon} - \frac{1}{s'-i\varepsilon} \} \sqrt{1 - \frac{4m^2}{s'}} \qquad (5.10)$$

so that $I_1(s)$ is finite and $I_1(0)=0$.

Because the ρ has a finite width there is a nominal threshold of $s=4m^2$ for $\gamma\gamma \rightarrow \rho\rho$. The $\sigma(\gamma\gamma \rightarrow \rho\rho)$ is non-zero below the nominal threshold, substantially so in the neutral channel which peaks around $s=4m^2$. Thus making subtractions at, say, nominal threshold to the dispersive integrals for $\gamma\gamma \rightarrow \rho\rho$ amplitudes would mean a loss in predictivity for the model. This would be most unsatisfactory.

Equation 5.4 is the simplest loop integral, but in the process $\gamma\gamma \rightarrow \rho\rho$ there are 'bubble','triangle' and 'box' diagrams (2,3 and 4 internal lines repectively) each with up to 4 powers of loop momentum (q) in the numerator (this includes those terms that are unrenormalisable).

To ensure that the dispersion relation 5.8 is used correctly it is essential to seperate out the external kinematical factors from the "invariant amplitudes", to which the dispersion relation 5.8 is applied. As an example consider the bubble diagram integral :

$$\int d^4q \frac{q^\alpha q^\beta}{(q^2 - m^2 + i\varepsilon)((q-k)^2 - m^2 + i\varepsilon)} = 2\pi^2 i \left(g^{\alpha\beta} e_1(k^2) + k^\alpha k^\beta e_2(k^2) \right) \tag{5.11}$$

The RHS of the above equation is the most general form possible, the tensor can only be constructed out of the quantities $g^{\alpha\beta}$ and $k^\alpha$and the invariant amplitudes e_j can only be functions of k^2. It is shown in appendix D that the judicious application of the Cutkosky rule gives Im e_j j=1,2 as solutions to a pair of linear equations which can be easily solved by hand; this becomes impracticable for higher powers of q in the numerator, and the triangle diagrams, so the algebraic programming system REDUCE is used to solve the sets of linear equations. Taking the solutions Im e_j j=1,2 from appendix D and using equation 5.8 to reconstruct the real part of e_j gives :

$$e_j(k^2) = \frac{1}{\pi} \int_{4m^2}^{s_c} dk'^2 \frac{\text{Im } e_j(k'^2)}{k'^2 - k^2 - i\varepsilon} \tag{5.12}$$

(iii) Box Diagram Approximation

The invariant amplitudes for the bubble and triangle diagrams are functions of only one of the Mandelstam variables s,t,u , and because there are no anomalous thresholds associated with these diagrams when there is a ρ in the loop, a single dispersion relation is a sufficient representation. Whereas the box diagram invariant amplitudes are functions of two Mandelstam variables, for example consider the box diagram below:

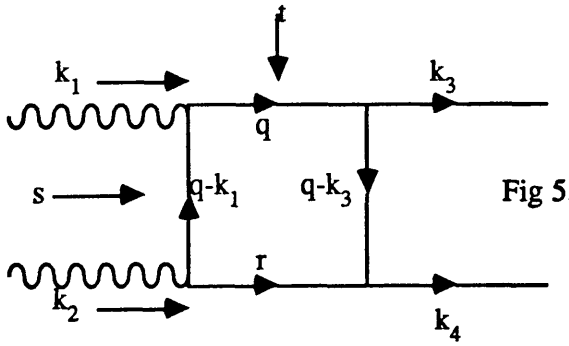

Fig 5.3

The basic integral (numerator=1) corresponding to this diagram is

$$\int \frac{d^4q}{(q^2-m^2)((q-k_3)^2-m^2)(r^2-m^2)((q-k_1)^2-m^2)} = 2\pi^2 i\,\Psi(s,t) \quad (5.13)$$

$$r=q-k_1-k_2=q-k_3-k_4$$

The full analytic expression for $\Psi(s,t)$ is a double dispersion relation [69] in s and t.

$$\Psi(s,t) = \frac{1}{\pi^2}\iint_{\mathfrak{R}} \frac{\mathrm{Im}(\mathrm{Im}\Psi(s,t))\,ds'\,dt'}{(s'-s-i\varepsilon)(t'-t-i\varepsilon)} \quad (5.14)$$

This is not true if the particles in the loop are light, $(2m_{loop})<m$, such as π,k...[69] and [70] because the resultant anomalous thresholds introduce cuts into

the s and t plane which makes the application of Cauchy's theorem much more difficult. That is the double dispersion relations given by Costantini et al [69] are not valid when any of the external masses are greater than the internal loop particle masses. Brehm and Sucher [70] have addressed this problem in the context of pion-deuteron scattering from a dispersive approach, but it is such that one is just as well going to the 't Hooft -Veltman [66] prescription.

In fact the $\rho\pi\pi$ and $\gamma\pi\pi$ couplings , Feynman rules 1 and 2 appendix B, generate a box diagram with pion (or kaon) in the loop for the process $\gamma\gamma\rightarrow\rho\rho$; but given the above difficulties with such diagrams it was decided to leave these until one had a better indication of how the ρ loop diagrams behaved.

The region of integration $\Re$ in the integral 5.14 is determined by the 'spectral function' $\mathrm{ImIm}\Psi(s,t)$, we shall sketch over the calculation of $\mathrm{ImIm}\Psi(s,t)$ here.

Holding t fixed let s increase from zero, at $s=4m^2$ there is sufficient energy for pair production (just as in the bubble diagram case considered in detail in appendix D) so the propagators $(q^2- m^2)^{-1}$ and $(r^2- m^2)^{-1}$ go 'on-shell' and $\mathrm{Im}\Psi(s,t)$ can thus be calculated (see appendix E equations E12/13) using the Cutkosky rule :

$$\mathrm{Im}\ \Psi(s,t) = \int d^4q \frac{\delta(q^2- m^2)\,\delta(r^2- m^2)}{((q-k_3)^2- m^2)((q-k_1)^2- m^2)} \qquad (5.15)$$

Which reduces to a solid angle integration, giving

$$\mathrm{Im}\ \Psi(s,t) = \frac{\pi}{s(s-4m^2)\,\sqrt{\lambda(s,t)}}\, 2Q_0\left(\frac{\alpha_1\alpha_2 - z}{\sqrt{\lambda(s,t)}}\right) \qquad (5.16)$$

where α_1, α_2 and z are defined in appendix A and also

$$\lambda(s,t) = \alpha_1^2 + \alpha_2^2 + z^2 - 1 - 2\alpha_1\alpha_2 z \qquad (5.17)$$

Rewriting α_1, α_2 and z as functions of s and t $\lambda(s,t)$ becomes

$$\lambda(s,t) = \frac{4}{s(s-4m^2)^2}\left((s-4m^2)\, t^2 - 4m^2(s-2m^2)\, t - 4m^6 \right) \qquad (5.18)$$

The single dispersion relation (in s) for $\Psi(s,t)$ is

$$\Psi(s,t) = \frac{1}{\pi}\int_{4m^2}^{\infty} ds' \, \frac{\mathrm{Im}\Psi(s',t)}{s'-s-i\varepsilon} \qquad (5.19)$$

However it has already been noted that the full analytic expression for $\Psi(s,t)$ is a double dispersion relation, this is because the function Im $\Psi(s,t)$ can itself be written as dispersion relation in t. Assume that t>0 and allow t to increase then there is a threshold $t_0(s)$, a function of s and not necessarily equal to $4m^2$, at which point the function Im $\Psi(s,t)$ develops a pole due to the propagators $((q-k_3)^2 - m^2)^{-1}$ and $((q-k_1)^2 - m^2)^{-1}$ going 'on-shell'; this is calculated in appendix E and it is found that:

$$\mathrm{Im}(\mathrm{Im}\,\Psi(s,t)) = \begin{cases} \dfrac{2\pi^2}{s(s-4m^2)\sqrt{\lambda(s,t)}} & t>t_0 \\ 0 & t<t_0 \end{cases} \qquad (5.20)$$

Thus Im $\Psi(s,t)$ can be written as a dispersion relation in t

$$\mathrm{Im}\,\Psi(s,t) = \frac{1}{\pi}\int_{t_0}^{\infty} dt' \, \frac{\mathrm{Im}(\mathrm{Im}\Psi(s,t'))}{t'-t-i\varepsilon} \qquad (5.21)$$

Inserting equation 5.21 into 5.19 gives the double dispersion relation 5.14 with the region of integration $\Re$ defined to be

$$\Re \begin{cases} (s-4m^2)\,t^2 - 4m^2(s-2m^2)\,t - 4m^6 \geq 0 \\ \\ s > 0, t > 0 \end{cases} \qquad (5.22)$$

The first part of 5.22 follows from the requirement that Im(Im $\Psi(s,t)$) is a real function of s and t, the second part is assumed when the Cutkosky rule is applied.

Equation 5.14 is the exact dispersive expression for $\Psi(s,t)$ so in the spirit of estimating the loop corrections to 20-30% accurracy, $\Psi(s,t)$ is approximated by the single dispersion relation in s with a cut-off. Equation 5.19 is modified to

$$\Psi(s,t) \approx \frac{1}{\pi} \int_{4m^2}^{s_c} ds' \, \frac{\text{Im}\,\Psi(s',\,t)}{s'-s-i\varepsilon} \qquad (5.23)$$

Ignoring the dispersion relation in t is a reasonable approximation provided that the cut on the real t-axis is "far enough away" from the physical value of t, that it could only give a small effect. Rewriting equation 5.22 with $x,y := s/m^2, t/m^2$ gives

$$(x-4)\,y^2 - 4\,(x-2)\,y - 4 = 0 \qquad (5.24)$$

This quadratic equation in t can be solved to give $t_0(=m^2 y_0)$, the point at which the t-channel cut begins

$$y_0(x) = \frac{2}{x-4}\left(x - 2 + \sqrt{x\,(x-3)} \right) \qquad (5.25)$$

Taking $\sqrt{s}$=1.6GeV, which is around the $\rho^0\rho^0$ peak, then equation 5.25 gives $t_0(s) \approx 16.5\ \text{GeV}^2$ which is to be compared with physical values of t which lie in the

range $\approx$[-1.05,-0.33]. Also t_0 is well outside the range $|t_0| < (2.5\ \text{GeV}/\ m_\rho)^2 \approx 10$ where one believes the imaginary part of the loop diagrams. It is also interesting to note that the symmetric solution, $t_0 = s_0 \approx 6.9$, to (5.25) is also outside this region. The function (5.25) is plotted in graph (5.1).

Thus the t-channel cut begins well outside the physical region for t in the process $\gamma\gamma \rightarrow \rho\rho$.

(iv) Conclusions

The loop corrections to the process $\gamma\gamma \rightarrow \rho\rho$ are to be estimated in the spirit of chiral perturbation theory. This is to check the possibility of whether or not there is a conspiracy between the helicity amplitudes causing the $\sigma(\gamma\gamma \rightarrow \rho^+\rho^-)$ to be decreased by an order of magnitude and increasing $\sigma(\gamma\gamma \rightarrow \rho^0\rho^0)$ from zero to$\approx$100nb.

The imaginary parts of the loop diagrams are given by applying Cutkosky's rule, the real parts being reconstructed by an approximation to a dispersive integral.The use of a single dispersion relation for the box diagram is an approximation (for both real and imaginary parts), but one which is justified in the kinematical region in which we are interested.

The cut-off parameter s_c enters as the upper limit of the dispersive integral, s_c is taken to lie within a range of values. It might be hoped to vary s_c so that the model gives an optimum fit to the data.

Chapter 6 Loop Calculation II

(i) Introduction

The calculation of the one loop corrections to $\gamma\gamma \rightarrow \rho\rho$ is an extensive task. Although it is made easier by breaking it up into more manageable parts whose results can tell us a lot about the progress of the calculation, rather than doing the whole thing before trying to interpret the results. To this end first parts to be tackled are:

(i) the process $\gamma\gamma \rightarrow \rho^0\rho^0$ which is zero at the tree level, so that there are fewer Feynman diagrams to be considered , for instance there are no "self-energy" corrections to the wavefunctions.

(ii) by considering those diagrams arising from the gauge boson 'self-interactions' and ignoring for the time being the other possible diagrams such as a box diagram with a π or k in the loop or the phenomological diagrams arising from nucleons N (spin 1/2) or N** (spin 3/2), which being fermionic will have a relative '-' sign to the bosonic diagrams.

There are three sorts of loop diagram with intermediate ρ mesons (the paper by Boudjema [71] considering the process $\gamma\gamma \rightarrow \gamma\gamma$ in the Standard Model is a useful reference here), the two-point ("bubble") the three-point ("triangle") and the four-point ("box") diagram.

The simplest is the 'bubble diagram' which has already been mentioned in Chapter 5, in the context of estimating the loop corrections. The 's-channel' bubble diagram is constructed using Feynman rules 5 and 6 from appendix B and is shown in Fig.(6.1) below ('s-channel' meaning that the integral formulae are coefficients of s-only)

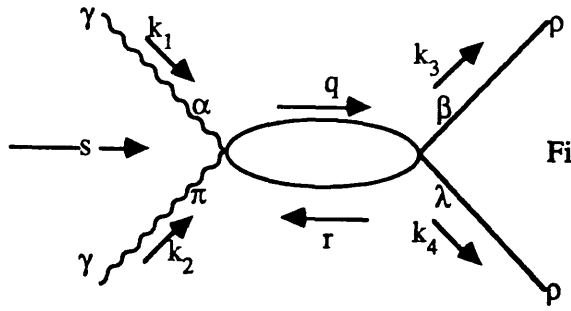

Fig. 6.1

The Feynman amplitude for this diagram is

$$M^{\alpha\pi\beta\lambda} = (-i)\frac{e^2f^2}{16\pi^4}\int d^4q \frac{1}{(q^2 - m^2 + i\varepsilon)(r^2 - m^2 + i\varepsilon)}$$

$$\times i\left(g^{\alpha\mu}g^{\pi\theta} + g^{\alpha\theta}g^{\pi\mu} - 2g^{\alpha\pi}g^{\theta\mu}\right) i\left(-g_{\mu\nu} + \frac{q_\mu q_\nu}{m^2}\right)$$

$$\times i\left(g^{\beta\nu}g^{\lambda\omega} + g^{\beta\omega}g^{\lambda\nu} - 2g^{\beta\lambda}g^{\nu\omega}\right) i\left(-g_{\theta\omega} + \frac{r_\theta r_\omega}{m^2}\right) \qquad (6.1)$$

Where $r \equiv q-k$ and $k^2=s$, also for future convenience define the following coupling costant to be

$$\beta := \frac{e^2}{4\pi}\frac{f^2}{4\pi} \qquad (6.2)$$

Equation (6.1) is integrated using the formulae in appendix D, equations D16,... . There are two other bubble diagrams, the t-channel diagram is obtained from (6.1) by $k_2 \leftrightarrow -k_3$, $\pi \leftrightarrow \beta$, $s \leftrightarrow t$ interchange and the u-channel diagram by $k_2 \leftrightarrow -k_4$, $\pi \leftrightarrow \lambda$, $s \leftrightarrow u$ interchange.

The 'triangle diagram' is constructed from the Feynman rules 3,4 and 5 (appendix B), two of the vertices are momentum dependent whi ch makes the diagram somewhat more complicated than the bubble diagram. The basic diagram,

from which all the others can be obtained, is:

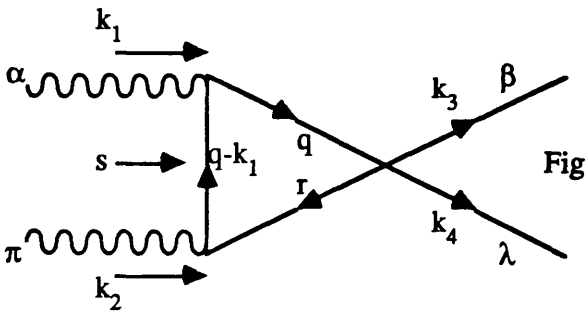

Fig 6.2

For which the Feynman amplitude is :

$$M^{\alpha\pi\beta\lambda} = (-i)\frac{\beta}{\pi^2}\int d^4q \frac{1}{(q^2 - m^2)(r^2 - m^2)((q-k_1) - m^2)}$$

$$\times i\left(g^{\alpha\mu}(q+k_1)^{\tau} + g^{\alpha\tau}(q-2k_1)^{\mu} + g^{\mu\tau}(k_1-2q)^{\alpha}\right) i\left(-g_{\mu\nu} + \frac{q_\mu q_\nu}{m^2}\right)$$

$$\times i\left(g^{\beta\nu}g^{\lambda\rho} + g^{\beta\rho}g^{\lambda\nu} - 2g^{\beta\lambda}g^{\nu\rho}\right) i\left(-g_{\eta\rho} + \frac{r_\eta r_\rho}{m^2}\right)$$

$$\times i\left(g^{\pi\sigma}(r+2k_2)^{\eta} + g^{\pi\eta}(r-k_2)^{\sigma} - g^{\sigma\eta}(k_2+2r)^{\pi}\right) i\left(-g_{\sigma\tau} + \frac{(q-k_1)_\sigma (q-k_1)_\tau}{m^2}\right) \qquad (6.3)$$

Which is integrated using the formulae D.16,...,D.25 (appendix D).

The diagram Figure 6.2 can be be described using the four momentum labels of the external particles as (12 (34)), this is using Boudjema's notation [71], the (34) denotes symmetry under 3↔4 interchange ie (12 (34))≡(12 (43)).

Then all twelve triangle diagrams are given by permutations of (ij (lm)) :

s-channel (12 (34)) , (21 (34)) , (34 (12)) , (43 (12)) (6.4a)

t-channel (13 (24)) , (31 (24)) , (24 (13)) , (42 (13)) (6.4b)

u-channel (14 (23)) , (41 (23)) , (23 (14)) , (32 (14)) (6.4c)

Where "s-channel" means that the integral formulae depend only on s, t-channel formulae depend only on t and so on ; this is the notation used for both bubble and triangle diagrams.

To obtain the diagram (13 (24), for example, from (12 (34)) one changes $k_2 \rightarrow -k_3$ and $s \rightarrow t$ and interchange $\alpha \leftrightarrow \pi$ in the integrated form of equation (6.3).

The 'box diagram' is constructed from Feynman rules 3 and 4, each vertex is momentum dependent and as a result is much more complicated by comparison with the triangle and bubble diagrams.

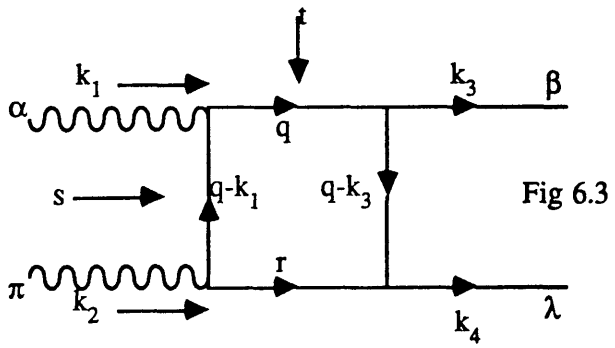

Fig 6.3

The (1234) box diagram, again using Boudjema's notation, is shown above in figure 6.3 and has Feynman amplitude given by equation 6.5 on the next page.

There are six box diagrams in total, but three of these can be obtained from the remaining three by reversing the direction of the arrow in the loop, so the total box diagram contribution to $\gamma\gamma \rightarrow \rho^0\rho^0$ is given by:

$$2((1234) + (2134) + (1432)) \qquad (6.6)$$

$$M^{\alpha\pi\beta\lambda} = (-i)\frac{\beta}{\pi^2}\int d^4q \frac{1}{(q^2-m^2)((q-k_3)^2-m^2)(r^2-m^2)((q-k_1)^2-m^2)}$$

$$\times i\left[g^{\alpha\mu}(q+k_1)^{\tau}+g^{\alpha\tau}(q-2k_1)^{\mu}+g^{\mu\tau}(k_1-2q)^{\alpha}\right] i\left(-g_{\mu\nu}+\frac{q_\mu q_\nu}{m^2}\right)$$

$$\times i\left[g^{\beta\nu}(q+k_3)^{\varphi}+g^{\beta\varphi}(q-2k_3)^{\nu}+g^{\nu\varphi}(k_3-2q)^{\beta}\right]$$

$$\times i\left(-g_{\varphi\psi}+\frac{(q-k_3)_\varphi (q-k_3)_\psi}{m^2}\right)$$

$$\times i\left[g^{\lambda\psi}(r+2k_4)^{\rho}+g^{\lambda\rho}(r-k_4)^{\psi}-g^{\rho\psi}(k_4+2r)^{\lambda}\right] i\left(-g_{\eta\rho}+\frac{r_\eta r_\rho}{m^2}\right)$$

$$\times i\left[g^{\pi\sigma}(r+2k_2)^{\eta}+g^{\pi\eta}(r-k_2)^{\sigma}-g^{\sigma\eta}(k_2+2r)^{\pi}\right]$$

$$\times i\left(-g_{\sigma\tau}+\frac{(q-k_1)_\sigma (q-k_1)_\tau}{m^2}\right) \qquad (6.5)$$

(ii) Calculation

Considering the number and complexity of the Feynman diagrams the following strategy is adopted:

(a) each Feynman amplitude $M^{\alpha\pi\beta\lambda}$ is split into two parts :

$$M^{\alpha\pi\beta\lambda} = M_0^{\alpha\pi\beta\lambda} + M_L^{\alpha\pi\beta\lambda} \qquad (6.7)$$

$M_o^{\alpha\pi\beta\lambda}$ is the amplitude calculated when the momentum dependent terms "$q_\mu q_\nu/m^2$" in the numerator of the ρ meson propagator are ignored , $M_L^{\alpha\pi\beta\lambda}$ is given by the remainder. For example take equation (6.1) and multiply out the numerators from the two propagator terms to give equation (6.8):

$$\left(-g_{\mu\nu}+\frac{q_\mu q_\nu}{m^2}\right)\left(-g_{\theta\omega}+\frac{r_\theta r_\omega}{m^2}\right) = g_{\mu\nu}g_{\theta\omega} \qquad (6.8a)$$

$$\frac{g_{\mu\nu}r_\theta r_\omega}{m^2} - \frac{g_{\theta\omega}q_\mu q_\nu}{m^2} + \frac{q_\mu q_\nu r_\theta r_\omega}{m^2} \qquad (6.8b)$$

Where (6.8a) gives $M_o{}^{\alpha\pi\beta\lambda}$ and $M_L{}^{\alpha\pi\beta\lambda}$ is given by (6.8b).

(b) The calculation is also greatly simplified by, initially, considering only the imaginary part of the Feynman amplitude for $\gamma\gamma\rightarrow\rho^0\rho^0$. Only the s-channel diagrams contribute to the imaginary part, this further reduces the number of diagrams.

The momentum dependent terms "$q_\mu q_\nu/m^2$" in the ρ propagator are due to the longitudinal polarizations of the ρ meson and it is these terms that go towards making the HLS model non-renormalisable [72], but recall from chapter two that we are forced to work with the HLS model entirely in the unitary gauge.

If this were $\gamma\gamma\rightarrow Z^0Z^0$ in the Standard Model in the unitary gauge then there would be diagrams invlving Higgs boson exchange which would "counteract" the bad high energy behaviour of $M_L{}^{\alpha\pi\beta\lambda}$.Although if this were a renormalisable gauge theory then it would be most sensible to calculate the loop diagarams in a renormalisable gauge, such as the Feynman- 't Hooft gauge $\xi=1$, in which case there would be explicit would-be-Goldstone bosons and ghosts. These unphysical particles are not present in the HLS model as they are all supposedly buried within the underlying fundamental theory.

The imaginary parts of the $\gamma\gamma\rightarrow\rho^0\rho^0$ amplitudes can then be compared with the tree-level amplitudes for $\gamma\gamma\rightarrow\rho^+\rho^-$ calculated in chapter 4.

The s-channel diagrams contributing to the imaginary part of the amplitude are (6.1),(6.4a) and two box diagrams (6.5) (1234) and (2134). The calculation of the bubble diagram and the triangle diagrams is relativley straight forward, on the other

hand the calculation of the box diagrams was incredibly involved and long winded. Only the final result for the imaginary part of $M^{\alpha\pi\beta\lambda}$ is given , with some restrictions, as there simply is no room to present the (rather non-intuitive) calculation in its entirety.

Firstly there is the usual subsidiary co ndition equation (4.3), as discussed in chapter 4, setting

$$k_1^\alpha = k_2^\pi = k_3^\beta = k_4^\lambda = 0 \qquad (4.3)$$

certainly simplifies the loop diagram calculation. Using the polarization vectors to project out the different helicity amplitudes it is convenient to set

$$k_1^\pi = k_2^\alpha = 0 \text{ , because } k_{2\alpha}\varepsilon^\alpha_{1\pm} = 0 = k_{1\pi}\varepsilon^\pi_{2\pm}$$

the same is true of the outgoing ρ mesons provided that their longitudinal polarizations are ignored, which is what we will do.

(iii) Results

Using the integration formulae for the bubble and triangle diagrams (appendix D) and those for the box diagram (appendix E) one obtains the following formula for the Feynman amplitude after very many hours of work!

$$
\begin{aligned}
M_0^{\alpha\pi\beta\lambda} = 2\beta \{\ & g^{\alpha\pi}g^{\beta\lambda}\,\bar{C}_1^0 + g^{\alpha\beta}g^{\pi\lambda}\,C_2^0 + g^{\alpha\lambda}g^{\pi\beta}\,C_2^0 \\
& + g^{\alpha\pi}\,k_1^\beta\,k_1^\lambda\,B_1^0 + g^{\beta\lambda}\,k_3^\alpha\,k_3^\pi\,B_2^0 \\
& + \left(g^{\alpha\beta}k_1^\lambda k_3^\pi - g^{\pi\beta}k_1^\lambda k_3^\alpha - g^{\alpha\lambda}k_1^\beta k_3^\pi + g^{\pi\lambda}k_1^b k_3^\alpha\right) B_3^0 \\
& + \left(g^{\alpha\beta}k_1^\lambda k_3^\pi - g^{\pi\lambda}k_1^\lambda k_3^\alpha - 4g^{\alpha\lambda}k_1^\beta k_3^\pi + 4g^{\pi\lambda}k_1^\beta k_3^\alpha\right) 4m^2 W_{13}(s) \\
& + \left(k_1^\beta k_1^\lambda + k_2^\beta k_2^\lambda\right) k_3^\alpha\,k_3^\pi\,B_4^0 \qquad \} \qquad (6.9)
\end{aligned}
$$

All the functions C_i and B_i are functions of s :

$$\bar{C}_1^0 = C_1^0 + \frac{128}{3}\,k^2k'\Psi(s)\,P_2(z)$$

$$
\begin{aligned}
C_1^0 = {} & 136\,Z(s) + 4(30m^2 - 32s)\,W(s) + 16\,I_1(s) + 64k^2k'^2\left(\tfrac{1}{3}+\alpha_1^2\right)\Psi(s) \\
& + (-32b_1 + 2s(9J-a_1) - 4m^2J)(s,k_1) \\
& + (-32b_1 + 2(s-4m^2)(9J-a_1) + 44m^2J)(s,k_3)
\end{aligned}
$$

$$C_2^0 + C_3^0 = 272\,Z(s) + 8(16s-5m^2)W(s) + 4(2s-m^2)(3s-2m^2)\,\Psi(s)$$

$$C_2^0 - C_3^0 = -\frac{128s}{\alpha_1}\,W(s)\,P_1(z)$$

$$
\begin{aligned}
B_1^0 = {} & 136\,Z_{11}(s) + 4(25m^2 - 16s)W_{11}(s) + 64s\,V_1(s) \\
& + 16(3m^2 - 2s)\Psi(s) + 4(8a_1 - 3b_2 + 2J)(s,k_1)
\end{aligned}
$$

$$
\begin{aligned}
B_2^0 = {} & 136\,Z_{33}(s) + 4(25m^2 - 16s)W_{33}(s) + 16(4s-m^2)V_3(s) \\
& + 16(m^2-2s)\Psi(s) - 4(2a_1 - b_2 - 4J)(s,k_3)
\end{aligned}
$$

$$B_3^0 = -128W(s) - 16(3m^2 - 2s)V_3(s) - 16(m^2 - 2s)V_1(s)$$

$$B_4^0 = 68\,Z_{1133}(s) \qquad (6.10)$$

The functions Z(s),W(s),... are given in appendix E equation (E.23) and one piece of shorthand notation used above is $(2a_1\text{-}4J)(s,k_1)\equiv 2a_1(s,k_1) - 4J(s,k_1)$.

Similarly the expression for the "longitudinal component' of the amplitude is

$$M_L^{\alpha\pi\beta\lambda} = 2\beta \{ g^{\alpha\pi}g^{\beta\lambda}\bar{C}_1^L + g^{\alpha\beta}g^{\pi\lambda}C_2^L + g^{\alpha\lambda}g^{\pi\beta}C_2^L + g^{\alpha\pi}k_1^\beta k_1^\lambda B_1^L + g^{\beta\lambda}k_3^\alpha k_3^\pi B_2^L + (g^{\alpha\beta}k_1^\lambda k_3^\pi - g^{\pi\beta}k_1^\lambda k_3^\alpha - g^{\alpha\lambda}k_1^\beta k_3^\pi + g^{\pi\lambda}k_1^b k_3^\alpha) B_3^L + (k_1^\beta k_1^\lambda + k_2^\beta k_2^\lambda) k_3^\alpha k_3^\pi B_4^L \} \qquad (6.11)$$

$$\bar{C}_1^L = \frac{(6s\text{-}16m^2)}{m^4} e_1(s) + \frac{4s^2}{m^4} e_2(s) + \frac{(s^2 - 6m^2s - 8m^4)}{m^4} I_1(s) + \left(4\frac{(m^2 - 2s)}{m^2} b_1 + 8sc_1 - 2s(a_1 + 2a_2) + 2(s+14m^2)J\right)(s,k_1) + \left(\frac{2s}{m^2} b_1 + 2(s-4m^2)c_1 + 8m^2 J\right)(s,k_3) + 8Z(s) - 48m^2 W(s)$$

$$C_2^L = C_3^L = 8Z(s) + 2m^2(2s-3m^2)\Psi(s) - 4m^2 J(s,k_1) - 4m^2 J(s,k_3)$$

$$B_1^L = 8Z_{11}(s) - 20m^2 W_{11}(s)$$

$$B_2^L = 8Z_{33}(s) - 2m^2 W_{33}(s) + 8m^2 V_3(s) - 8m^2\Psi(s)$$

$$B_3^L = 16m^2 V_1(s) - 2m^2 W_{13}(s) \ , \ B_4^L = 4\, Z_{1133}(s) \qquad (6.12)$$

Using the polarization vectors (C.13)

and the notation of appendix C, the partial wave helicity amplitudes are easily obtained :

$$T_0^{++++} = \frac{2\beta}{3}\left(3C_1 + C_2 + C_3 - \frac{64s}{\alpha_1} W(s) - k^2 B_1 - k'^2 B_2 + 2kk' B_3 + \frac{4}{5} k^2 k'^2 B_4 + 20kk' m^2 W_{13}(s) \right) \qquad (6.13a)$$

$$T_0^{+\,+\,-\,-} = \frac{2\beta}{3}\Big(3C_1 + C_2 + C_3 + \frac{64s}{\alpha_1} W(s) - k^2 B_1 - k'^2 B_2 - 2kk' B_3 + \frac{4}{5} k^2 k'^2 B_4 - 20kk' m^2 W_{13}(s) \Big) \qquad (6.13b)$$

$$T_2^{+\,+\,+\,-} = -\frac{\beta}{5}\sqrt{\frac{2}{3}}\Big(C_2 + C_3 + 2k^2 B_1 + \frac{12}{7} k^2 k'^2 B_4 + 24kk' m^2 W_{13}(s)\Big) \qquad (6.13c)$$

With the condition on equations a,b,c above that the $W_{13}(s)$ term is only present for the non-longitudinal amplitudes $M_0^{\alpha\alpha\beta\lambda}$.

$$T_2^{+\,-\,+\,+} = -\frac{\beta}{5}\sqrt{\frac{2}{3}}\Big(C_2 + C_3 + 2k'^2 B_2 + \frac{12}{7} k^2 k'^2 B_4\Big) \qquad (6.13d)$$

$$T_2^{+\,-\,+\,-} = T_2^{+\,-\,-\,+} = \frac{2\beta}{5}\Big(C_2 + C_3 + \frac{8}{21} k^2 k'^2 B_4\Big) \qquad (6.13e)$$

These helicity amplitudes are easily evaluated numerically using the functions $J(s,k_1), a_i(s,k_1)$,...given in appendix D and the $\Psi(s), W(s)$,... given in appendix E. They are compared with the corresponding tree-level helicity amplitudes for $\gamma\gamma \to \rho^+\rho^-$, around the experimental $\gamma\gamma \to \rho^0\rho^0$ peak at $\sqrt{s} \approx 1.6$GeV.

$\sqrt{s}$=1.6 GeV	TREE $\gamma\gamma \to \rho^+\rho^-$	LOOP ('0') $\gamma\gamma \to \rho^0\rho^0$	LOOP ('0+L') $\gamma\gamma \to \rho^0\rho^0$
$T_0^{+\,+\,+\,+}$	0.31	0.56 i	0.30 i
$T_0^{+\,+\,-\,-}$	0.10	0.52 i	0.26 i
$T_2^{+\,+\,+\,-}$	0	-0.07 i	-0.09 i
$T_2^{+\,-\,+\,-}$	-0.06	-0.17 i	-0.19 i
$T_2^{+\,-\,+\,-}$	0.15	0.44 i	0.51 i
$\sigma(\gamma\gamma \to \rho\rho)$ nb	≈150	≈1200	≈1350

TABLE 6.1

The imaginary part of the loop helicity amplitudes for $\gamma\gamma\rightarrow\rho^0\rho^0$, calculated from $M_o^{\alpha\pi\beta\lambda}$, are between 2 and 5 times larger than the corresponding tree-level amplitudes. Including the longitudinal part of the propagating ρ in the loop decreases the J=0 amplitudes but the J=2 amplitudes are made larger. A large contribution is found to come from the $\Psi(s)$ terms the 'simplest' box diagram integration.It is interes ting to note that $\gamma\gamma\rightarrow\gamma\gamma$ [69] and gluon fusion processes involving the box diagram [73] all find a significant contribution from the box diagram near the threshold for the internal particles.

The final row of table 6.1 is the cross-section arising from the transverse (only) helicity amplitudes shown in the table. Clearly the cross-section corresponding to the imaginary part of the one loop $\gamma\gamma\rightarrow\rho^0\rho^0$ amplitudes in the HLS model is completely "wild" by comparison with the experimental data! Including the real-parts of the loop amplitudes will simply make the 'loop' cross-section larger still, as will including the helicity amplitudes corresponding to the production of longitudinally polarized ρ's.

(iv) Conclusions

The loop amplitudes are much larger than the order of magnitude estimate, and the fact that the loop amplitudes are generally larger than the tree-level amplitudes indicates a breakdown of perturbation theory in the HLS model of vector mesons. This breakdown would appear to be independent of any cut-off (Λ) since the imaginary part of the amplitude does not depend on Λ.

An independent check on the loop calculation is required because either the calculation is correct and the loop expansion breaks down making perturbation theory invalid for the HLS model or a mistake has been made in the loop calculation. Thus an independent check will tell us whether to abandon the loop calculation or to go back over it looking for a mistake.

As a result of the above conclusion the HLS model is used to calculate $\rho^+\rho^-$

scattering amplitudes at the tree-level, which are of order f^2.These scattering amplitudes are tested to see if they violate unitarity since the $\rho\rho$ scattering amplitude, rather than the weak $\gamma\gamma\rightarrow\rho\rho$ amplitude, is expected to be responsible for the big loop corrections found above.

Obviously at very high energies ($s\rightarrow\infty$) unitarity will be violated because there is no Higgs exchange (cf the Standard Model and WW scattering); but the question is whether or not the coupling f (of the ρ meson as gauge boson) is so strong that unitarity is even violated close $\rho\rho$ threshold.

Chapter 7 Testing ρρ Unitarity

(i) Introduction

In the conclusions to the preceeding chapter it was argued that testing the unitarity of $\rho^+\rho^-$ scattering amplitudes in the HLS model would be an independent test of the loop calculation of chapter 6.

In this first section we use the unitarity of the S-matrix to obtain a relation between the imaginary part of a scattering amplitude and the "square" of the that amplitude. This will then be used to derive tests for the unitarity of spinless particle scattering (section ii) and spinning particles (section iii) , these will then be applied to the $\rho^+\rho^-$ scattering amplitudes in section iv.

The S-matrix element for the process $|i\rangle_{initial} \rightarrow |f\rangle_{final}$ state is

$$S_{fi} = \delta_{fi} + i\,(2\pi)^4\,\delta^4(P_f - P_i)\,M_{fi} \qquad (7.1)$$

Where $P_{i,f}$ are the initial and final state four-momenta respectively and M_{fi} is the Feynman amplitude calculated from the Feynman rules in appendix B (and with the polarization vectors applied.

The S-matrix must conserve probability for quantum mechanical consistency, that is it must be unitary :

$$SS^\dagger = S^\dagger S = 1 \qquad (7.2)$$

applying the unitary relation (7.2) to the expression for S_{fi} in (7.1) gives the following relation:

$$-i\,(M_{fi} - M_{fi}^{*}) = \sum_{n} \int d\rho_n\, M_{nf}^{*}\, M_{ni} \qquad (7.3)$$

n = number of intermediate states

$d\rho_n$ = n-body phase space

$$(7.3) \Rightarrow 2\,\mathrm{Im}\, M_{fi} = \sum_{n} \int d\rho_n\, M_{nf}^{*}\, M_{ni} \qquad (7.4)$$

(ii) Two Body Unitarity Test - Spinless Particles

The simplest two body unitarity relation is that for the scattering of two spinless particles. Equation (7.4) is used here to derive a bound on the partial wave amplitudes of M_{fi}.

Diagramatically the two body unitarity for states of equal mass (m) is

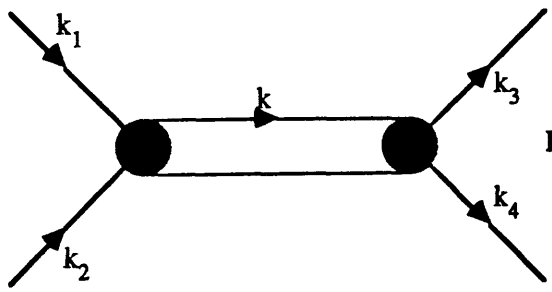

Fig 7.1

In the centre of mass frame k=(2E,k) and

$$k_1 + k_2 = k_3 + k_4 \qquad (7.6)$$

$$k_1 = (E,k_i) \quad , \quad k_3 = (E,k_f) \qquad (7.7)$$

The 'external' scattering angle θ is defined by

$$z = \cos\theta = \frac{\mathbf{k}_i.\mathbf{k}_f}{k_i\, k_f}\ ,\ k_i = |\mathbf{k}_i| \text{ and } k_f = |\mathbf{k}_f| \qquad (7.8a)$$

and the 'internal' scattering angles by

$$z' = \cos\theta' = \frac{\mathbf{k}.\mathbf{k}_i}{k\, k_i}\ ,\ z'' = \cos\theta'' = \frac{\mathbf{k}.\mathbf{k}_f}{k\, k_f} \qquad (7.8b,c)$$

k_i and k_f defined above and $k = |\mathbf{k}|$

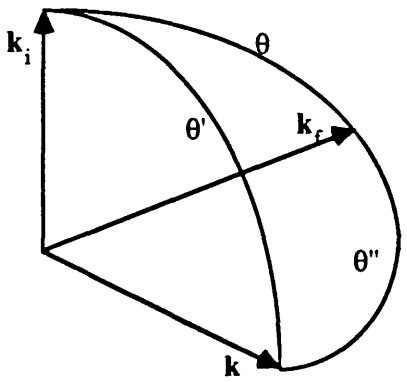

Fig 7.2

The cosine z'' can be related to z,z' and the azimuthal angle φ by

$$z'' = z\, z' + (1-z^2)^{\frac{1}{2}} (1-z'^2)^{\frac{1}{2}} \cos\varphi \qquad (7.9)$$

and two body phase space is

$$d\rho_2 = \frac{1}{16\pi^2} \sqrt{\frac{s - 4m^2}{4s}}\, d\Omega \qquad (7.10)$$

solid angle $d\Omega = \sin\theta\, d\theta\, d\varphi$

The unitarity relation (7.4) for n=2 is:

$$2\,\mathrm{Im}\,M_{fi}(s,z) = \int d\rho_2\, M^{*}_{2f}(s,z'')\; M_{2i}(s,z') \qquad (7.11)$$

Since all the particles are spinless the partial wave expansion of M (dropping the i,f subscripts) is given by:

$$M(s,\theta) = \sum_{J}(2J+1)\, T_J(s)\, P_J(z) \qquad (7.12)$$

Where $P_J(z)$ are the Legendre polynomials defined in appendix A.

Using the expansion (7.12) in equation (7.11) and the orthogonality of the Legendre polynomials to project out each partial wave amplitude gives

$$\mathrm{Im}\,T_J = \lambda \int d\Omega \int_{-1}^{1} dz\, P_J(z) \sum_{l',l''} (2l'+1)T_{l'}\, P_{l'}(z')\; (2l''+1)T^{*}_{l''}P_{l''}(z'') \qquad (7.13)$$

where the argument (s) of the T_J has been dropped and λ is defined to be

$$\lambda = \frac{1}{64\pi^2}\sqrt{\frac{s-4m^2}{4s}} \qquad (7.14)$$

Using the standard identity (A.3) for $P_{l''}(z'')$ the integrations in (7.13) are easily performed, with the result $\mathrm{Im}T_J = 8\pi\lambda\,|T_J|^2$ (7.15), this then implies that

$$8\pi\lambda\,|T_J|^2 \le |T_J|$$

and finally yields the unitarity bound on the T_J

$$|T_J| \le 16\pi\sqrt{\frac{s}{s-4m^2}} \qquad (7.16)$$

Thus for the S-matrix to be unitary each partial wave amplitude must satisfy the bound (7.16).

(iii) Two-Body Unitarity Test - Spinning Particles

To test the unitarity of the $\rho^+ \rho^-$ scattering amplitudes (from the HLS model) is a little more complicated than that for spinless particles. This is because the sum on the RHS of equation (7.4) also has to run over all possible intermediate polarizations.

So given a $\rho^+\rho^-$ scattering amplitude M^{abcd}, calculated at the tree level in section (iv), the unitarity test becomes a comparison between

$$2\,|M^{abcd}| \quad \text{and} \quad \sum_{i,j} \int d\rho_2\, M^{abij}\, M^{*ijcd} \tag{7.17}$$

where the sum i,j is over all possible intermediate polarizations.

To compare partial wave amplitudes, using the notation of appendix C, the comparison is between $|T_J{}^{abcd}|$ and $(\Sigma MM^*)_J$, where $(\Sigma MM^*)_J$ is shorthand for

$$(\Sigma MM^*)_J = \frac{1}{4} \int_{-1}^{1} dz\, d^J_{\lambda\lambda'}(z) \sum_{i,j} \int d\rho_2\, M^{abij}(s,z')\, M^{*ijcd}(s,z'') \tag{7.18}$$

Where the $d^J_{\lambda\lambda'}(z)$ function is used to project out the J^{th} partial wave corresponding to $|T_J{}^{abcd}|$.

So unitarity is violated if $|T_J{}^{abcd}| < (\Sigma MM^*)_J$.

(iv) Testing ρρ Scattering Amplitudes

The Feynman rules 4 and 8 (appendix B) are used to calculate the $\rho^+\rho^-$ scattering amplitudes, which are of the order f^2 at the tree level. This ignores those tree diagrams involving photon exchange since they are of the order e^2 and are only tiny O(1%) corrections to the strong ρρ amplitudes.

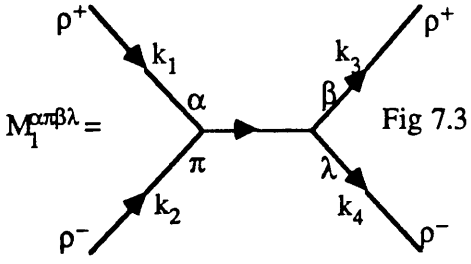

Fig 7.3

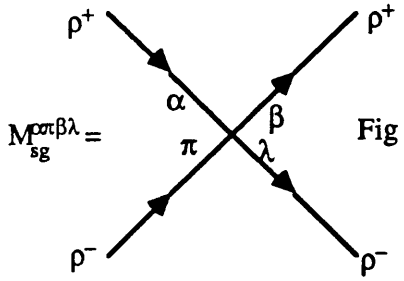

Fig 7.6

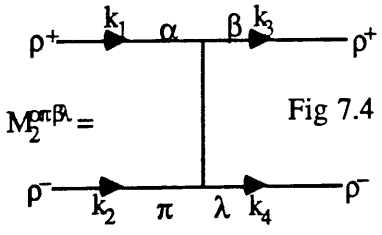

Fig 7.4

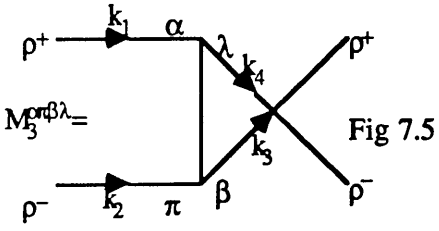

Fig 7.5

$$M_1^{\alpha\pi\beta\lambda} = \frac{f^2}{s - m^2}\{\, g^{\alpha\pi}g^{\beta\lambda}(u - t) + 2g^{\alpha\pi}((k_1 - k_2)^{\lambda}k_4^{\beta} - (k_1 - k_2)^{\beta}k_3^{\lambda}) + 2g^{\beta\lambda}((k_3 - k_4)^{\pi}k_2^{\alpha} - (k_3 - k_4)^{\alpha}k_1^{\pi}) + 4g^{\alpha\beta}k_1^{\pi}k_3^{\lambda} + 4g^{\pi\beta}k_2^{\alpha}k_3^{\lambda} - 4g^{\alpha\lambda}k_1^{\pi}k_4^{\beta} - 4g^{\pi\lambda}k_2^{\alpha}k_4^{\beta}\,\} \quad (7.19a)$$

$$M_2^{\alpha\pi\beta\lambda} = (\, M_1^{\alpha\pi\beta\lambda} \text{ with } s \leftrightarrow t,\ \alpha \leftrightarrow \pi \text{ and } k_2 \leftrightarrow -k_3 \text{ interchanged}) \quad (7.19b)$$

$$M_3^{\alpha\pi\beta\lambda} = (M_2^{\alpha\pi\beta\lambda} \text{ with } t\leftrightarrow u\ ,\ \beta\leftrightarrow\lambda \text{and } k_3\leftrightarrow\ k_4 \text{ interchanged}) \tag{7.19c}$$

$$M_{sg}^{\alpha\pi\beta\lambda} = f^2\{\, 2\, g^{\alpha\lambda}g^{\pi\beta} - g^{\alpha\pi}g^{\beta\lambda} - g^{\alpha\beta}g^{\pi\lambda}\,\} \tag{7.20}$$

The polarization vectors (appendix C, equation C.13) are used to project out the various helicity amplitudes. To a very good approximation each helicity amplitude M^{abcd} (these are given in appendix C) is given by the first non-zero wave in the partial wave expansion. This makes calculating $(\Sigma MM^*)_J$ a great deal easier.

The following calculations have not included intermediate ρ^0's in the sum $(\Sigma MM^*)_J$, they will simply act to increase $(\Sigma MM^*)_J$ by ≈50%.

The test for the M^{++++} amplitude is to compare $|T_J^{++++}|$ with

$$\frac{1}{4}\int_{-1}^{1} dz\, d^J_{00}(z) \sum_{i,j}\int d\rho_2\, M^{++\,ij}(s,z')\, M^{*ij\,++}(s,z'') \tag{7.21}$$

The helicity amplitudes used are:

$$\begin{aligned}
M^{++++} &= T_0^{++++} P_0(z) \\
M^{++--} &= T_0^{++--} P_0(z) \\
M^{++00} &= T_0^{++00} P_0(z) \\
M^{+++0} &= 3\, T_1^{+++0}\, d^1_{01}(z) = -M^{++0+} \\
M^{++-0} &= 3\, T_1^{++-0}\, d^1_{0\,-1}(z) = -M^{++0-} \\
M^{+++-} &= 5\, T_2^{+++-}\, d^2_{02}(z) = M^{++-+}
\end{aligned} \tag{7.22}$$

Dropping the explicit s dependence of the T_J for convenience.

So to test the J=0 amplitude $|T_0^{++++}|$ put the amplitudes (7.22) into equation (7.21) and do the integrations, which can be performed analytically and yields:

$$\frac{1}{32\pi^2}\sqrt{\frac{s-4m^2}{4s}}\left\{4\pi\,|T_0^{+\,+\,+\,+}|^2+4\pi\,|T_0^{+\,+\,-\,-}|^2+4\pi\,|T_0^{+\,+\,0\,0}|^2\right.$$
$$+18\frac{\pi^3}{8}\,|T_1^{+\,+\,+\,0}|^2+18\frac{\pi^3}{8}\,|T_1^{+\,+\,-\,0}|^2$$
$$\left.+50\,\frac{2\pi}{3}\,|T_2^{+\,+\,+\,-}|^2\right\} \qquad (7.23)$$

This also uses the fact that $M^{abcd} = M^{cdab}$.

Although there is no proof it is generally taken that the partial wave projections of tree-graphs in renormalisable field theories should go 'like-logarithms' [74]. For this reason it might be suspected that the seagull term (7.20) is responsible for making the ρρ scattering non-unitary, although the indications from chapter 6 are that it is more likely to be the Born terms.

So to probe the structure of the scattering amplitudes we consider :

(a) BORN + SEAGULL terms contributing to the amplitude

(b) BORN ONLY terms contributing to the amplitude

Evaluating the amplitudes just above the ρρ threshold at $s=5m^2$ and with $f^2=34.3$

T_0^{++++}	=	(a) 147.0	(b) 170.4	
T_0^{++--}	=	(a) 46.8	(b) 69.7	
T_0^{++00}	=	(a) 93.8	(b) 131.0	
T_1^{+++0}	=	(a) -25.6i	(b) -6.4i	
T_1^{++-0}	=	(a) -12.8i	(b) 6.4i	
T_2^{+++-}	=	(a) -16.2	(b) -13.4	(7.24)

So taking the values (a) above and putting into equation (7.23) and writing them out in the same order

$$(\Sigma MM^*)_0 = (193.8 + 19.5 + 78.3 + 40.5 + 19.5) \qquad (7.25)$$

Which is to be compared with $T_0^{+\,+\,+\,+}=147.0$. Clearly the $T_0^{+\,+\,+\,+}$ amplitude violates unitarity on its own (ie without the sum over intermediate polarizations), this violation simply becomes worse when the rest of the terms are included.

Case (b), the corresponding result is compare $T_0^{+\,+\,+\,+}=170.4$ with

$$(\Sigma MM^*)_0 = (258.6 + 43.2 + 152.7 + 4.0 + 13.3) \qquad (7.26)$$

Clearly unitarity is again violated, in fact the violation in this case seems to be worse than (a) which included the seagull term. This is illustrated by graph (7.1) which compares $|T_0^{+\,+\,+\,+}|$ to $|(\Sigma MM^*)_0|$ for cases (a) and (b). Unitarity is clearly violated very close to the $\rho\rho$ threshold. Graph (7.2) illustrates the relative contributions of the different terms in equation (7.23) which combine to give $(\Sigma MM^*)_0$.

As a second example consider an amplitude M^{abcd} in which $a,b \neq c,d$ ie 'non-diagonal' helicity amplitudes such as $M^{+\,-\,+\,+}$. Because in this case there are some relative minus signs between the terms in $(\Sigma MM^*)_J$ due to intermediate longitudinally polarized ρ mesons.

The test in this case is to compare $|T_2^{+-++}|$ with $(\Sigma MM^*)_2$, which is given by

$$(\Sigma MM^*)_2 = \frac{1}{8}\sqrt{\frac{2}{3}}\,\frac{1}{16\pi^2}\sqrt{\frac{s-4m^2}{4s}}\,\Big\{\, 10\sqrt{\frac{2}{3}}\pi\, T_2^{+-++} T_0^{*+++} + 10\sqrt{\frac{2}{3}}\pi\, T_2^{+--+} T_0^{*-++} + 10\sqrt{\frac{2}{3}} T_2^{+-00} T_0^{*00++} + 15\frac{9\pi^3}{32\sqrt{2}}\big(T_2^{+-+0} T_1^{*+0++} + T_2^{+-0-} T_0^{*0-++} - T_2^{+-0+} T_1^{*0+++} - T_2^{+--0} T_1^{*-0++} \big) + 25\frac{34}{25}\sqrt{\frac{2}{3}}\pi\big(T_2^{+-+-} T_2^{*+-++} + T_2^{+--+} T_2^{*-+++} \big) \,\Big\}$$

(7.27)

Making use of the following relations between the T^{abcd} amplitudes :

$$\begin{aligned}
T_1^{+++0} &= -T_1^{+0++} = -T_1^{0+++} \\
T_1^{++-0} &= -T_1^{0-++} = -T_1^{-0++} \\
T_2^{+++-} &= T_2^{+-++} = T_2^{-+++} \\
T_2^{+-+0} &= -T_2^{+-0-}, \quad T_2^{+--0} = -T_2^{+-0+} \\
T_2^{+-+-} &= T_2^{+--+}
\end{aligned} \qquad (7.28)$$

T_2^{+-+0}	=	(a) -32.2i	(b) -26.8i	
T_2^{+--0}	=	(a) -43.0i	(b) -48.4i	
T_2^{+-00}	=	(a) 33.8	(b) 26.8	
T_2^{+-+-}	=	(a) 59.7	(b) 52.8	(7.29)

Thus taking the BORN+SEAGULL part (a) first of all we see that the comparison is between

$|T_2^{+-++}| = |-16.2|$ and

$|(\Sigma MM^*)_2| = |-8.8 - 2.8 + 11.75 - 12.8 - 24.4|$ (7.30)

Again the numbers for $|(\Sigma MM^*)_2|$ are written out so as to correspond to the different contributions in equation (7.27). The +10.3 contribution coming from the term where both intermediate ρ's are longitudinally polarized does decrease the sum, but not enough to stop the amplitude T_2^{+-++} from violating unitarity. Similarly if one considers case (b) without the SEAGULL contribution one finds

$$|(\Sigma MM^*)_2| = |-8.5 - 3.5 + 13.0 - 12.8 - 17.8| \qquad (7.31)$$

and again unitarity is violated.

The amplitude T_2^{+-+-}, for instance, satisfies the simple unitarity bound equation (7.16) around ρρ threshold

$$|T_2^{+-+-}| \leq 16\pi \sqrt{\frac{s}{s - 4m^2}}$$

and only violates unitarity when the summation over all possible intermediate helicity states is taken.

There are two factors contributing to the unitarity violation of the ρρ scattering amplitudes

- the large coupling constant f
-the complex spin structure of the interaction.

So to examine the structure of this violation further consider the ππ scattering amplitude due to only ρ exchange, given by Feynman rule 2 (appendix B). There are three Born graphs as in ρρ scattering , but no seagull graph; it has already been shown that the seagull graph does not make a significant contribution to the violation of unitarity around the ρρ threshold.

The coupling for the ππ scattering amplitude is $(f_{\rho\pi\pi})^2$ which is exactly the same as the ρρ case because of the universality ($f_{\rho\pi\pi} = f_{\rho NN} = f = ...$) of the ρ coupling constant (f) in the HLS model.

Basically the difference between the $\pi\pi$ and the $\rho\rho$ cases is the spin structure, because the π is spin zero the $\pi\pi$ scattering amplitude unitarity can be tested without the complex spin structure clouding the issue.

The amplitude corresponding to figure 7.7 is

$$M = f^2\left\{ \frac{u-t}{s-m^2} + \frac{u-s}{t-m^2} + \frac{t-s}{u-m^2} \right\} \qquad (7.32)$$

Where m is the ρ mass and the π mass is denoted m_π, the Mandelstam variables for the process are given in appendix A.

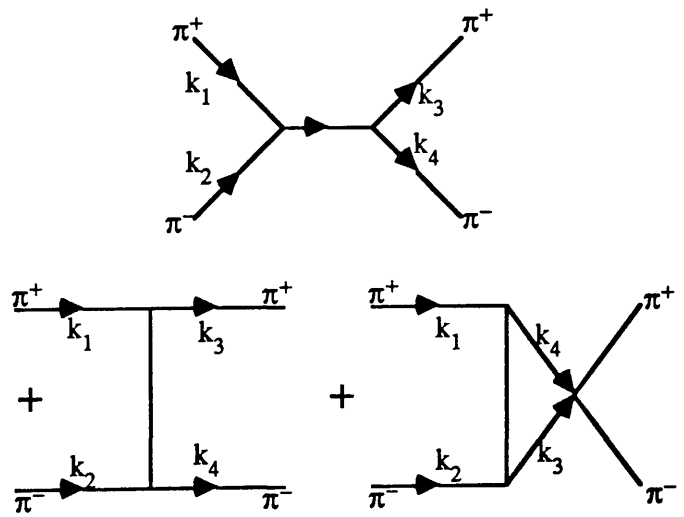

Figure 7.7

The amplitude M has the following partial wave expansion

$$M = \sum_J (2J+1)\, T_J\, P_J(z) \qquad (7.33)$$

$$T_0 = 2f^2\left((\gamma_1+\gamma_2)\, Q_0(\gamma_1) - 1 \right)$$

$$T_1 = -\frac{f^2}{3}\left(\frac{s-4m_\pi^2}{s-m^2}\right)$$

$$T_J = f^2 (\gamma_1+\gamma_2)\left(1+(-1)^J\right) Q_J(\gamma_1)\ ,\ J>1 \qquad (7.34)$$

The functions γ_i i=1,2 are defined in appendix A, and have the following form:

$$\gamma_1 = 1 + \frac{2m^2}{s - 4m_\pi^2} \quad , \quad \gamma_2 = 1 + \frac{2s}{s - 4m_\pi^2} \qquad (7.35)$$

The unitarity test for the $\pi^+ \pi^-$ scattering amplitudes T_J is equation (7.16), thus for the s-wave amplitude T_0 to be unitary it must satisfy

$$|T_0| \leq 16\pi \sqrt{\frac{s}{s - 4m_\pi^2}} \qquad (7.36)$$

Just above $\pi\pi$ threshold at $s = 5m_\pi^2$, analogous to $s = 5m^2$ at $\rho\rho$ peak, one finds that

$$T_0 = 12.3 \quad \text{and} \quad 16\pi \sqrt{\frac{s}{s - 4m_\pi^2}} = 112.4$$

Thus equation (7.36) is satisfied and T_0 is unitary just above $\pi\pi$ threshold; this is just as well because the pertubative calculation of $\Gamma(\rho \rightarrow \pi\pi)$ using Feynman rule 2, and coupling = $f_{\rho\pi\pi}$, is within 10% of the experimental data. This is illustrated in graph (7.3) for the s- and p-wave amplitudes T_0 and T_1.

However at the much higher energy of $s=5m^2$, the scale at which the $\rho\rho$ amplitudes were tested but would correspond to $\approx 150m^2$ in units of external mass if taken over to $\rho\rho$, ie well outside the expected domain of validity. One finds that

$$T_0 = 202.6 \quad \text{and} \quad 16\pi \sqrt{\frac{s}{s - 4m_\pi^2}} = 50.9$$

Obviously in this case (7.36) is <u>not satisfied</u>, T_0 violates unitarity.

(v) Conclusions

It has been shown that the $\rho^+\rho^-$ scattering amplitudes violate unitarity and that this is principally due to the strong gauge coupling (f) of the ρ meson in the HLS model.

This shows that the one loop calculation of $\gamma\gamma\rightarrow\rho^0\rho^0$ in chapter 6 is correct, in that the imaginary part of the loop amplitudes are larger than the corresponding $\gamma\gamma\rightarrow\rho^+\rho^-$ tree-level amplitudes, just as one would be expect given the results of this chapter.

The overall conclusion of this chapter is that the chiral loop expansion in the HLS model fails. One of the consequences of this is that the model fails to describe the process $\gamma\gamma\rightarrow\rho\rho$ perturbatively. There is absolutely nothing to be gained by evaluating the real parts of the $\gamma\gamma\rightarrow\rho^0\rho^0$ loop amplitudes, because a perturbative calculation is meaningless in this model. Although it is worth mentioning that in fact the real parts have been estimated to some extent and whilst not trustworthy in the 'perturbative sense' (above) they generally turn out to be larger than the imaginary parts ; which is contrary to what Moussallam assumed (see chapter 5 section i) in the preprint version of his paper [59].

Thus by proceeding judiciously one has been saved from a great deal of time consuming, and what would have been pointless, computing.

However there is still the possibility that the model might work non-perturbatively!

Chapter 8 Conclusions and Discussion

The aim of this thesis has been to test the HLS model of ρ mesons against experimental data on the process $\gamma\gamma\rightarrow\rho\rho$. It is only feasible to calculate $\gamma\gamma\rightarrow\rho\rho$ perturbatively in the HLS model. In the preceeding chapters (4,6 and 7) it has been shown that the HLS model fails to describe the process $\gamma\gamma\rightarrow\rho\rho$ perturbatively.

However it seemed a reasonable assumption in chapter 2(iv) that if the model were valid up to $\sqrt{s}\approx 2$ GeV for calculating Skyrmion properties then it should be reasonable to expect the model to describe other processes involving ρ mesons in this extrapolated energy range, such as $\gamma\gamma\rightarrow\rho\rho$. It was shown in chapter 7 that the HLS model $\rho^+\rho^-$ scattering amplitudes violate unitarity just above ρρ threshold, this suggests that the "meson loops" could become significant. Recalling that as pointed out in chapter 2(iii) the "meson loops" are explicitly ignored in the calculation of Skyrmion properties, the ρ field is treated classically.

So it would be most instructive to investigate how sensitive the Skyrmion properties are to the region ρρ threshold $\leq \sqrt{s} \leq 2$ GeV, before one can dismiss the HLS model outright. If the Skyrmion is insensitive to this region of $\sqrt{s}$ and the loop effects (ρ kinetic term), then there would be no problem for the Skyrmion model; this fits in with Ball's idea [20] that the vector mesons should not be crucial to the Skyrmion properties and the HLS model should not be useful above $\sqrt{s} \approx 1$ GeV. Resolution of thisquestion will require numerical studies of Skyrmion properties. An exact calculation of the quantum corrections ("meson loops") to the equations of motion is probably intractable, although one might gain some insight by putting in "by hand" form factors which would have the effect of making $\rho\rightarrow 0$, such as an exponential fall off with energy, above ρρ threshold, this could be part of the programme of investigating the 'sensitivity' of the Skyrmion properties.

So, that if it is found that the Skyrmion properties are relatively insensitive to the 'extrapolated region' (including loop effects) of the HLS model then there is no need to necessarily abandon the model as a mechanism of Skyrmion stabilization,

although as a model of ρ dynamics it would remain invalid (perturbatively). It could well be that in this energy range that the ρ is so far from being 'point-like' that the quark structure is playing a significant role and should be included in any 'effective' description.

Also very much along the lines of only believing the HLS model below ρρ threshold is the following , inspired by the work of Truong [75]. As was pointed out in chapter 3 Poppe [23] regards as serious the omission from the 4-quark 'exotic' models of the $\gamma\rho^+\rho^-$ vertex which gives Born amplitudes. In this thesis we have taken those Born amplitudes at face value and calculated cross sections (above ρρ threshold) which are found to be in serious disagreement with the data. It would be most interesting if one could use the Born amplitudes below ρρ threshold to place constraints on the 4-quark amplitudes.

Here we shall outline Truong's [75] approach to ππ scattering and then explain how it might be adapted to the process $\gamma\gamma\rightarrow\rho\rho$.

First of all Truong takes the Weinberg [76] low-energy ππ scattering amplitude, this gives a scattering length that is much smaller than the value extracted from experimental data, this is clearly unsatisfactory. However using ππ phase shifts to unitarize the scattering amplitude, via the 'N/D' method, a satisfactory value for the scattering length can be obtained. In this method the low-energy Weinberg amplitude is only believed in a region of s below ππ threshold and is extended to the physical region via a dispersion relation; in this way the phase shifts take into account the final state interactions. Truong emphasises the advantages of this unitary approach over the more conventional chiral perturbation theory, especially if the interactions become strong as they do for ρρ scattering.

Truong then considers a narrow resonance model for the ππ phase shifts, a combined linear σ model [77] and the ρ gauged chiral model [12] in which the σ (0^+) is assumed to be a narrow resonance in 'some approximation'. This model gives a ππ scattering amplitude with 2 terms involving ρ exchange (t and u-channels) and an s-channel σ exchange term. Truong then matches this model

amplitude with the unmodified Weinberg amplitude in the region in which it is believed ie below $\pi\pi$ threshold, the unphysical region. The matching is in the s-waves and is good up to corrections of the order $(m_\pi/m_\sigma)^2$ and $(m_\pi/m_\rho)^2$.

The 'high energy' (ie above $\pi\pi$ threshold) narrow resonance model of $\pi\pi$ scattering is thus constrained by the matching condition; the constrained model is found to give scattering lengths in good agreement with experimental data.

The matching condition works when the s-channel resonance of the model is the σ, isoscalar 0^+ state, with linear σ model couplings; if one were to use, say, an I=2 resonance instead then this would probably lead to 'bad matching'. Thus the choice of resonance is not completely arbitrary.

In summary Truong constructs a narrow resonance model of $\pi\pi$ phase shifts by constraining the resonance model with a matching condition; the resonance model then gives results previously obtained by unitarization of the scattering amplitude.

So how might this be adapted to the process $\gamma\gamma\to\rho\rho$? Corresponding to the unmodified Weinberg $\pi\pi$ scattering amplitude we have the HLS model tree-level amplitudes for $\gamma\gamma\to\rho\rho$, which we only want to believe below $\rho\rho$ threshold. Clearly $\gamma\gamma\to\rho\rho$ is a much more complicated spin system than $\pi\pi\to\pi\pi$, for instance there are twelve helicity amplitudes for $\gamma\gamma\to\rho\rho$ instead of one for $\pi\pi\to\pi\pi$ which makes things more difficult.

There is no data on $\rho\rho$ phase shifts so an 'N/D' unitarization of $\gamma\gamma\to\rho\rho$, to take into account final state interactions, is not feasible. The lack of $\rho\rho$ phase shift data means that we can only adopt the second of Truong's approaches, ie construct narrow resonance models which are to be constrained by matching them with the HLS model amplitudes below $\rho\rho$ threshold.

Thus following Truong one might try a narrow resonance model in which the s-channel resonance is a 'qq' state, in appendix F it is shown that only the I=0 component of this couples to $\rho\rho$ (I=1 coupling $v^o\rho\rho = 0$), so in effect the resonance would be the isoscalar σ. It is conceivable that such a resonance model could be

matched with the HLS model below ρρ threshold, since as pointed out in chapter 3 an s-channel I=0 resonance mechanism gives

$$\frac{\sigma(\gamma\gamma\rightarrow\rho^0\rho^0)}{\sigma(\gamma\gamma\rightarrow\rho^+\rho^-)} = \frac{1}{2} \qquad (3.1)$$

and the HLS model gives the ratio to be zero. However both of these are incompatible with the experimental data which gives the ratio to be >1 (≈4); so a simple σ resonance model is unviable for obtaining a fit to the data.

We are thus naturally led to consider a toy 4-quark model of 0^+ and 2^+ narrow resonances, as in the work of Li and Liu [45]-[47] and Achasov et al [48]-[50] described in chapter 3, such that in the physical region the ratio of neutral to charged cross sections is > 1. The general aim would be to extrapolate these 4-quark resonance model amplitudes below ρρ threshold and by matching them with the HLS model amplitudes thus put constraints on the 4-quark resonance model. And so implicitly include the $\gamma\rho^+\rho^-$ vertex effects in the 'exotic' models.

Although it may well be that $\gamma\gamma\rightarrow\rho^0\rho^0$ zero at the tree-level in the HLS modelis simply too strong a condition to allow matching at low energies of the 4-quark model amplitudes to those of the HLS model.

However it should be emphasised that such a 'matching programme' requires a great deal of work. This is because of the large domain of parameters, especially if channels other than ρρ involved in the 4-quark resonance models are considered, such as ωρ, ωω, k*k*, etc. For example there are twelve independent helicity amplitudes for $\gamma\gamma\rightarrow\rho\rho$, a suitable scale is required at which the matching would be done and there is the question of exactly which 4-quark resonances should be included? Also because of the different mass scales involved a single expansion parameter is not immediately obvious for the process of extrapolating the 'high-energy' narrow resonance model to below ρρ threshold for the matching. All of which would require investigation before one could reach any definite conclusions, so the matching procedure is a long programme of work.

It is interesting to consider further the possibility of a Pomeron mechanism giving dominace of the $\rho^0\rho^0$ final state in the process $\gamma\gamma\rightarrow\rho\rho$. Diffraction scattering, or Pomeron exchange, amplitudes can be generated by summing over all possible intermediate states through the unitarity relation [78], an example of this with two body intermediate states as an attempt to understand the Pomeron at low-energies is given in reference [79].

So what are the possible intermediate states that one could use in this manner to generate a Pomeron amplitude for $\gamma\gamma\rightarrow \rho^0\rho^0$? Firstly we consider the electric couplings of the photon to two pseudoscalar (0^-) states $\pi^+\pi^-$, k^+k^- applying the two body unitarity relation to the diagram in Figure 8.1

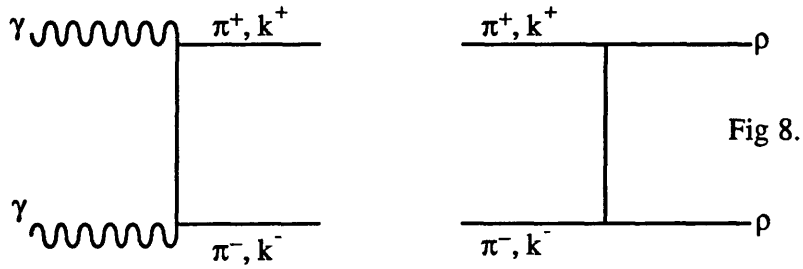

Fig 8.1

unfortunately the best that this can give is $\sigma(\gamma\gamma\rightarrow \rho^0\rho^0) \approx \sigma(\gamma\gamma\rightarrow \rho^+\rho^-)$, which is obviously of no use for giving neutral channel dominance.

Four body intermediate states, such as four pseudoscalars (π,k), is in general too difficult to compute; but in an approximation could be considered as a two-body intermediate state of two body resonances such as $\rho\rho$ or $\sigma\sigma$ ($0^+\,0^+$). The $\rho\rho$ case has already been dismissed; the σ is believed to have mass$\geq$900MeV this is simply too heavy for it to produce a diffraction peak at $\sqrt{s}\approx$1.6 GeV since it would be likely to give a cross section rising to a maximum around $\sqrt{s}\approx$2 GeV.

One is thus led to consider the 'non-electric' couplings of the photon generated by the Wess-Zumino action [80]; incorporating the Wess-Zumino term into the HLS model (see chapter 7.3 of ref.[19]) gives $\gamma\omega\pi^o$ and $\rho^o\omega\pi^o$ vertices. In

this case the imaginary part of the $\gamma\gamma \rightarrow \rho\rho$ amplitude is given by applying the two body unitarity relation to the diagram in Figure 8.2

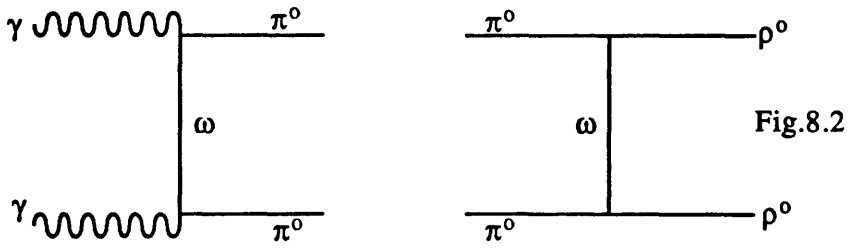

Fig.8.2

This guarrantees $\sigma(\gamma\gamma \rightarrow \rho^0\rho^0) \gg \sigma(\gamma\gamma \rightarrow \rho^+\rho^-)$, given that the γ and ρ^o couplings are given by the Wess-Zumino term. So in this way the $\rho^+\rho^-$ final state is suppressed with respect to the $\rho^0\rho^0$ final state as required by experiment.

However the same model can be used to calculate the process $\gamma\gamma \rightarrow \omega\omega$, the diagram for this process is Fig.8.3

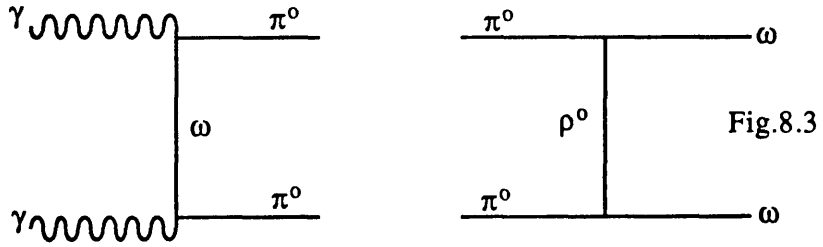

Fig.8.3

which can be seen to have exactly the same coupling as the diagram for $\gamma\gamma \rightarrow \rho^0\rho^0$, so that near threshold of $\sqrt{s}$=1.6 GeV this model would give $\sigma(\gamma\gamma \rightarrow \omega\omega) \approx \sigma(\gamma\gamma \rightarrow \rho^0\rho^0)$ whereas the experimental data in this region gives

$$\frac{\sigma(\gamma\gamma \rightarrow \rho^0\rho^0)}{\sigma(\gamma\gamma \rightarrow \omega\omega)} \approx 5.0\text{-}10.0$$

So this approach to diffractive scattering, with non-electric couplings fails. The failure of this 'low-energy' Pomeron approach to provide a satisfactory mechanism

for the processes $\gamma\gamma\rightarrow\rho^0\rho^0$ and $\gamma\gamma\rightarrow\omega\omega$ makes it hard to understand exactly why the t-channel factorization approach of Alexander et al [53] should work.

If the Pomeron were to dominate the process $\gamma\gamma\rightarrow\rho\rho$ and one applied the Truong type matching to the Pomeron amplitudes then there is no problem with the neutral channel (both zero below $\rho\rho$ threshold),but the HLS model amplitude for $\gamma\gamma\rightarrow\rho^+\rho^-$ is so large and has a functional dependence contrary to the experimental data that it would seem unlikely to be able to achieve a satisfactory matching.

The violation of unitarity by the $\rho^+\rho^-$ scattering amplitudes suggests another very interesting line of investigation which would tie-in very nicely with the $\gamma\gamma\rightarrow$VV physics. The unitarity violation is an indication of the possibility of ('$\rho\rho$') resonance formation, recalling from chapter 3 that both I=0 and I=2 resonances are required in the 4-quark explana tion of $\gamma\gamma\rightarrow\rho\rho$ then we also need to consider the case of the $\rho^+\rho^+$ scattering amplitudes as an I=2 resonance would be 'built' from $\rho^+\rho^+$. In fact the Born amplitudes (t and u-channels but no s-channel) for $\rho^+\rho^+$ are the same as those for $\rho^+\rho^-$ apart from an overall '-' sign, the seagull terms will be different but it was shown in chapter 7 that these are not a major factor in the violation of unitarity just above $\rho\rho$ threshold. So it would seem that the $\rho^+\rho^+$ amplitudes also violate unitarity.

Although we have shown that the HLS model fails perturbatively there seems to be no reason *a priori* to disbelieve it non-perturbatively. So a non-perturbative calculation showing up I=2 '$\rho\rho$' resonances would be most interesting since it could be regarded as a dynamical model for 4-quark states, which have so far only been considered in a 'static' bag model description. This would be a 'challenging' calculation for the lattice!

Another approach to the process $\gamma\gamma\rightarrow\rho\rho$ that might be considered is to extend the HLS model so as to include higher derivative, or'non-minimal', terms; to

generate tree-level diagrams for both $\gamma\gamma \rightarrow \rho^+\rho^-$ and $\gamma\gamma \rightarrow \rho^0\rho^0$. Such an effective Lagrangian approach includes any term allowed by the symmetries of the theory, but with arbitary coefficients to be fixed by experimental data; it should be noted that fitting the data by as many terms as needed means a loss of predictivity. In this way one could certainly generate tree-level diagrams for the neutral channel, which is required to be 'dominant, but at the same time this would also generate diagrams for the charged channel which is required to be small compared to the neutral channel. Unfortunately the indications are that for a given higher derivative term, with an overall coupling constant which is a parameter to be fixed, every neutral channel diagram generated there are several charged channel diagrams so on this basis alone it would seem unlikely that dominace of the neutral channel will occur.

So although the content of the thesis might seem some what negative, it certainly suggests several very interesting lines of investigation for future work.

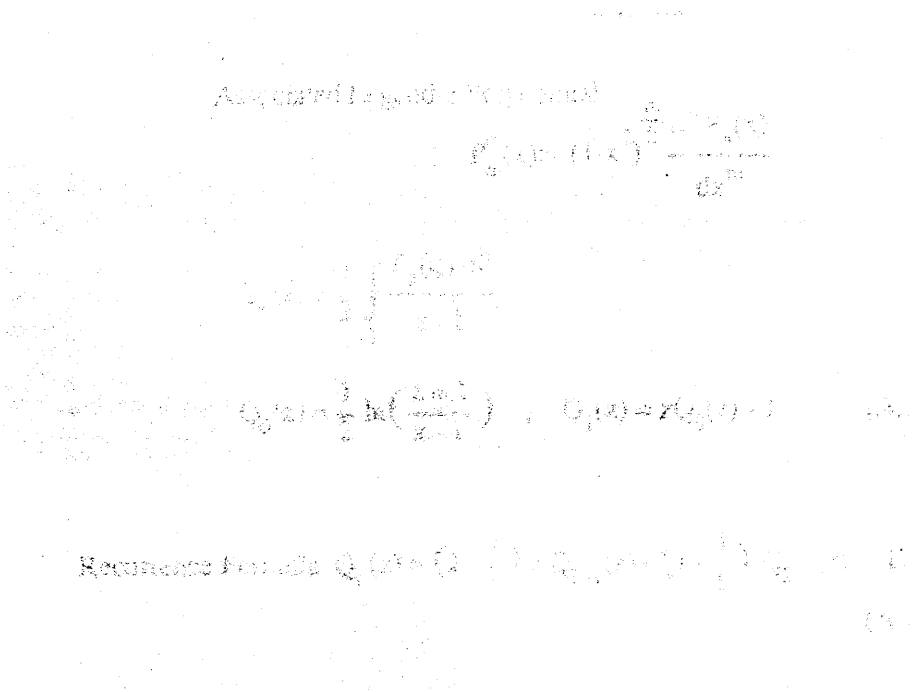

Appendix A

General Notation:

Metric $g_{\mu\nu}$= diag(1,-1,-1,-1)

A is defined to be equal to B A:=B

Trace of matrix M TrM

RHS, LHS := right,left -hand side

$\{T^a\}$ a = 1,2,3 are the generators of SU(2), normalised as $Tr(T^a T^b) = \delta^{ab}/2$

Formulae and Functions for Partial Waves:

$$\text{Legendre Polynomials } P_n(x) := \frac{1}{2^n n!}\frac{d^n}{dx^n}(x^2-1)^n$$

Associated Legendre Polynomial

$$P_n^m(x) := (1-x^2)^{\frac{m}{2}}\frac{d^m P_n(x)}{dx^m}$$

$$Q_n(z) := \frac{1}{2}\int_{-1}^{1}\frac{P_n(\xi)\,d\xi}{z-\xi}$$

$$Q_0(z) = \frac{1}{2}\ln\left(\frac{z+1}{z-1}\right) \quad , \quad Q_1(z) = zQ_0(z) - 1 \qquad \text{(A.1)}$$

$$\text{Recurrence Formula } Q_L(z) = \left(2-\frac{1}{L}\right) z\, Q_{L-1}(z) - \left(1-\frac{1}{L}\right) Q_{L-2}(z) \ , \ L>1 \qquad \text{(A.2)}$$

Addition Theorem

$$P_n(\cos\theta_1\cos\theta_2 + \sin\theta_1\sin\theta_2\cos\varphi) =$$

$$P_n(\cos\theta_1)\,P_n(\cos\theta_2) + 2\sum_{m=1}^{\infty}\frac{\Gamma(n-m+1)}{\Gamma(n+m+1)}P_n^m(\cos\theta_1)\,P_n^m(\cos\theta_2)\cos m\varphi \qquad \text{(A.3)}$$

$$\frac{1}{\alpha - z} = \sum_{n=0}^{\infty}(2n+1)\,Q_n(\alpha)\,P_n(z) \qquad \text{(A.4)}$$

converges provided that $|z + \sqrt{(z^2 - 1)}| < |\alpha + \sqrt{(\alpha^2 - 1)}|$

Dynamical Variables for the reactions $1 + 2 \longrightarrow 3 + 4$

Where 1,2 = $\gamma\gamma$, $\rho^+\rho^-$, $\pi^+\pi^-$ and 3,4 = $\rho^0\rho^0$, $\rho^+\rho^-$, $\pi^+\pi^-$

Conservation of four momentum: $k_1 + k_2 = k_3 + k_4$ (A.5)

Mandelstam Variables $s=(k_1+k_2)^2$, $t=(k_1-k_3)^2$, $u=(k_1-k_4)^2$ (A.6)

In the centre of mass frame

$$k_1^\alpha = (E, \mathbf{k}),\quad k_2^\alpha = (E, -\mathbf{k}),\quad k_1^2 = k_2^2,\quad \mathbf{k}^2 = E^2 - k_1^2$$

$$k_3^\alpha = (E, \mathbf{k}'),\quad k_4^\alpha = (E, -\mathbf{k}'),\quad k_3^2 = k_4^2,\quad \mathbf{k}'^2 = E^2 - k_3^2 \qquad \text{(A.7)}$$

and the scattering angle (θ) is defined by

$$\cos\theta = z := \frac{\mathbf{k}.\mathbf{k}'}{kk'} \qquad \text{(A.8)}$$

where $k = |\mathbf{k}|$ and $k' = |\mathbf{k}'|$

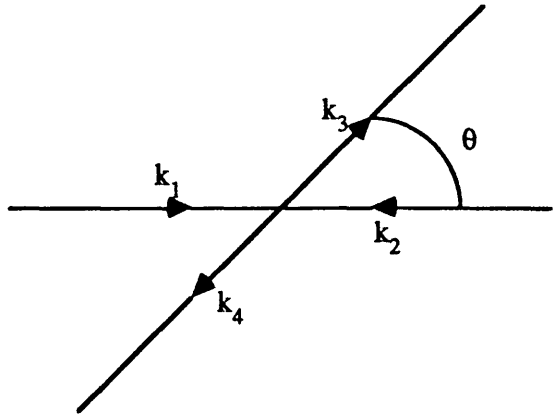

Figure A.1

Particles 1 and 2 along the z-axis so $\mathbf{k} = (0,0,k)$

Particles 3 and 4 in the x-z plane so $\mathbf{k}' = (k'\sin\theta, 0, k'\cos\theta)$ (A.9)

(i) $\gamma\gamma \rightarrow \rho\rho$

$$k_1^2 = k_2^2 = 0 \ , \ k_3^2 = k_4^2 = m^2 \ , \ k \neq k' \ , \ s = 4E^2$$

$$t - m^2 = -2kk'(\alpha_1 - z) \ , \ u - m^2 = -2kk'(\alpha_1 + z)$$

$$\text{where } \alpha_1 = \frac{k}{k'} = \sqrt{\frac{s}{s - 4m^2}}$$

(ii) $\rho\rho \rightarrow \rho\rho$

$$k_1^2 = k_2^2 = k_3^2 = k_4^2 = m^2 \ , \ k = k' \ , \ s = 4E^2$$

$$t - m^2 = -2kk'(\alpha_2 - z) \ , \ u - m^2 = -2kk'(\alpha_2 + z)$$

$$\text{where } \alpha_2 = 1 + \frac{2m^2}{s - 4m^2}$$

$$t = -2kk'(1-z) \ , \ u = -2kk'(1+z)$$

(iii) $\pi\pi \rightarrow \pi\pi$

$$k_1^2 = k_2^2 = k_3^2 = k_4^2 = m_\pi^2 \quad , \quad k = k' \quad , \quad s = 4E^2$$

$$t = -2kk'(1-z) \quad , \quad u = -2kk'(1+z)$$

$$t - m^2 = -2kk'(\gamma_1 - z) \quad , \quad u - m^2 = -2kk'(\gamma_1 + z)$$

where $\gamma_1 = 1 + \dfrac{2m^2}{s - 4m_\pi^2}$

$$u - s = -2kk'(\gamma_2 - z) \quad , \quad t - s = -2kk'(\gamma_2 + z)$$

where $\gamma_2 = 1 + \dfrac{2s}{s - 4m_\pi^2}$

Appendix B

Diagonalization of the HLS Lagrangian and the Feynman rules.

In chapter 2 the HLS lagrangian for π,V and B fields (equation 2.21) was derived, in this appendix the lagrangian is diagonalized to give mass and charge eigenstates.

$$L = \frac{1}{2}(\partial_\mu \vec{\pi})^2 + \frac{a}{2} f \vec{V}_\mu.(\vec{\pi} \times \partial^\mu \vec{\pi}) + \frac{a}{2} f_\pi^2 f^2 \vec{V}_\mu^2 - \frac{1}{2} \mathrm{Tr} V_{\mu\nu}^2$$

$$+ \frac{(2-a)}{2} g' B_\mu (\vec{\pi} \times \partial^\mu \vec{\pi})_3 - a f_\pi^2 f\, g' B_\mu V_3^\mu + \frac{a}{2} f_\pi^2\, g'^2\, B_\mu^2 - \frac{1}{4} B_{\mu\nu}^2 \qquad (2.21)$$

The physical fields are defined as follows

$$\pi_3 = \pi^0$$

$$B_\alpha = \cos\theta\, A_\alpha - \sin\theta\, \rho_\alpha^0$$

$$V_3^\alpha = \sin\theta\, A^\alpha + \cos\theta\, \rho^{0\alpha} \qquad (B.1)$$

$$\lambda^\pm = \frac{1}{\sqrt{2}} (\lambda_1 \mp i\lambda_2) \qquad (B.2)$$

Where $\lambda^\pm$ destroys $\pm$ and $\lambda_i = \pi_i$, V_i $i = 1,2,3$.

The kinetic term for the HLS is given by equation 2.12, it can be shown that

$$-\frac{1}{2} \mathrm{Tr}\, V_{\mu\nu}^2 \equiv -\frac{1}{4} F_{a\mu\nu} F_a^{\mu\nu} - f \partial_\mu \vec{V}_\nu.(\vec{V}^\mu \times \vec{V}^\nu)$$

$$-\frac{f^2}{4} (\vec{V}_\mu \times \vec{V}_\nu).(\vec{V}^\mu \times \vec{V}^\nu)$$

Where $F_a^{\mu\nu} \equiv (\partial^\mu V^\nu - \partial^\nu V^\mu)_a$.

Using the above definitions of the physical fields the Lagrangian 2.21 becomes :

$$L = \partial_\alpha \pi^+ \partial^\alpha \pi^- + \frac{1}{2}\partial_\alpha \pi^0 \partial^\alpha \pi^0 - \frac{1}{4}(\partial_\alpha A_\beta - \partial_\beta A_\alpha)^2$$

$$\frac{1}{4}(\partial_\alpha \rho^0_\beta - \partial_\beta \rho^0_\alpha)^2 + \frac{1}{2} m^2_{\rho^0} \rho^0_\alpha \rho^{0\alpha}$$

$$\frac{1}{2}(\partial_\alpha \rho^+_\beta - \partial_\beta \rho^+_\alpha)(\partial^\alpha \rho^{-\beta} - \partial^\beta \rho^{-\alpha}) + m^2_{\rho^\pm} \rho^+_\alpha \rho^{-\alpha}$$

$$+ i g_{\gamma\pi\pi} A_\alpha (\pi^- \partial^\alpha \pi^+ - \pi^+ \partial^\alpha \pi^-) + i g_{\rho^0\pi\pi} \rho^0_\alpha (\pi^- \partial^\alpha \pi^+ - \pi^+ \partial^\alpha \pi^-)$$

$$+ i g_{\rho^\pm\pi\pi} \rho^+_\alpha (\pi^0 \partial^\alpha \pi^- - \pi^- \partial^\alpha \pi^0) + i g_{\rho^\pm\pi\pi} \rho^-_\alpha (\pi^+ \partial^\alpha \pi^0 - \pi^0 \partial^\alpha \pi^+)$$

$$+ i f \cos\theta \left[(\rho^+_\alpha \rho^-_\beta - \rho^-_\beta \rho^+_\alpha)\partial^\alpha \rho^{0\beta} \right.$$
$$\left. + (\partial_\alpha \rho^-_\beta - \partial_\beta \rho^-_\alpha)\rho^{0\alpha} \rho^{+\beta} - (\partial_\alpha \rho^+_\beta - \partial_\beta \rho^+_\alpha)\rho^{0\alpha} \rho^{-\beta} \right]$$

$$+ i f \sin\theta \left[(\rho^+_\alpha \rho^-_\beta - \rho^+_\beta \rho^-_\alpha)\partial^\alpha A^\beta \right.$$
$$\left. + (\partial_\alpha \rho^-_\beta - \partial_\beta \rho^-_\alpha) A^\alpha \rho^{+\beta} - (\partial_\alpha \rho^+_\beta - \partial_\beta \rho^+_\alpha) A^\alpha \rho^{-\beta} \right]$$

$$+ f^2 \cos^2\theta \left[\rho^+_\alpha \rho^-_\beta \rho^{0\alpha} \rho^{0\beta} - \rho^+_\alpha \rho^{-\alpha} \rho^0_\beta \rho^{0\beta} \right]$$

$$+ f^2 \sin^2\theta \left[\rho^+_\alpha \rho^-_\beta A^\alpha A^\beta - \rho^+_\alpha \rho^{-\alpha} A_\beta A^\beta \right]$$

$$+ f^2 \cos\theta \sin\theta \left[\rho^+_\alpha \rho^-_\beta (A^\alpha \rho^{0\beta} + A^\beta \rho^{0\alpha}) - 2\, \rho^+_\alpha \rho^{-\alpha} A_\beta \rho^{0\beta} \right]$$

$$+ \frac{f^2}{2} \rho^+_\alpha \rho^-_\beta \left[\rho^{+\alpha} \rho^{-\beta} - \rho^{+\beta} \rho^{-\alpha} \right] \qquad \text{(B.3)}$$

The mixing angle θ is given by $\tan\theta = g'/f$ and the mass eigenstaes are

$$m^2_{\rho^0} = a\,(f^2 + g'^2)\, f^2_\pi \quad , \quad m^2_{\rho^\pm} = a\, f^2 f^2_\pi$$

the vector couplings to the pion current are given by

$$g_{\gamma\pi\pi} = g' \cos\theta + \frac{a}{2}(f \sin\theta - g' \cos\theta) \qquad \text{(B.4)}$$

$$g_{\rho^0\pi\pi} = \frac{a}{2} f \cos\theta + \frac{(a-2)}{2} g' \sin\theta \qquad \text{(B.5)}$$

$$g_{\rho^{\pm}\pi\pi} = \frac{a f}{2} \qquad \text{(B.6)}$$

Since the weak interactions have not been included in this lagrangian then one can immediately identify the $U(1)_Q$ coupling constant g' with the electric charge e, that is g'=e, where $e^2/4\pi = 1/137$ (B.7).The HLS coupling constant f is determined from the (KSRF) mass relation given above. The input is the measured ρ mass = 770MeV, the pion decay constant f_π=93MeV and a=2 (as discussed in chapter2), this yields f=5.85(B.8). Consequently $\cos\theta \approx 1$ and $\sin\theta \approx 0$ numerically, and for the purposes of calculation f cosθ = f and f sinθ = e (B.9).

As a result of the above the vector couplings to the pion current become $g_{\gamma\pi\pi}$= e and $g_{\rho\pi\pi}$= f. It is interesting to note that the "a" dependence of $g_{\gamma\pi\pi}$ disappears whatever the value of θ, since f sinθ - g' cosθ = 0. Which is presumably a reflection of the universality of the electromagnetic couplimg, so that the π charge couples with 'e'.

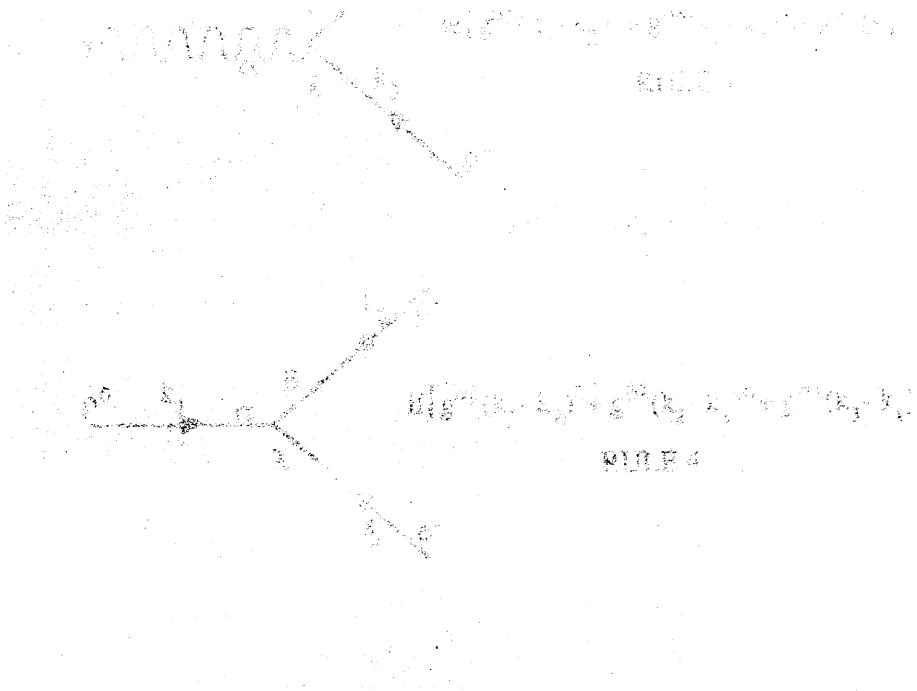

The Feynman rules arising from the Lagrangian (B.3) are as follows, all four momentum are 'going into' the vertex:

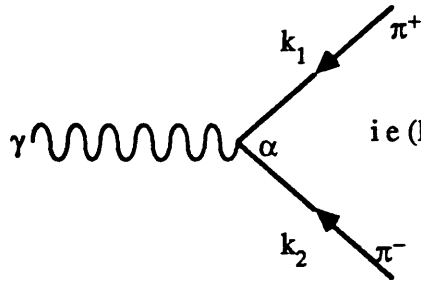

$i\,e\,(k_2 - k_1)_\alpha$ RULE 1

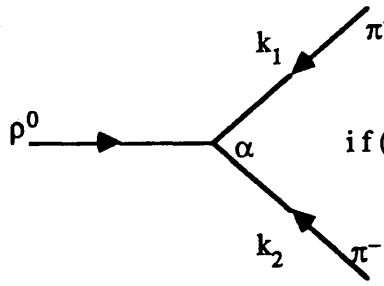

$i\,f\,(k_2 - k_1)_\alpha$ RULE 2

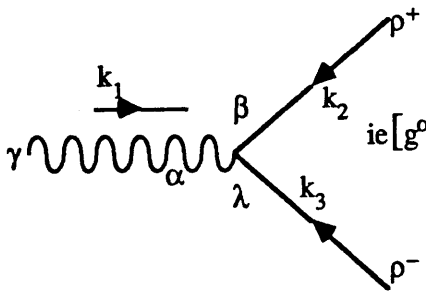

$ie[g^{\alpha\beta}(k_1 - k_2)^\lambda + g^{\beta\lambda}(k_2 - k_3)^\alpha + g^{\alpha\lambda}(k_3 - k_1)^\beta]$

RULE 3

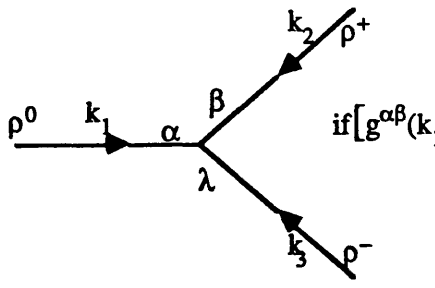

$if[g^{\alpha\beta}(k_1 - k_2)^\lambda + g^{\beta\lambda}(k_2 - k_3)^\alpha + g^{\alpha\lambda}(k_3 - k_1)^\beta]$

RULE 4

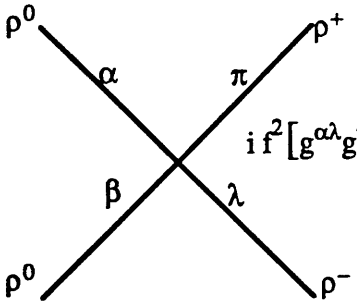

$$i f^2 [g^{\alpha\lambda} g^{\pi\beta} + g^{\alpha\pi} g^{\beta\lambda} - 2 g^{\alpha\beta} g^{\pi\lambda}]$$

RULE 5

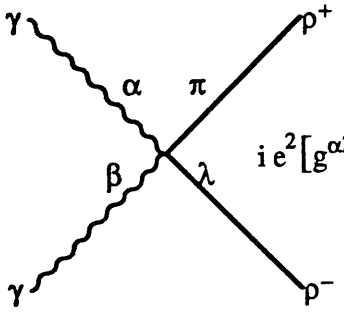

$$i e^2 [g^{\alpha\lambda} g^{\pi\beta} + g^{\alpha\pi} g^{\beta\lambda} - 2 g^{\alpha\beta} g^{\pi\lambda}]$$

RULE 6

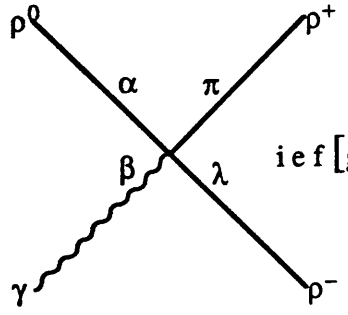

$$i e f [g^{\alpha\lambda} g^{\pi\beta} + g^{\alpha\pi} g^{\beta\lambda} - 2 g^{\alpha\beta} g^{\pi\lambda}]$$

RULE 7

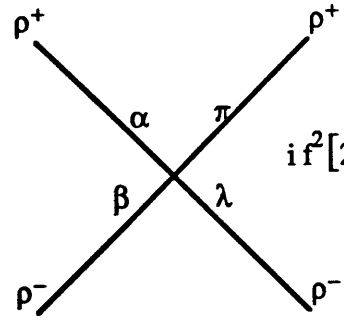

$$i f^2 [2 g^{\alpha\pi} g^{\beta\lambda} - g^{\alpha\beta} g^{\pi\lambda} - g^{\alpha\lambda} g^{\pi\beta}]$$

RULE 8

ρ propagator 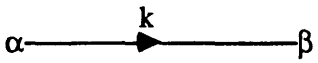

RULE 9

$$i\frac{(-g_{\alpha\beta} + k_\alpha k_\beta/m^2)}{k^2 - m^2 + i\varepsilon} \quad , \ \varepsilon>0 \ .$$

For an intial photon or vector meson take the polarization vector and for a final photon or vector meson take the complex conjugate of the polarization vector

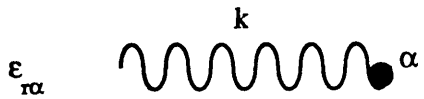

$\varepsilon_{r\alpha}$ RULE 10a

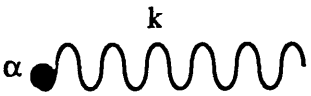

$\varepsilon^*_{r\alpha}$ RULE 10b

Appendix C Partial Wave Amplitudes

(i) Helicity Amplitude Notation

The processes $\gamma(1) + \gamma(2) \rightarrow \rho(3) + \rho(4)$ and $\rho(1) + \rho(2) \rightarrow \rho(3) + \rho(4)$ will have helicity amplitudes denoted by M^{abcd} which is obtained from the Feynman amplitude (calculated using the rules in appendix B) $M^{\alpha\pi\beta\lambda}$

$$M^{abcd} = \varepsilon^{\alpha}_{1a}\ \varepsilon^{\pi}_{2b}\ \varepsilon^{\beta}_{3c}\ \varepsilon^{\lambda}_{4d}\ M_{\alpha\pi\beta\lambda} \qquad (C.1)$$

Where ε_1 is the polarization vector for particle 1 and so on. The letters a,b,c,d label the helicity of particles 1,2,3,4 respectively and they can take the values

$$a,b,c,d = \pm 1\ ,\ 0 \qquad (C.2)$$

except in the case of the reaction $\gamma(1) + \gamma(2) \rightarrow \rho(3) + \rho(4)$ longitudinally polarized photons are excluded ($a,b \neq 0$).

Following the notation of Jacob and Wick [81], the total spin component of the initial(final) particles along the direction of motion is

$$\lambda = a - b \quad (\lambda' = c - d) \qquad (C.3)$$

and the partial wave expansion of the helicity amplitude is

$$M^{abcd}(s,\theta) = \sum_{J} (2J+1)\ T_J^{abcd}(s)\ d^{J}_{\lambda\lambda'}(\theta) \qquad (C.4)$$

Where s is the centre of mass energy squared and θ is the scattering angle as defined in appendix A.

The $d_{\lambda\lambda'}$ have the following useful proerties :

$$\text{Orthogonality} \quad \int_0^{\pi} \sin\theta\, d\theta\, d^{J}_{\lambda\lambda'}(\theta)\, d^{J'}_{\lambda\lambda'}(\theta) = \frac{2}{2J+1}\,\delta_{JJ'} \qquad (C.5)$$

$$d_{\lambda,\mu} = d_{-\mu,-\lambda} = (-1)^{\lambda-\mu}\, d_{\mu,\lambda} \quad \text{(for any J)} \qquad (C.6)$$

$$d^J_{\lambda,\mu\pm1} = \frac{1}{\sqrt{[(j\pm\mu+1)(J\mp\mu)]}} \{ \frac{-\lambda}{\sin\theta} + \mu\cot\theta \mp \frac{\partial}{\partial\theta} \} d^J_{\lambda,\mu} \quad \text{(C.7)}$$

$$d^J_{00} = P_J(\cos\theta) \quad \text{(C.8)}$$

$$d^J_{10} = -\sqrt{\frac{1}{J(J+1)}} \sin\theta \frac{dP_J(\cos\theta)}{d\cos\theta} \quad \text{(C.9)}$$

$$d^2_{20} = d^2_{02} = \frac{1}{2}\sqrt{\frac{3}{2}} \sin^2\theta \quad \text{(C.10)}$$

$$d^2_{21} = -d^2_{12} = \frac{1}{2}(1+\cos\theta)\sin\theta$$

$$d^2_{2-1} = -d^2_{-12} = \frac{1}{2}(1-\cos\theta)\sin\theta \quad \text{(C.11)}$$

$$d^2_{22} = d^2_{-2\,-2} = \frac{1}{4}(1+\cos\theta)^2$$

$$d^2_{2\,-2} = d^2_{-2\,2} = \frac{1}{4}(1+\cos\theta)^2 \quad \text{(C.12)}$$

(ii) Polarization Vectors

The 4 momenta k_i are as defined in appendix A, in the centre of mass frame with the incoming particles (1&2) along the z axis and the outgoing particles (3&4) in the x-z plane. Then the polarization vectors which project out states of definite helicity (these are the same as those used by Poppe [23] with final state vectors constructed by rotation , see Scadron [82]).

$$\varepsilon_{1+} = \frac{1}{\sqrt{2}}(0,-1,-i,0) \quad , \quad \varepsilon_{1-} = \frac{1}{\sqrt{2}}(0,1,-i,0)$$

$$\varepsilon_{2+} = \frac{1}{\sqrt{2}}(0,1,-i,0) \quad , \quad \varepsilon_{2-} = \frac{1}{\sqrt{2}}(0,-1,-i,0)$$

If the particles 1&2 are ρ mesons then their longitudinal polarization vectors are

$$\varepsilon_{10} = \frac{1}{m}(k,0,0,E) \quad , \quad \varepsilon_{20} = \frac{1}{m}(k,0,0,-E)$$

$$\varepsilon_{3+} = \frac{1}{\sqrt{2}}(0,-\cos\theta,-i,\sin\theta) \quad , \quad \varepsilon_{3-} = \frac{1}{\sqrt{2}}(0,\cos\theta,-i,-\sin\theta)$$

$$\varepsilon_{4+} = \frac{1}{\sqrt{2}}(0,\cos\theta,-i,-\sin\theta) \quad , \quad \varepsilon_{4-} = \frac{1}{\sqrt{2}}(0,-\cos\theta,-i,\sin\theta)$$

$$\varepsilon_{30} = \frac{1}{m}(k', E\sin\theta, 0, E\cos\theta) \quad , \quad \varepsilon_{40} = \frac{1}{m}(k',-E\sin\theta,0,-E\cos\theta)$$

(C.13)

(iii) $\gamma\gamma \rightarrow \rho^+\rho^-$

The polarization vectors on page are used to project out the tree level $\gamma\gamma \rightarrow \rho^+\rho^-$ helicity amplitudes M^{abcd} from the Feynman amplitude $M^{\alpha\sigma\tau\beta\lambda}$ equation 4.4 .

$$M^{++++} = M^{----}$$

$$= -2e^2\left\{1 + \frac{k^2(1+z)^2 + (k+k')^2\sin^2\theta}{t-m^2} + \frac{k^2(1-z)^2 + (k+k')^2\sin^2\theta}{u-m^2}\right\}$$

$$M^{++--} = M^{--++}$$

$$= -2e^2\left\{1 + \frac{k^2(1-z)^2 + (k-k')^2\sin^2\theta}{t-m^2} + \frac{k^2(1+z)^2 + (k-k')^2\sin^2\theta}{u-m^2}\right\}$$

$$M^{+++-} = M^{++-+} = M^{--+-} = M^{---+} = 0$$

$$M^{+-++} = M^{-+++} = M^{+---} = M^{-+--}$$

$$= 2e^2m^2\sin^2\theta\left\{\frac{1}{t-m^2} + \frac{1}{u-m^2}\right\}$$

$$M^{+-+-} = M^{-+-+}$$

$$= -2e^2k^2(1+z)^2\left\{\frac{1}{t-m^2} + \frac{1}{u-m^2}\right\}$$

$$M^{+--+} = M^{-++-}$$

$$= -2e^2k^2(1-z)^2\left\{\frac{1}{t-m^2}+\frac{1}{u-m^2}\right\}$$

$$M^{+++0} = M^{++0+} = M^{--0-} = M^{---0} = 0$$

$$M^{++-0} = M^{++0-} = M^{--0+} = M^{--+0} = 0$$

$$M^{++00} = M^{--00}$$

$$= -2e^2\left\{\frac{(k^2+k'^2)}{m^2} - \frac{skk'z}{m^2}\left(\frac{1}{t-m^2}-\frac{1}{u-m^2}\right)\right.$$

$$\left.\left(\frac{2k^2(k^2+k'^2)}{m^2}+\frac{(k^2+m^2)\sin^2\theta}{m^2}\right)\left(\frac{1}{t-m^2}+\frac{1}{u-m^2}\right)\right\}$$

$$M^{+-00} = M^{-+00}$$

$$= -2e^2(k^2+m^2)\sin^2\theta\left\{\frac{1}{t-m^2}+\frac{1}{u-m^2}\right\}$$

$$M^{+-+0} = M^{-+-0} = -M^{+-0-} = -M^{-+0+}$$

$$= -e^2(2\sqrt{2}\,k\,m\,i)(1+z)\sin\theta\left\{\frac{1}{t-m^2}+\frac{1}{u-m^2}\right\}$$

$$M^{+--0} = M^{-++0} = -M^{+-0+} = -M^{-+0-}$$

$$= e^2(2\sqrt{2}\,k\,m\,i)(1-z)\sin\theta\left\{\frac{1}{t-m^2}+\frac{1}{u-m^2}\right\}$$

The partial wave amplitudes are then projected out using the orthogonality and symmetry properties of the $d_{\lambda\lambda'}$ functions and the expansion (A.4).

$$T_J^{+\,+\,+\,+} = e^2 \frac{(1+\alpha_1)^2}{\alpha_1} \left(1 + (-1)^J\right) Q_J(\alpha_1)$$

$$T_J^{+\,+\,-\,-} = e^2 \frac{(1-\alpha_1)^2}{\alpha_1} \left(1 + (-1)^J\right) Q_J(\alpha_1)$$

$$T_2^{+\,-\,+\,+} = -e^2 \sqrt{\frac{2}{3}} \left(\frac{16m^2\alpha_1}{5s}\right) \left\{ Q_0(\alpha_1) - \frac{10}{7} Q_2(\alpha_1) + \frac{3}{7} Q_4(\alpha_1) \right\}$$

$$T_2^{+\,-\,+\,-} = T_2^{+\,-\,-\,+} = e^2 \frac{8\alpha_1}{5} \left\{ Q_0(\alpha_1) + \frac{10}{7} Q_2(\alpha_1) + \frac{1}{14} Q_4(\alpha_1) \right\}$$

$$T_0^{+\,+\,0\,0} = e^2 \left\{ \frac{4}{3}\alpha_1 \frac{(s+4m^2)}{s} \left(Q_0(\alpha_1) - Q_2(\alpha_1) \right) - 4\, Q_1(\alpha_1) + \frac{(s-2m^2)}{m^2} \right\}$$

$$T_2^{+\,-\,+\,0} = -T_2^{+\,-\,-\,0} = -e^2 \frac{4\sqrt{2}\, m\, i}{5k'} \left(Q_0(\alpha_1) - \frac{5}{7} Q_2(\alpha_1) - \frac{2}{7} Q_4(\alpha_1) \right)$$

(iv) $\rho^+\rho^- \rightarrow \rho^+\rho^-$

The polarization vectors are used to project out the $\rho^+\rho^-$ scattering amplitudes from the Feynman amplitude (7.19), the Born and seagull terms are kept seperate :

$$M^{++++} = M^{----}$$

$$= f^2 \{ \frac{u-t}{s-m^2} - \frac{1}{t-m^2}\left(\frac{(1+z)^2}{4}(s-u) + 8k^2\sin^2\theta\right) - \frac{1}{u-m^2}\left(\frac{(1-z)^2}{4}(s-t) + 8k^2\sin^2\theta\right) + \frac{1}{4}(z^2 - 6z - 3) \quad \text{seagull} \}$$

$$M^{++--} = M^{--++}$$

$$= f^2 \{ \frac{u-t}{s-m^2} - \frac{s-u}{t-m^2}\frac{(1-z)^2}{4} - \frac{s-t}{u-m^2}\frac{(1+z)^2}{4} + \frac{(z^2+6z-3)}{4} \quad \text{seagull} \}$$

$$M^{+++-} = M^{++-+} = M^{--+-} = M^{---+} =$$

$$M^{+-++} = M^{-+++} = M^{+---} = M^{-+--}$$

$$= \frac{f^2}{4} \{ \frac{(t+4m^2)\sin^2\theta}{t-m^2} + \frac{(u+4m^2)\sin^2\theta}{u-m^2} - \sin^2\theta \quad \text{seagull} \}$$

$$M^{+-+-} = M^{-+-+}$$

$$= \frac{f^2}{4} \{ \frac{(u-s)}{t-m^2}(1+z)^2 + \frac{(t-s)}{u-m^2}(1+z)^2 + (1+z)^2 \quad \text{seagull} \}$$

$$M^{+--+} = M^{-++-}$$

$$= \frac{f^2}{4}\{\frac{(u-s)}{t-m^2}(1-z)^2 + \frac{(t-s)}{u-m^2}(1-z)^2$$

$$+ (1-z)^2 \quad \text{seagull} \quad \}$$

$$M^{++00} = M^{--00} = M^{00++} = M^{00--}$$

$$= \frac{f^2}{m^2}\Big\{ 4k^2\frac{(2E^2+m^2)}{s-m^2}z$$

$$+\frac{1}{2}\frac{[(4k^2(2E^2+m^2) - E^2(s-u))\sin^2\theta - 2sk^2(1-z)^2]}{t-m^2}$$

$$+\frac{1}{2}\frac{[(4k^2(2E^2+m^2) - E^2(s-t))\sin^2\theta - 2sk^2(1+z)^2]}{u-m^2}$$

$$-\frac{(2E^2+3k^2)}{3} - \frac{E^2}{2}P_2(z) \quad \text{seagull} \quad \Big\}$$

$$M^{+-00} = M^{-+00} = M^{00+-} = M^{00-+}$$

$$= \frac{f^2}{2m^2}\Big\{ \frac{[4k^2(2E^2+m^2) - E^2(s-u)]\sin^2\theta}{t-m^2}$$

$$+\frac{[4k^2(2E^2+m^2) - E^2(s-t)]\sin^2\theta}{u-m^2}$$

$$+E^2\sin^2\theta \quad \text{seagull} \quad \Big\}$$

$$M^{+++0} = M^{---0} = M^{+0++} = M^{-0--}$$
$$= -M^{++0+} = -M^{0+++} = -M^{--0-} = -M^{0---}$$
$$= f^2 \frac{i E \sin\theta}{2\sqrt{2}\, m} \left\{ \frac{-16k^2}{s - m^2} + \frac{(8k^2(3z-1)-(s-u)(1+z))}{t - m^2} + \frac{(8k^2(3z+1)+(s-t)(1-z))}{u - m^2} + (z-3) \quad \text{seagull} \right\}$$

$$M^{++-0} = M^{--+0} = M^{-0++} = M^{+0--}$$
$$= -M^{++0-} = -M^{0-++} = -M^{--0+} = -M^{0+--}$$
$$= f^2 \frac{i E \sin\theta}{2\sqrt{2}\, m} \left\{ \frac{16k^2}{s - m^2} + \frac{(t+4m^2)}{t - m^2}(1-z) + \frac{(u+4m^2)}{u - m^2}(1+z) + (z+3) \quad \text{seagull} \right\}$$

$$M^{+-+0} = M^{-+-0} = M^{+0+-} = M^{-0-+}$$
$$= -M^{+-0-} = -M^{0-+-} = -M^{-+0+} = -M^{0+-+}$$
$$= f^2 \frac{i E \sin\theta}{2\sqrt{2}\, m} \left\{ \frac{(t+4m^2)}{t - m^2}(1+z) - \frac{(u+4m^2)}{u - m^2}(1+z) + (1+z) \quad \text{seagull} \right\}$$

$$M^{+--0} = M^{-++0} = M^{-0+-} = M^{+0+-}$$
$$= -M^{+-0+} = -M^{-+0-} = -M^{0+-+} = -M^{0-++}$$
$$= f^2 \frac{i E \sin\theta}{2\sqrt{2}\, m} \left\{ \frac{(t+4m^2)}{t - m^2}(1-z) + \frac{(u+4m^2)}{u - m^2}(1-z) - (1-z) \quad \text{seagull} \right\}$$

The partial wave amplitudes are then projected out using the orthogonality and symmetry properties of the $d_{\lambda\lambda'}$ functions and the expansion (A.4). For convenience we define the following variables:

$x = \alpha_1 = 1 + 2m^2/4k^2$, $y = 1 + 2s/4k^2$ where $4k^2 = s-4m^2$

$$T_0^{++++} = \frac{2}{3}f^2\{-1 + (x+y)\left(Q_0(x)+\frac{3}{2}Q_1(x)+\frac{1}{2}Q_2(x)\right) + 8\left(Q_0(x)-Q_2(x)\right)$$

$$- 1 \text{ seagull} \quad \}$$

$$T_0^{+--} = \frac{2}{3}f^2\{-1 + (x+y)\left(Q_0(x) - \frac{3}{2}Q_1(x) + \frac{1}{2}Q_2(x)\right)$$

$$- 1 \text{ seagull} \quad \}$$

$$T_2^{+-++} = \sqrt{\frac{2}{3}}\, f^2\{\frac{1}{5} - (x-1)\left(Q_0(x) - \frac{10}{7}Q_2(x) + \frac{3}{7}Q_4(x)\right)$$

$$-\frac{1}{10} \text{ seagull} \quad \}$$

$$T_2^{+-+-} = \frac{f^2}{5}\{(x+y)\left(2Q_0(x)+\frac{4}{35}Q_2(x)+\frac{1}{175}Q_4(x)\right) - 2$$

$$+ 1 \quad \text{seagull} \quad \}$$

$$T_2^{+-+-} = T_2^{+--+}$$

$$T_0^{+00} = \frac{4}{3}f^2\{\frac{s}{m^2}\left(Q_0(x) - \frac{3}{2}Q_1(x) + \frac{1}{2}Q_2(x) - \frac{1}{8}\right)$$

$$+\frac{s+m^2}{s-4m^2}\left(Q_0(x) - Q_2(x)\right)$$

$$-\frac{(5s-12m^2)}{16m^2} \text{ seagull} \quad \}$$

$$T_2^{+-00} = f^2\, 2\sqrt{\frac{2}{3}} \left\{ \frac{1}{5}\left(\frac{E^2}{m^2}\,(x+y-4) - 2\right)\left(Q_0(x) - \frac{2}{35}Q_2(x) + \frac{3}{175}Q_4(x)\right) \right.$$

$$\left. - \frac{E^2}{5m^2} + \frac{E^2}{10m^2}\ \text{seagull} \right\}$$

$$T_1^{+++0} = f^2 \left(\frac{iE}{m}\right) \left\{ \frac{-8k^2}{3(s-m^2)} - \frac{1}{2}\ \text{seagull} \right\}$$

$$T_1^{++-0} = f^2 \left(\frac{iE}{m}\right) \left\{ \frac{8k^2}{3(s-m^2)} - \frac{1}{2}\ \text{seagull} \right\}$$

$$T_2^{+-+0} = f^2 \left(\frac{-iE}{2\sqrt{2}\,m}\right) \left\{ \frac{4}{5}(x+y-4)\left(Q_0(x) - \frac{1}{35}Q_2(x) - \frac{2}{175}Q_4(x)\right) - \frac{4}{5} \right.$$

$$\left. + \frac{2}{5}\ \text{seagull} \right\}$$

$$T_2^{+--0} = f^2 \left(\frac{-iE}{2\sqrt{2}\,m}\right) \left\{ \frac{4}{5}(x+y-4)\left(Q_0(x) - \frac{1}{35}Q_2(x) - \frac{2}{175}Q_4(x)\right) + \frac{4}{5} \right.$$

$$\left. - \frac{2}{5}\ \text{seagull} \right\}$$

Appendix D Loop Diagram Results

(i) Cutkosky's Rule

Take the bubble diagram as an example to work with, ρ mesons in the loop

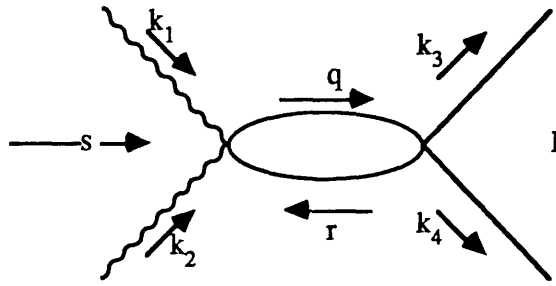

Fig. D.1

Diagram for $\gamma\gamma\rightarrow\rho\rho$ figure D.1 is constructed from Feynman rules 6 and 5/8 in appendix B. The basic integration has the form

$$\int d^4q \frac{1}{(q^2 - m^2 + i\varepsilon)(r^2 - m^2 + i\varepsilon)} = 2\pi^2 i \; I_1(s) \qquad (D.1)$$

When $s \geq 4m^2$ there is sufficient energy for ρ pair production, $s=4m^2$ is the threshold for the process $\gamma\gamma\rightarrow\rho\rho$. Consequently when $s \geq 4m^2$ the particles in the loop become 'real' and go on-shell, so the above diagram develops a cut starting at $s=4m^2$.

The imaginary part is calculated using Cutkosky's rule [68], the prescription is that each propagator "going on-shell" is replaced by a delta function:

$$\frac{1}{q^2 - m^2 + i\varepsilon} \rightarrow 2\pi i \, \delta(q^2 - m^2)$$

$$\frac{1}{r^2 - m^2 + i\varepsilon} \rightarrow 2\pi i \, \delta(r^2 - m^2) \qquad (D.2)$$

Applying this prescription to the integrand of equation (D.1) gives

$$\int d^4q\, 2\pi i\, \delta(q^2 - m^2)\; 2\pi i\, \delta(r^2 - m^2) = 2\pi^2 i\,(\,2i\, \mathrm{Im}\, I_1(s)\,)$$

$$\Rightarrow \quad \mathrm{Im}\, I_1(s) = \int d^4q\; \delta(q^2 - m^2)\, \delta(r^2 - m^2) \qquad \text{(D.3)}$$

The two delta functions project out

$$q^\alpha q_\alpha - m^2 = 0 \;\text{(a)}\;,\; q^\alpha q_\alpha - m^2 + k^2 - 2k^\alpha q_\alpha = 0 \;\text{(b)} \qquad \text{(D.4)}$$

The equations a and b above determine two of the four degrees of freedom in the loop momentum q^α

$$q^\alpha = (\frac{\sqrt{s}}{2}, \mathbf{q})\;,\; q = |q| = \sqrt{\frac{s}{4} - m^2}$$

$$\mathbf{q} = q\,(\sin\theta\cos\varphi,\, \sin\theta\sin\varphi,\, \cos\theta) \qquad \text{(D.5)}$$

Where θ and φ are the "polar-co-ordinates" for the solid angle integration over the two remaining degrees of freedom

$$d\Omega = \sin\theta\, d\theta\, d\varphi\;,\; 0 \le \theta \le \pi\;,\; 0 \le \varphi \le 2\pi$$

The integration (D.3) is best performed [83] by making a change of variable

$$d^4q = |q|\, \varepsilon\, d\varepsilon\, dq^0\, d\Omega\;,\; \text{where}\; \varepsilon^2 = |q|^2 + m^2 \qquad \text{(D.6)}$$

with the result that (D.3) is rewritten as

$$\mathrm{Im}\, I_1(s) = \int |q|\, \varepsilon\, d\varepsilon\, dq^0\, d\Omega\, \delta(\,(q^0)^2 - \varepsilon^2)\, \delta(\,(q^0)^2 - \varepsilon^2 + s - 2k^\alpha q_\alpha) \qquad \text{(D.7)}$$

the dq^0 integration is easily performed

$$\text{Using } \delta((q^0)^2 - \varepsilon^2) = \frac{1}{2\varepsilon}\delta(q^0 - \varepsilon)$$

$$\Rightarrow \text{Im } I_1(s) = \int \frac{|q|}{2}\, \delta(s - 2\sqrt{s}\, q^0)\, dq^0\, d\Omega$$

$$\Rightarrow \text{Im } I_1(s) = \frac{1}{8}\sqrt{1 - \frac{4m^2}{s}} \int d\Omega \qquad \text{(D.8)}$$

With the final result that

$$\text{Im } I_1(s) = \frac{\pi}{2}\sqrt{1 - \frac{4m^2}{s}} \qquad \text{(D.9)}$$

(ii) 'Deriving' the Dispersive Integral

Let f be an analytic function in the s-plane; assume that f has no poles at the origin and that as $s \to \infty$ then lim f(s)=0.

Cauchy's theorem staes that for any contour C

$$\frac{1}{2\pi i}\int_C \frac{f(s)}{s - s_0}\, ds = f(s_0) \qquad \text{(D.10)}$$

The contour C, see Fig.D.2 (overleaf), avoids the cut in the s-plane $[0,+\infty)$ along the real s-axis. Letting $R \to \infty$ and $r \to 0$ the integrals around C_R and $C_r \to 0$ leaving just the integrals above and below the cut, thus

$$f(s_0) = \frac{1}{2\pi i}\int_0^\infty \frac{f(s^+) - f(s^-)}{s - s_0}\, ds \qquad \text{(D.11)}$$

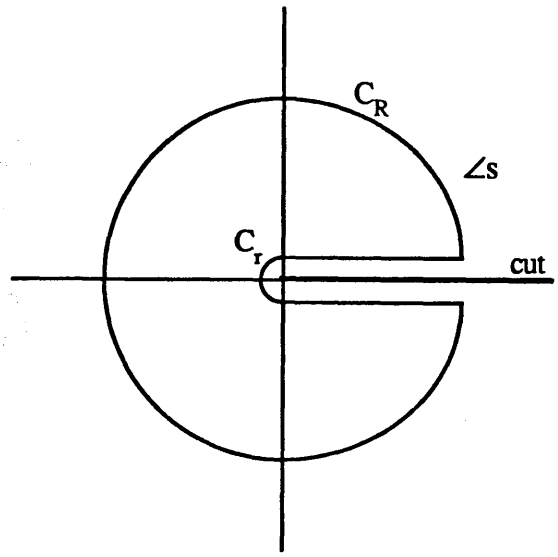

Figure D.2

C_R,C_r are circles of radius R,r with R>r.

Where $s^{\pm}$ is the value of s just above/below the cut, the numerator of the integrand of (D.11) is the discontinuity of the function f across the cut

$$f(s^{+}) - f(s^{-}) = 2\,i\,\mathrm{Im}\,f(s) \qquad \text{(D.12)}$$

So the integral may be rewritten as:

$$f(s_0) = \frac{1}{\pi}\int_0^{\infty} \frac{\mathrm{Im}\,f(s)\,ds}{s - s_0} \qquad \text{(D.13)}$$

In the case of the ρ loop diagrams the cut is in the interval $[4m^2,+\infty)$ along the real s-axis, there is no imaginary part for $s<4m^2$, therefore (D.12) is modified to

$$f(s) = \frac{1}{\pi}\int_{4m^2}^{\infty} \frac{\mathrm{Im}\,f(s')\,ds'}{s' - s - i\varepsilon}, \quad \varepsilon>0 \qquad \text{(D.14)}$$

In general given the imaginary part of a function f the real part can be reconstructed using equation (D.13) up to n-subtraction constants where

$$|\,f(s\to\infty)\,| \le \text{constant} \times |\,s\,|^{n-\alpha} \quad n=1,2,\ldots \text{ and } 0<\alpha<1 \qquad \text{(D.15)}$$

(iii) Bubble Diagram Integration Formulae

The integration formulae for the bubble diagram , figure D1 , are:

$$\int d^4q \frac{1;\, q^\alpha;\, q^\alpha q^\pi;\, q^\alpha q^\pi q^\beta}{(q^2 - m^2)(r^2 - m^2)} = 2\pi^2 i\, I_1(k^2) \quad \text{D.16} \; ; \; 2\pi^2 i\, I_2(k^2) \quad \text{D.17} \; ;$$

$$2\pi^2 i \left(g^{\alpha\pi} e_1(k^2) + k^\alpha k^\pi e_2(k^2) \right) \quad \text{D.18} \; ;$$

$$2\pi^2 i \left([g^{\alpha\pi} k^\beta]\, f_1(k^2) + k^\alpha k^\pi k^\beta\, f_2(k^2) \right) \quad \text{D.19}$$

With the notation $[g^{\alpha\pi}k^\beta]$ meaning symmmetrise the terms in the square brackets will be used throughout appendices D and E , ie

$$[\, g^{\alpha\pi}\, k^\beta \,] \equiv g^{\alpha\pi}k^\beta + g^{\alpha\beta}k^\pi + g^{\pi\beta}k^\alpha$$

Equation (D.16) has already been calculated, see (D.9), applying the same method to (D.17) in reducing the d^4q integration to a solid angle integration yields

$$k^\alpha \, \mathrm{Im}\, I_2(k^2) = \frac{1}{8} \sqrt{1 - \frac{4m^2}{k^2}} \int d\Omega \, q^\alpha \qquad \text{(D.20)}$$

contracting both sides of this equation with k^α, replacing kq with $k^2/2$ using equation(D.4) (ie as a result of the Cutkosky rule) one obtains

$$\mathrm{Im}\, I_2(k^2) = \frac{1}{16} \sqrt{1 - \frac{4m^2}{k^2}}\, 4\pi = \frac{1}{2}\, \mathrm{Im}\, I_1(k^2) \qquad \text{(D.21)}$$

The functions Im $e_j(k^2)$ and Im $f_j(k^2)$ are similarly obtained by contracting equations (D.17) and (D.18) with $g_{\alpha\pi}$ and k_α and applying the Cutkosky rules (ie equation (D.4)). This leads to sets of linear equations whose solutions are Im $e_j(k^2)$ and Im $f_j(k^2)$.

For example, by contracting (D.17) with k_α and then $g_{\alpha\pi}$ yields the following two equations, Im e_j and Im I_1 all functions of k^2:

$$\text{Im } e_1 + k^2 \text{ Im } e_2 = \frac{k^2}{4} \text{Im } I_1$$
$$4 \text{ Im } e_1 + k^2 \text{Im } e_2 = m^2 \text{ Im } I_1$$

which have the following solutions

$$\text{Im } e_1 = -\frac{(k^2 - 4m^2)}{12} \text{Im } I_1 \ , \ \text{Im } e_2 = \frac{(k^2 - m^2)}{3k^2} \text{Im } I_1 \qquad \text{(D.22)}$$

and similarly for the Im f_j

$$\text{Im } f_1 = \frac{1}{2} \text{Im } e_1 \ , \ \text{Im } f_2 = \frac{(k^2 - 2m^2)}{4k^2} \text{Im } I_1 \qquad \text{(D.22)}$$

The formulae D.9/14/21/22 are then used to reconstruct the real part of the loop integral, as discussed in chapter 5. For example

$$e_j(k^2) = \frac{1}{\pi} \int_{4m^2}^{\infty} \frac{dk'^2}{k'^2 - k^2 - i\varepsilon} \text{Im } e_j(k'^2) \qquad \text{(D.23)}$$

$$\frac{1}{x' - x - i\varepsilon} = P\frac{1}{x' - x} + i\pi\, \delta(x' - x) \qquad \text{(D.24)}$$

These formulae are valid for the s,t and u-channel diagrams. In the case of the s-channel diagram figure D.1 $k^\alpha = (k_1 + k_2)^\alpha$ and $k^2 = s$, the t-channel diagram below

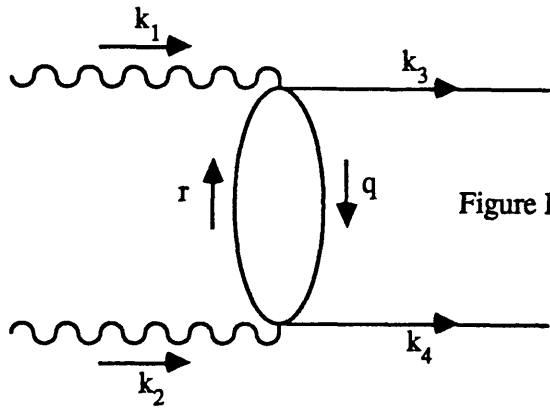

Figure D.3

is obtained from the s-channel by $k_2 \leftrightarrow -k_3$ and $\pi \leftrightarrow \beta$ interchange so that $k^\alpha = (k_2 - k_3)^\alpha$ and $k^2 = t$ (<0). Similarly for the u-channel diagram by $k_2 \leftrightarrow -k_4$ and $\pi \leftrightarrow \lambda$ interchange .

(iv) Triangle Diagram Integration Formulae

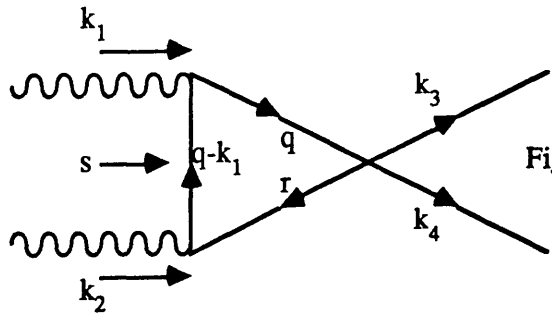

Fig D.4

Consider the triangle diagram above from which all other triangle diagrams can be obtained by suitable interchanges.

The integration formulae are:

$$\int d^4q \frac{1;\, q^\alpha;\, q^\alpha q^\pi}{(q^2 - m^2)((q-k)^2 - m^2)((q-k_1)^2 - m^2)} = 2\pi^2 i\, J(k^2,k_1) \qquad \text{(D.25)};$$

$$2\pi^2 i \left(k_1^\alpha a_1(k^2,k_1) + k^\alpha a_2(k^2,k_1)\right) \qquad \text{(D.26)};$$

$$2\pi^2 i \left(g^{\alpha\pi} b_1(k^2,k_1) + k_1^\alpha k_1^\pi b_2(k^2,k_1) + k^\alpha k^\pi b_3(k^2,k_1) + [k^\alpha k_1^\pi] b_4(k^2,k_1)\right) \qquad \text{(D.27)}$$

Applying Cutkosky's rule (D.2) to the two propagators which go on-shell at $\rho\rho$ threshold ($s=4m^2$) , then equation (D.25) becomes:

$$\int d^4q \frac{\delta(q^2 - m^2)\, \delta(r^2 - m^2)}{(q-k_1)^2 - m^2} = \text{Im}\, J(k^2,k_1) \qquad \text{(D.28)}$$

proceeding as before, in the bubble diagram case equations (D.3) to (D.8), this reduces to a solid angle integration

$$\text{Im}\, J(k^2,k_1) = \frac{1}{8}\sqrt{1 - \frac{4m^2}{k^2}} \int d\Omega \frac{1}{k_1^2 - 2k_1^\alpha q_\alpha} \qquad \text{(D.29)}$$

Defining z_1 to be the cosine of the angle between **k** and**q** ,then the denominator of (D.29) is rewritten as

$$k_1^2 - 2k_1^\alpha q_\alpha = -2\,|\mathbf{k}|\,|\mathbf{q}|\,(\alpha - z_1) \qquad \text{(D.30)}$$

where $k_1^\alpha = (k_1^\circ, \mathbf{k})$ and

$$\alpha = \frac{2k_1^\circ q^\circ - k_1^2}{2\,|\mathbf{k}|\,|\mathbf{q}|} \qquad \text{(D.31)}$$

So that the solid angle integration now has the form:

$$\text{Im } J(k^2,k_1) = \frac{-1}{8\sqrt{k^2}\,|k|}\int \frac{d\Omega}{\alpha - z_1} \qquad \text{(D.32)}$$

Which is easily integrated to give

$$\text{Im } J(k^2,k_1) = \frac{-\pi}{2\sqrt{k^2}\,|k|} Q_0(\alpha) \qquad \text{(D.33)}$$

and where $Q_0(z)$ is defined in appendix A.

Dropping the explicit (k^2,k_1) dependence, for the time being, of the functions J,a_i and b_i. Consider equation (D.26), apply the Cutkosky rule to give

$$\int d^4q \frac{\delta(q^2 - m^2)\,\delta(r^2 - m^2)}{(q-k_1)^2 - m^2}\, q^\alpha = k_1^\alpha \text{ Im } a_1 + k^\alpha \text{ Im } a_2 \qquad \text{(D.34)}$$

contract (D.34) with k_α , then substitute $kq = k^2/2$ using (D.4) and use (D.28) to give

$$\frac{k^2}{2}\text{Im } J = kk_1 \text{ Im } a_1 + k^2 \text{ Im } a_2 \qquad \text{(D.35)}$$

Contract (D.34) with $-2k_{1\alpha}$ and add this to k_1^2 multiplying equation (D.28) :

$$\int d^4q \frac{\delta(q^2 - m^2)\,\delta(r^2 - m^2)}{(q-k_1)^2 - m^2}\,(k_1^2 - 2k_1q) = k_1^2 \text{ Im } J - 2\left(k_1^2 \text{ Im } a_1 + kk_1 \text{ Im } a_2\right) \qquad \text{(D.36)}$$

The denominator is thus cancelled giving:

$$\text{Im } I_1 = k_1^2\left(\text{Im } J - 2\text{Im } a_1\right) - 2kk_1 \text{ Im } a_2 \qquad \text{(D.37)}$$

The linear equations (D.35) and (D.37) are easily solved to give:

$$\text{Im } a_1 = \frac{-k^2 \text{ Im } I_1 + k^2(k_1^2 - kk_1) \text{ Im } J}{2(k^2k_1^2 - (kk_1)^2)}$$

$$\text{Im } a_2 = \frac{kk_1 \text{ Im } I_1 + k_1^2(k^2 - kk_1) \text{ Im } J}{2(k^2k_1^2 - (kk_1)^2)} \qquad \text{(D.38)}$$

The same procedure is applied to equation (D.27) to obtain the coeficients $\text{Im}b_i$ as functions of k^2, k_1^2, kk_1, ImJ and $\text{Im}I_1$. However this time , since there are more coefficients to find the algebraic programming system REDUCE is used.

In fact use of REDUCE is essential for obtaining these coefficients and those for the integrals with 3 and 4 powers of loop momentum in the numerator (Im c_i and Im d_i respectively).

$$\text{Im } b_1 = \frac{k^2(k_1^2 - kk_1) \text{ Im } I_1 + \left(k^2k_1^2(2kk_1 - k_1^2 - k^2) - 4m^2(kk_1)^2\right) \text{Im } J}{8(k_1^2k^2 - (kk_1)^2)}$$

$$\text{Im } b_2 = \frac{1}{8(k_1^2k^2(k_1^2k^2 - 2(kk_1)^2) + (kk_1)^4)} \{ 3(kk_1 - k_1^2)(k^2)^2 \text{Im } I_1$$

$$+k^2\left(k^2k_1^2(3k_1^2 - 6kk_1 + k^2 - 4m^2) + 2(kk_1)^2(k^2 + 2m^2)\right) \text{Im } J \}$$

$$\text{Im } c_1 = \frac{k^2(kk_1 - k_1^2) \text{ Im } b_1 - k^2 \text{ Im } e_1}{2((kk_1)^2 - k_1^2k^2)}$$

(D.39)

To perform the dispersive integration the functions J, a_i and b_i must be expressed in terms of the Mandelstam variables s,t,u.

For exmple take the basic triangle diagram figure D.4 , called (12 (34)) in the notation of chapter 6, then we substitute the following

$$k^2 = s \ , \ |\mathbf{k}| = \frac{\sqrt{s}}{2} \ , \ kk_1 = \frac{s}{2} \ \text{and} \ k_1^2 = 0 \ \text{(photon on-shell)}$$

into the expressions for J, a_i and b_i. With the result that

$$\text{Im } J(s,k_1) = -\frac{\pi}{s} Q_0(\alpha_1) \ , \ \alpha_1 = \sqrt{\frac{s}{s - 4m^2}} \qquad \text{(D.40)}$$

$$\text{Im } a_1(s,k_1) = \frac{2}{s} \text{Im } I_1(s) + \text{Im } J(s,k_1)$$

$$\text{Im } a_2(s,k_1) = -\frac{1}{s} \text{Im } I_1(s)$$

$$\text{Im } b_1(s,k_1) = \frac{1}{4} \text{Im } I_1(s) + \frac{m^2}{2} \text{Im } J(s,k_1) \qquad \text{(D.41)}$$

The integral coefficients corresponding to the diagram (34 (12))

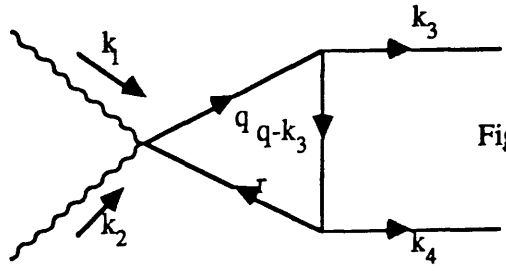

Fig D.5

are easily obtained by those derived for the (12 (34)) diagram simply by the change $k_1 \rightarrow k_3 = (\sqrt{s}/2, \mathbf{k}')$, the coefficients are still functions of s but have a different form because k_3 is the four momentum of a massive particle. So one uses

$k^2 = s$, $|\mathbf{k}'| = \sqrt{\frac{s}{4} - m^2}$, $kk_3 = \frac{s}{2}$ and $k_3^2 = m^2$ (ρ meson on-shell)

$$\text{Im } J(s,k_3) = \frac{-\pi}{s - 4m^2}\sqrt{1 - \frac{4m^2}{s}}\, Q_0(\alpha_2) \qquad \text{(D.42)}$$

$$\alpha_2 = 1 + \frac{2m^2}{s - 4m^2} \qquad \text{(D.43)}$$

and equation (D.38) gives

$$\text{Im } a_1(s,k_3) = \frac{2}{s - 4m^2}\text{Im } I_1(s) + \frac{s - 2m^2}{s - 4m^2}\text{Im } J(s,k_3)$$

$$\text{Im } a_2(s,k_3) = \frac{-1}{s - 4m^2}\text{Im } I_1(s) - \frac{m^2}{s - 4m^2}\text{Im } J(s,k_3)$$

$$\text{Im } b_1(s,k_3) = \frac{s - 2m^2}{4(s - 4m^2)}\text{Im } I_1(s) + \frac{(s - 3m^2)m^2}{2(s - 4m^2)}\text{Im } J(s,k_3) \qquad \text{(D.44)}$$

To calculate the functions ImJ, Ima_i and Imb_i for the t or u-channel diagrams, equations (6.4b&c) requires a little more care. For instance consider the (13 (24)) triangle diagram

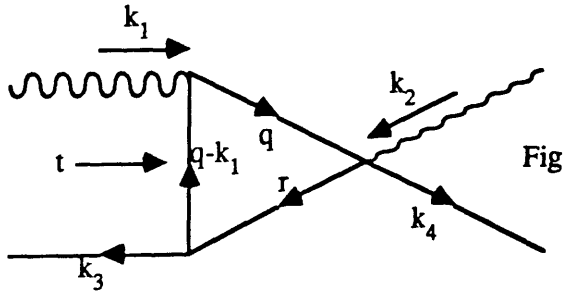

Fig D.6

The function Im$J(k^2,k_1)$ is calculated in the centre of mass frame of the process

$$\gamma(k_1) + \rho(-k_3) \longrightarrow \gamma(-k_2) + \rho(k_4) \qquad \text{(D.45)}$$

So that conservation of four momentum now reads

$$k_1 - k_3 = k = k_4 - k_2 \qquad (D.46)$$

and $k^2 = s$ the centre of mass energy squared for the process (D.45)

$$k_1^\alpha = (k_1^o, \mathbf{k}) \ , \ k_1^2 = 0 \Rightarrow |\mathbf{k}| = k_1^o = \frac{s - m^2}{2\sqrt{s}} \qquad (D.47)$$

Putting this into equation (D.33) gives:

$$\text{Im } J(s,k_1) = \frac{-\pi}{s - m^2} Q_0(\alpha_1) \qquad (D.48)$$

Finally to obtain the expression for ImJ in the centre of mass frame of the process

$$\gamma(k_1) + \gamma(k_2) \longrightarrow \rho(k_3) + \rho(k_4) \qquad (D.49)$$

the interchange $s \leftrightarrow t$ (ie $k_2 \leftrightarrow -k_3$) is made so that finally

$$\text{Im } J(t,k_1) = \frac{-\pi}{t - m^2} Q_0(\alpha_3) \ , \ \alpha_3 = \sqrt{\frac{t}{t - 4m^2}} \qquad (D.50,51)$$

The dispersive integral then approximates a reconstruction of the function:

$$J(t,k_1) = \frac{1}{\pi} \int_{4m^2}^{\infty} \frac{\text{Im}J(t',k_1)\, dt'}{t' - t - i\varepsilon} \qquad (D.52)$$

Noting that for the process (D.50) $t<0$ and so the function $J(t,k_1)$ is real, there are no poles.

The rest of the functions Ima_i and Imb_i are easily calculated from the formulae (D.38) and (D.39) simply by, noting that for the (13 (24)) diagram (say) $k=k_1 - k_3$, substituting the following

$$k^2 = t \ , \ k_1^2 = 0 \ , \ kk_1 = \frac{t - m^2}{2}$$

without the need to go to some other process and then convert back by $s \leftrightarrow t$ interchange.

Appendix E Box Diagram Results

(i) Integration Formulae for Box Diagram (1234)

The integration formulae for the box diagram (1234),figure 5.3, are:

$$\int d^4q \frac{1\ ;\ q^\alpha\ ;\ q^\alpha q^\pi}{(q^2-m^2)((q-k_3)^2-m^2)(r^2-m^2)((q-k_1)^2-m^2)} =$$

$$2\pi^2 i\ \Psi(s,t) \qquad \text{(E.1)};$$

$$2\pi^2 i \left(k^\alpha V_0(s,t) + k_1^\alpha V_1(s,t) + k_3^\alpha V_3(s,t) \right) \qquad \text{(E.2)};$$

$$2\pi^2 i \left(g^{\alpha\pi} Ws,t) + k_1^\alpha k_1^\pi\ W_{11}(s,t) + k_3^\alpha k_3^\pi W_{33}(s,t) + k^\alpha k^\pi W_{00}(s,t) \right.$$

$$\left. +[k^\alpha k_1^\pi]\ W_{01}(s,t) + [k^\alpha k_3^\pi]\ W_{03}(s,t) + [k_1^\alpha k_3^\pi]\ W_{13}(s,t) \right)$$

(E.3)

With {X(s,t)} and {Z(s,t)} the coefficients of the integrals with three and four powers of loop momentum respectively in the numerator of the integrand, using a notation that is a natural continuation of (E.2) and (E.3) above, but not given in full form here for lack of space. For example Z(s,t) is the coefficient of the $[g^{\alpha\pi}\, g^{\beta\lambda}]$ term whilst $Z_{11}(s,t)$ is the coefficient of the $[g^{\alpha\pi}\, k_1{}^\beta\, k_1{}^\lambda]$ term.

Proceeding as before with the bubble diagram calculation in appendix D, the Cutkosky rules are applied to the integrand of equation (E.1) giving:

$$\text{Im}\ \Psi(s,t) = \frac{q}{4\sqrt{s}} \int d\Omega \frac{1}{((q-k_1)^2-m^2)((q-k_3)^2-m^2)} \qquad \text{(E.4)}$$

then applying (D.4) to the denominator means it can be rewritten using

$$(q-k_1)^2 - m^2 = -2qk\,(\alpha_1 - z_1) \qquad \text{(E.5a)}$$

$$(q-k_3)^2 - m^2 = -2qk'(\alpha_2 - z_2) \qquad \text{(E.5b)}$$

where $q^\alpha = (\sqrt{s}/2\,,\,\mathbf{q})$, $q = |\mathbf{q}|$ and k_1 and k_3 as given in appendix A for the reaction $\gamma\gamma \to \rho\rho$.

$$z_1 = \frac{\mathbf{k}.\mathbf{q}}{kq}\,,\quad z_2 = \frac{\mathbf{k}'.\mathbf{q}}{k'q} \qquad \text{(E.6a)}$$

$$\alpha_1 = \frac{s - 2k_1^2}{4kq}\,,\quad \alpha_2 = \frac{s - 2k_3^2}{4k'q} \qquad \text{(E.6b)}$$

Using $k = \frac{\sqrt{s}}{2}$ and $k' = \sqrt{\frac{s}{4} - m^2}$ one obtains

$$\alpha_1 = \sqrt{\frac{s}{s - 4m^2}} \quad \text{and} \quad \alpha_2 = 1 + \frac{2m^2}{s - 4m^2} \qquad \text{(E.7)}$$

and z is related to the Mandelstam variables as

$$z = \frac{t - u}{4kk'}\,,\quad s+t+u = 2m^2$$

So that (E.4) simplifies to

$$\text{Im}\,\Psi(s,t) = \frac{1}{16\sqrt{s}\,q\,k\,k'} \int \frac{d\Omega}{(\alpha_1 - z_1)(\alpha_2 - z_2)} \qquad \text{(E.8)}$$

The easiest way to do the solid angle integration in (E.8) above is to use the expansion (A.4), so that

$$\text{Im}\,\Psi(s,t) = \frac{1}{16\sqrt{s}\,qkk'} \sum_{n=0}^{\infty} (2n+1)\,Q_n(\alpha_2) \int d\Omega\, \frac{P_n(z_2)}{\alpha_1 - z_1} \qquad \text{(E.9)}$$

(recall that $P_n(z)$ and the associated $Q_n(z)$ are defined in appendixA)

The two 'internal' scattering angles θ_1 and θ_2 ($z_1 = \cos\theta_1$ and $z_2 = \cos\theta_2$) are

related (the same situation as the two body unitarity in chapter 7, equation (7.9))

$$z_2 = z\,z_1 + (1-z_1)^{\frac{1}{2}}(1-z^2)^{\frac{1}{2}}\cos\varphi \qquad \text{(E.10)}$$

where z is the cosine of the 'external' scttering angle (4.5). Thus $P_n(z_2)$ can be rewritten using a standard identity, equation (A.3), the integration over $\cos(m\varphi)$ vanishes for all m so the final result is :

$$\text{Im}\,\Psi(s,t) = \frac{4\pi}{16\sqrt{s}\,qkk'}\sum_{n=0}^{\infty}(2n+1)\,Q_n(\alpha_1)\,Q_n(\alpha_2)\,P_n(z) \qquad \text{(E.11)}$$

Barut [84] shows that the integration (E.8) can be done in closed form:

$$\int \frac{d\Omega}{(\alpha_1 - z_1)(\alpha_2 - z_2)} = \frac{4\pi}{\sqrt{\lambda}}\,Q_0\left(\frac{\alpha_1\alpha_2 - z}{\sqrt{\lambda}}\right) \qquad \text{(E.12)}$$

$$\text{where } \lambda \equiv \alpha_1^2 + \alpha_2^2 + z^2 - 1 - 2\alpha_1\alpha_2 z \qquad \text{(E.13)}$$

This can also be obtained by simply making use of the following identity , from Whittaker and Watson [85],

$$\sum_{n=0}^{\infty}(2n+1)\,Q_n(\alpha_1)\,Q_n(\alpha_2)\,P_n(z) = \frac{1}{\sqrt{\lambda}}\,Q_0\left(\frac{\alpha_1\alpha_2 - z}{\sqrt{\lambda}}\right) \qquad \text{(E.14)}$$

A slightly different method of calculation is adopted for the higher order integrals (equations (E.2),(E.3) etc) to that used for the bubble and triangle diagrams. Using the four vectors k,k_1,k_3 to determine a set of linear equations of which {ImV(s,t)} , {ImW(s,t)} etc are the solutions , introduces 'spurious cuts' in the t-channel , thus making the single dispersion relation approach unviable. However if the Legendre expansion, of the form (E.11), is used then the coefficients have a relatively simple form. In which case it seems to be only necessary when

calculating the numerical value (and so z is constant) of the imaginary part of the coefficient to take the first non-zero term in each expansion. It is not at all clear that this remains true when one applies the single dispersion relation and z is no longer constant but a function of s and t.

Consider an example of how the coefficients were evaluated. Apply the Cutkosky rules to (E.2) to give

$$\frac{1}{16q\sqrt{s}\ kk'}\int d\Omega \frac{q^{\alpha}}{(\alpha_1 - z_1)(\alpha_2 - z_2)} = k^{\alpha}ImV_0 + k_1^{\alpha}ImV_1 + k_3^{\alpha}ImV_3 \qquad (E.15)$$

We define the following four vectors to project out the components of q^{α}

$$P_x^{\alpha} = (0,1,0,0)\ ,\ P_y^{\alpha} = (0,0,1,0)\ ,\ P_z^{\alpha} = (0,0,0,1) \qquad (E.16a)$$

and note that we are working in the particular frame of reference in which

$$\begin{aligned} k^{\alpha} &= (\sqrt{s}, \mathbf{0})\ , \\ k_1^{\alpha} &= (\frac{\sqrt{s}}{2}, \mathbf{k})\ ,\ \mathbf{k} = (0,0,k) \\ k_3^{\alpha} &= (\frac{\sqrt{s}}{2}, \mathbf{k}')\ ,\ \mathbf{k}' = (k_x', 0, k_y') \end{aligned} \qquad (E.16b)$$

Contract both sides of equation (E.15) with the $P_{x,y,z}$ and k^{α} in turn giving a set of four equations, and recalling that the Cutkosky rules (D.4) means that $kq=k^2/2$ and that $kk_1=kk_3=s/2$

$$\frac{1}{16\sqrt{s}\ qkk'}\int d\Omega \frac{q_x}{(\alpha_1 - z_1)(\alpha_2 - z_2)} = k_x' ImV_3 \qquad (E.17a)$$

$$\frac{1}{16\sqrt{s}\ qkk'}\int d\Omega \frac{q_y}{(\alpha_1 - z_1)(\alpha_2 - z_2)} = 0 \qquad (E.17b)$$

$$\frac{1}{16\sqrt{s}\ qkk'}\int d\Omega \frac{q_z}{(\alpha_1 - z_1)(\alpha_2 - z_2)} = k\ ImV_1 + k_z' ImV_3 \qquad (E.17c)$$

$$\frac{1}{16\sqrt{s}\ qkk'}\int d\Omega \frac{k^{\alpha}q_{\alpha}}{(\alpha_1 - z_1)(\alpha_2 - z_2)} = k^2 ImV_0 + kk_1 ImV_1 + kk_3 ImV_3 \qquad (E.17d)$$

Using the expansion of $(\alpha_2 - z_2)^{-1}$ and $P_n(z_2)$ used in the evaluation of (E.9) the basic integrand is rewritten as

$$\int \frac{d\Omega}{(\alpha_1 - z_1)(\alpha_2 - z_2)} = \sum_{n=0}^{\infty}(2n+1)\, Q_n(\alpha_2) \left\{ P_n(z) \int d\Omega \frac{P_n(z_1)}{\alpha_1 - z_1} + 2 \sum_{m=1}^{\infty} \frac{\Gamma(n-m+1)}{\Gamma(n+m+1)} P_n^m(z) \int d\Omega \frac{P_n^m(z_1)\cos(m\varphi)}{\alpha_1 - z_1} \right\} \tag{E.18}$$

Noting that it follows from the definitions of z_1 and z_2 (E.6a) and the components of **k** and **k'** (E.16b) that in component form **q** is

$$\mathbf{q} = q\,(\sin\theta_1 \cos\varphi\,,\ \sin\theta_1 \sin\varphi\,,\ \cos\theta_1)$$

The LHS side of (E.17b) is zero because of the $\sin\varphi\, d\varphi$ integration, this then leaves three equations to determine three unknowns. The linear equations (E.17a,c,d) are solved, giving:

$$\mathrm{Im}V_0(s,t) = \frac{1}{2}\left\{ \frac{1}{16\sqrt{s}\, qkk'} \int d\Omega \frac{(1 - k^{-1}(q_z - q_x\cot\theta) - k_x'^{-1} q_x)}{(\alpha_1 - z_1)(\alpha_2 - z_2)} \right\} \tag{a}$$

$$\mathrm{Im}V_1(s,t) = \frac{k^{-1}}{16\sqrt{s}\, qkk'} \int d\Omega \frac{(q_z - q_x\cot\theta)}{(\alpha_1 - z_1)(\alpha_2 - z_2)} \tag{b}$$

$$\mathrm{Im}V_3(s,t) = \frac{k_x'^{-1}}{16\sqrt{s}\, qkk'} \int d\Omega \frac{q_x}{(\alpha_1 - z_1)(\alpha_2 - z_2)} \tag{c}$$

(E.19)

Using the expansion (E.18) and performing the $d\varphi$ integration in equation (c) above yields:

$$\mathrm{Im}V_3(s,t) = \frac{2\pi\, qk_x'^{-1}}{16\sqrt{s}\, qkk'} \sum_{n=1}^{\infty}(2n+1)\frac{(n-1)!}{(n+1)!} Q_n(\alpha_2) P_n^1(z) \int_{-1}^{1} dz_1 \frac{(1-z_1^2)^{\frac{1}{2}} P_n^1(z_1)}{\alpha_1 - z_1}$$

$$\mathrm{Im}V_3(s,t) = \frac{2\pi\, qk_x'^{-1}}{16\sqrt{s}\, qkk'} \left\{ \frac{3}{2!} Q_1(\alpha_2)\, P_1^1(z) \frac{4}{3} \left(Q_0(\alpha_1) - Q_2(\alpha_1) \right) \right.$$

$$+ \frac{5}{3!} Q_2(\alpha_2)\, P_2^1(z) \frac{12}{5} \left(Q_1(\alpha_1) - Q_3(\alpha_1) \right)$$

$$\left. + \ldots \right\} \qquad \text{(E.20)}$$

Evaluating at $\sqrt{s} \approx 1.6$GeV one finds that

$$Q_1(\alpha_2) \left(Q_0(\alpha_1) - Q_2(\alpha_1) \right) \gg Q_2(\alpha_2) \left(Q_1(\alpha_1) - Q_3(\alpha_1) \right)$$

Provided that z remains constant it is thus reasonable to take the first term in the curly brackets of (E.20) and usimg the facts that

$$P_1^1(z) = \sqrt{1 - z^2} \text{ and } k_x' = k' \sqrt{1 - z^2}$$

and expressing k and k' in terms of s one obtains

$$\mathrm{Im}V_3(s,t) = \frac{2\pi}{s\,(s - 4m^2)} Q_1(\alpha_2) \left(Q_0(\alpha_1) - Q_1(\alpha_1) \right) \qquad \text{(E.21)}$$

which is independent of z and hence independent of t. Similarly for $\mathrm{Im}V_1(s,t)$

$$\mathrm{Im}V_1(s,t) = \frac{2\pi\, \alpha_1}{s^2} Q_0(\alpha_2)\, Q_1(\alpha_1) \qquad \text{(E.22)}$$

Exactly the same methods are used to derive the rest of the integral formulae coefficients, again using the approximation of taking the first non-zero term in the expansion $Q_n(\alpha_2)$ this seems to be valid in that range of s values that we are interested. But when z becomes a function of s and t, such as when we try to reconstruct the real part by applying a single dispersion relation to s, then this scheme is almost certain to fail as there will probably be higher order terms making significant contributions.

$$\mathrm{Im}W(s,t) = \frac{-\pi}{6s} Q_0(\alpha_2)\big(Q_0(\alpha_1) - Q_2(\alpha_1)\big) \qquad \text{(a)}$$

$$\mathrm{Im}W_{11}(s,t) = \frac{\pi}{s^2} Q_0(\alpha_2)\big((3\alpha_1^2 - 1)Q_0(\alpha_1) - 3\alpha_1\big) \qquad \text{(b)}$$

$$\mathrm{Im}W_{33}(s,t) = \frac{4\pi}{3s(s - 4m^2)} Q_2(\alpha_2)\Big(Q_0(\alpha_1) - \frac{10}{7} Q_2(\alpha_1) + \frac{3}{7} Q_4(\alpha_1)\Big) \qquad \text{(c)}$$

$$\mathrm{Im}W_{13}(s,t) = \frac{2\pi}{s\,(s - 4m^2)\,\alpha_1} Q_1(\alpha_2)\big(Q_1(\alpha_1) - \alpha_1 Q_2(\alpha_1) \big) \qquad \text{(d)}$$

$$\mathrm{Im}\,Z = \frac{\pi\,(s - 4m^2)}{120\,s} Q_0(\alpha_2)\Big(Q_0(\alpha_1) - \frac{163}{70} Q_2(\alpha_1) + \frac{3}{7} Q_4(\alpha_1)\Big) \qquad \text{(e)}$$

$$\mathrm{Im}\,Z_{11} = \frac{-2\pi\,(s - 4m^2)}{28s^2} Q_0(\alpha_2)\big(Q_2(\alpha_1) - Q_4(\alpha_1)\big) \qquad \text{(f)}$$

$$\mathrm{Im}\,Z_{33} = \frac{3\pi}{56s} Q_2(\alpha_2)\Big(Q_0(\alpha_1) + \frac{20}{9} Q_2(\alpha_1) - \frac{12}{11} Q_4(\alpha_1) + \frac{20}{99} Q_6(\alpha_1)\Big) \qquad \text{(g)}$$

$$\mathrm{Im}\,Z_{1133} = \frac{\pi}{2\,s^2} Q_2(\alpha_2)\Big(Q_0(\alpha_1) + \frac{20}{21} Q_2(\alpha_1) - \frac{120}{77} Q_4(\alpha_1) + \frac{20}{33} Q_6(\alpha_1)\Big) \qquad \text{(h)}$$

(E.23)

These are the coefficients required for the calculation of the imaginary part of the $\gamma\gamma \to \rho\rho$ loop amplitudes.

The functions above (E.23) are all nominally functions of s and t but in the approximation taken the z (and hence t) dependence has disappeared. Thus these are also the integral formulae coefficients for the (2134) box diagram, which is obtained from the (1234) diagram by $k_1 \leftrightarrow k_2$, $t \leftrightarrow u$ and $\alpha \leftrightarrow \pi$ interchange.These are the coefficients required for the calculation of the imaginary part of the $\gamma\gamma \to \rho\rho$ loop (box diagram) amplitudes.

(ii) Spectral Function Im(ImΨ(s,t))

The function Im(ImΨ(s,t)) can be calculated by applying Cutkosky's rule to each of the four propagators in the box diagram (1234), making a change of variables and doing the integration. This is done in reference [83].

An easier method, is to follow Barut [84] and Mandelstam [86] in noting that the function

$$\int \frac{d\Omega}{(\alpha_1 - z_1)(\alpha_2 - z_2)} = \frac{4\pi}{\sqrt{\lambda}} Q_0\left(\frac{\alpha_1\alpha_2 - z}{\sqrt{\lambda}}\right) \qquad \text{(E.12)}$$

is an analytic function of z except for the cut $[z_c,+\infty)$, where

$$z_c := \alpha_1\alpha_2 + (\alpha_1^2 - 1)^{\frac{1}{2}} (\alpha_2^2 - 1)^{\frac{1}{2}} \qquad \text{(E.24)}$$

and the discontinuity of the function ImΨ(s,t) across this cut is easily calculated, noting that z is linearly related to t:

$$\frac{1}{2i}\{ \mathrm{Im}\Psi(s,z+i\varepsilon) - \mathrm{Im}\Psi(s,z-i\varepsilon) \} = \frac{4\pi^2}{16\sqrt{s}\, qkk'} \frac{1}{\sqrt{\lambda}}$$

Thus the double dispersive spectral function is :

$$\mathrm{Im}(\,\mathrm{Im}\Psi(s,t)\,) = \begin{cases} \dfrac{2\pi^2}{s(s-4m^2)\sqrt{\lambda}} & z > z_c \\ 0 & z < z_c \end{cases} \qquad \text{(E.25)}$$

Appendix F SU(3) Predictions for $\gamma\gamma \to VV$

We wish to calculate the relative strengths of the RV_1V_2 and $R\gamma\gamma$ couplings according to SU(3), where R is a resonance and V_1V_2 are the vector mesons ρ, ω, k* and φ.

The vector meson matrix M is

$$M = \begin{bmatrix} A & \rho^+ & k^{*+} \\ \rho^- & B & k^{*o} \\ k^{*-} & \overline{k^{*o}} & \varphi \end{bmatrix} \qquad \text{(F.1)}$$

$$A = \frac{1}{\sqrt{2}}(\rho^0 + \omega) \quad , \quad B = \frac{1}{\sqrt{2}}(-\rho^0 + \omega) \qquad \text{(F.2)}$$

Ignoring the off-diagonal terms the intermediate (pseudoscalar) resonance matrix is

$$M = \begin{bmatrix} a & . & . \\ . & b & . \\ . & . & s \end{bmatrix} \qquad \text{(F.3)}$$

$$a = \frac{1}{\sqrt{2}}(v^0 + \sigma) \quad , \quad b = \frac{1}{\sqrt{2}}(-v^0 + \sigma) \qquad \text{(F.4)}$$

The 'effective Lagrangian' for the RM_1M_2 vertex is

$$L_{RMM} = \mathrm{Tr}\{ R[M_1, M_2^\dagger]_+ \} \qquad \text{(F.5)}$$

where the subscript is the four momentum label of the vector meson and strictly speaking there should be a coupling costant in front of the trace in (F.5) but we can set this to =1 since only relative couplings are required.

Considering the diagonal elements only of R, these are the only ones that couple to $\gamma\gamma$, one obtains

$$L_{RVV} = \sqrt{2}\,\sigma\rho_1^0\rho_2^0 + \sqrt{2}\,\sigma(\rho_1^+\rho_2^- + \rho_2^+\rho_1^-)$$

$$+ \sqrt{2}\,\sigma\omega_1\omega_2 + \sqrt{2}\,v^0(\omega_1\rho_2^0 + \omega_2\rho_1^0)$$

$$+ \frac{1}{\sqrt{2}}(v^0 + \sigma + \sqrt{2}s)\,(k^{*+}(1)\,k^{*-}(2) + k^{*-}(1)\,k^{*+}(2))$$

$$+ \frac{1}{\sqrt{2}}(-v^0 + \sigma + \sqrt{2}s)\,(k^{*0}(1)\,\overline{k^{*0}}(2) + k^{*0}(2)\,\overline{k^{*0}}(1))$$

$$+ \; 2s\varphi_1\varphi_2 \qquad \text{(F.6)}$$

The particle identity (1 or 2) is written as an argument and not a subscript for the k*k* system.

Under SU(3) the electromagnetic current j_{em} transforms as:

$$j_{em}^{\alpha} = j_3^{\alpha} + \frac{1}{\sqrt{3}} j_8^{\alpha} \qquad \text{(F.7)}$$

j_3 is the Isovector component and j_8 the Isosinglet component

The Gell-Mann matrices λ_3 and λ_8 are

$$\lambda_3 = \text{diag}(1,-1,0) \quad , \quad \lambda_8 = \frac{1}{\sqrt{3}}\,\text{diag}(1,1,-2)$$

which implies that j_{em} has the following form:

$$j_{em}^{\alpha} = \frac{2}{3}\,\text{diag}(2,-1,-1)\,A^{\alpha} \qquad \text{(F.8)}$$

Thus the effective Lagrangian for $R\gamma\gamma$ is

$$L_{R\gamma\gamma} = \text{Tr}\{\, R[j_{em}^{\alpha}(1)\,,\, j_{em\alpha}(2)]_+ \,\} \qquad \text{(F.9)}$$

which simplifies to:

$$L_{R\gamma\gamma} = \frac{\sqrt{2}}{9}(3v^0 + 5\sigma + \sqrt{2}s)\,A_{\alpha}A^{\alpha} \qquad \text{(F.10)}$$

The couplings may now be read off from (F.6) and (F.10)

$$g_{\sigma\rho^0\rho^0} = g_{\sigma\rho^+\rho^-} = g_{\sigma\omega\omega} = g_{v^0\omega\rho^0} = \sqrt{2}$$

$$g_{s\varphi\varphi} = 2$$

and the following couplings to the k*'s

$$g_{v^{o}+-} = -g_{v^{o}00} = g_{\sigma+-} = g_{\sigma 00} = \frac{1}{\sqrt{2}}$$

$$g_{s+-} = g_{s00} = 1 \qquad \text{(F.11)}$$

The two-photon couplings are

$$g_{\sigma\gamma\gamma} = 5 \ , \ g_{v^{o}\gamma\gamma} = 3 \ , \ g_{s\gamma\gamma} = \sqrt{2} \qquad \text{(F.12)}$$

The couplings are then used to calculate ratios of the cross sections for $\gamma\gamma \rightarrow VV$, assuming that the underlying mechanism is pseudoscalar meson exchange.

For example the process $\gamma\gamma \rightarrow \rho\rho$ has the following amplitudes

$$M(\gamma\gamma \rightarrow \rho^{0}\rho^{0}) = g_{\sigma\rho^{o}\rho^{o}} g_{\sigma\gamma\gamma} T \frac{1}{\sqrt{2}}$$

$$M(\gamma\gamma \rightarrow \rho^{+}\rho^{-}) = g_{\sigma\rho^{+}\rho^{-}} g_{\sigma\gamma\gamma} T \qquad \text{(F.13)}$$

The $1/\sqrt{2}$ that is present for the neutral channel is because there are two identical outgoing particles, T represents the 'basic amplitude' which we do not know and thus has to be eliminated.

Taking the cross section to be the square of the amplitude we obtain

$$\frac{\sigma(\gamma\gamma \rightarrow \rho^{0}\rho^{0})}{\sigma(\gamma\gamma \rightarrow \rho^{+}\rho^{-})} = \frac{1}{2} \left(\frac{g_{\sigma\rho^{0}\rho^{0}}}{g_{\sigma\rho^{+}\rho^{-}}} \right)^{2}$$

but we know from (F.11) that the charged and neutral couplings to the I=0 resonance σ are equal, so

$$\frac{\sigma(\gamma\gamma \rightarrow \rho^{0}\rho^{0})}{\sigma(\gamma\gamma \rightarrow \rho^{+}\rho^{-})} = \frac{1}{2}$$

In this way we obtain all the other cross sections as multiples of one particular cross section, such as $\sigma(\gamma\gamma \rightarrow \omega\rho^{0})$, these results are given in table (3.1).

References

1. H.Georgi, Weak Interactions and Modern Particle Theory (The Benjamin/Cummings Publishing Company Inc., Wokingham,1984).
2. S.Coleman et al., Phys.Rev. **177**, 2239 (1969).
   C.Callan et al., Phys.Rev. **177**, 2247 (1969).
3. S.Weinberg, Phys.Rev.Lett. **18**, 188 (1967).
4. B.W.Lee, Chiral Dynamics, (Gordon & Breach, New York, 1972).
5. S.Weinberg, Physica **96A**, 327 (1979).
6. M.Bando et al., Phys.Rev.Lett. **54**, 1215 (1985).
7. E.Cremmer and B.Julia, Phys.Lett. **80B**, 48 (1978); Nucl.Phys. **B159**,141 (1979).
8. V.Golo and A.M.Perelomov, Phys.Lett. **79B**, 112 (1978);
   A.D'Adda, P. di Vecchia and M.Luscher, Nucl.Phys. **B146**, 63 (1978); **B152**, 125 (1979).
9. P.Breitenlohner and D.Maison, in Proceedings of Retzbach 1983 "Solutions of Einstein's Equations: Techniques and Results". p.76.
10. Kawarabayashi and M.Suzuki, Phys.Rev.Lett. **16**, 255 (1966).
    Riazuddin and Fayyazuddin, Phys.Rev. **147**, 1071 (1966).
11. J.J.Sakurai, Currents and Mesons (University of Chicago Press, Chicago,1969).
12. S.Weinberg, Phys.Rev.**166**, 1568 (1968).
13. T.H.R.Skyrme, Proc.Roy.Soc.(London) **260**, 127 (1961); ibid **262**, 237 (1961).
14. E.Witten, Nucl.Phys. **B223**, 433 (1983).
15. I.Zahed and G.E.Brown, Phys.Rep. **142**, 1 (1986).
16. Y.Igarashi et al., Nucl.Phys. **B259**, 721 (1985).
17. G.'t Hooft, Nucl.Phys. **B72**,461 (1974); **B75**, 461 (1974).
18. E.Witten, Nucl.Phys. **B160**, 57 (1979).

19. M.Bando, T.Kugo and K.Yamawaki, Phys.Rep. **164**, 218 (1988).

20. R.Ball, in Proceedings of the Workshop on Skyrmions and Anomalies, Krakow, Poland 20-24 Feb. 1987, eds. M.Jezabek and M.Praszatowicz (World Scientific, Singapore, 1987).

21. I.J.R.Aitchison, in Proceedings of the Workshop on Skyrmions and Anomalies, Krakow, Poland 20-24 Feb. 1987, eds. M.Jezabek and M.Praszatowicz (World Scientific, Singapore, 1987).

22. H.Kolanoski, Springer Tracts in Modern Physics Vol.105 (Springer-Verlag, Heidelberg, 1984).

23. M.Poppe, Int.Journal Mod.Phys. **A1**, 545 (1986).

24. TASSO Collaboration, R.Brandelik et al., Phys.Lett. **97B**, 448 (1980).

25. TASSO Collaboration, M.Althoff et al., Z.Phys. **C16**, 13 (1982).

26. D.L.Burke et al., Phys.Lett. **103B**, 153 (1981).

27. CELLO Collaboration, H.J.Behrend et al., Z.Phys. **C21**, 205 (1984).

28. TPC/Two-Gamma Collaboration, ABuijis et al., contributed paper to the 23rd Int. Conf. on High Energy Physics, Berkley 16-23 July (1986).

29. PLUTO Collaboration, Ch.Berger et al., Z.Phys. **C38**, 329 (1988).

30. JADE Collaboration, J.E.Olsson, Proc. of the 5th Int. Colloquium on $\gamma\gamma$ - Interactions, Aachen, p.45; ed. Ch.Berger, Lecture Notes in Physics, Vol. 191 (Spmger-Verlag, Heidelberg, 1983).

31. ARGUS Collaboration, A.W.Nilsson, Proc. of the 8th Int. Workshop on $\gamma\gamma$ - Collisions, Shoresh, Jerusalem Hills, Israel;April 24-28 1988. To be published.

32. P.Q.Hung, Phys.Lett. **168B**, 253 (1986).

33. K.Yamawaki, Phys.Rev. **D35**, 412 (1987).

34. J.Kunz and D.Masak, Phys.Lett. **179B**, 146 (1986).

35. J.Kunz and D.Masak, Phys.Lett. **184B**, 253 (1987).

36. J.Kunz, D.Masak and Toni Reitz, Phys.Lett. **195B**, 459 (1987).

37. D.Masak and J.Kunz, Phys.Lett. **209B**, 71 (1988).

38. ARGUS Collaboration, H.Albrecht et al., Phys.Lett. **196B**, 101 (1987).

39. ARGUS Collaboration, H.Albrecht et al., Phys.Lett. **198B**, 577 (1987).

40. ARGUS Collaboration, H.Albrecht et al., Phys.Lett. **198B**, 255 (1987).

41. ARGUS Collaboration, H.Albrecht et al., DESY 88-084.

42. ARGUS Collaboration, H.Albrecht et al., DESY 88-016.

43. R.L.Jaffe and K.Johnson, Phys.Lett. **60B**, 201 (1976).

44. R.L.Jaffe, Phys.Rev. **D15**, 281 (1977).

45. B.A.Li and K.F.Liu, Phys.Lett. **118B**, 435 (1982); **Phys.Lett. 124B**, 550(Erratum) (1983).

46. B.A.Li and K.F.Liu, Phys.Rev.Lett. **51**,1510 (1983).

47. B.A.Li and K.F.Liu, Phys.Rev. **D30**, 613 (1983).

48. N.N.Achasov, S.A.Devyanin and G.N.Shestakov, **Phys.Lett. 108B**, 134 (1982).

49. N.N.Achasov, S.A.Devyanin and G.N.Shestakov, **Z.Phys. C16**, 55 (1982).

50. N.N.Achasov, S.A.Devyanin and G.N.Shestakov, **Z.Phys. C27**, 99 (1985).

51. M.Feindt, in Proc. of the 8th Int. Workshop on $\gamma\gamma$-Collisions, Shoresh, Jerusalem Hills, Israel; April 24-28 1988. To be published.

52. U.Maor, Proc. of the 8th Int. Workshop on $\gamma\gamma$-Collisions, Shoresh, Jerusalem Hills, Israel; April 24-28 1988. To be published.

53. G.Alexander, U.Maor and P.G.Williams, Phys.Rev. **D26**, 1198 (1982); G.Alexander, A.Levy and U.Maor, Z.Phys. C30, 65 (1986).

54. H.Kolanoski, Z.Phys. C39, 543 (1988).

55. N.N.Achasov and G.N.Shestakov, Phys.Lett. **203B**, 309 (1988).

56. M.Hatzis and J.Paschalis, Lett.Nuovo Cimento **40**, 362 (1984).

57. S.J.Brodsky, G.Kopp and P.M.Zerwas, Phys.Rev.Lett. **58**, 443 (1987).

58. M.Prudden, Talk at the Institute of Physics Conference on Nuclear Physics and Particle Physics (Birmingham, April 1987).

59. B.Moussallam, Z.Phys. **C39**, 535 (1988).

60. P.D.Pesic, Phys.Rev. **D8**, 945 (1973).

61. G.Tupper and M.A.Samuel, Phys.Rev. **D23**, 1933 (1981).

62. M.Katuya, Phys.Lett. **124B**, 421 (1983).

63. J.Gasser and H.Leutwyler, Ann.Phys. **158**, 142 (1984).

64. J.Bijnens and F.Cornet, Nucl.Phys. **B296**, 557 (1988).

65. J.F.Donoghue, B.R.Holstein and Y.C.Liu, Phys.Rev. **D37**, 2423 (1988).

66. G.'t Hooft and M.Veltman, Nucl.Phys. **B153**, 365 (1979).

67. A.Devoto and D.W.Duke, Riv.Nuovo Cimento **7**, 1 (1984).

68. R.E.Cutkosky, Journal of Math.Phys. **1**, 429 (1960).

69. B.DeTollis, Nuovo Cimento **32**,757 (1964); ibid **35**, 1182 (1965).
V.Costantini, B.DeTollis and G.Pistoni, Nuovo Cimento **2A**, 733 (1971).

70. J.J.Brehm and J.Sucher, Ann.Phys. **25**, 1 (1963).

71. F.Boudjema, Phys.Lett. **187B**, 362 (1987).

72. T.Appelquist, Proc. of 21st Scottish Universities Summer Scool in Physics, Gauge Theories and Experiments At High Energies, eds. K.C.Bowler and D.G.Sutherland (SUSSP Publications, Edinburgh, 1981).

73. D.A.Dicus, C.Kao and W.W.Repko, Phys.Rev. **D36**, 1570 (1987);
D.A.Dicus, C.Kao and Scott S.D. Willenbrock, Phys.Lett. **203B**, 457 (1988).

74. I.J.R.Aitchison, An Informal Introduction to Gauge Field Theories (Cambridge University Press, Cambridge, 1982).

75. Tran N.Truong, "Modern application of Dispersion Relation: Chiral Perturbation vs. Dispersion Technique", preprint CERN-Th.4748/87
To appear in the Festschrift for Professor K.Nishijima of the University of Tokyo and the Research Institute of Fundamental Physics Kyoto University.

76. S.Weinberg, Phys.Rev.Lett.**17**, 616 (1966);
Y.Tomozawa, Nuovo Cimento **46A**, 707 (1966).

77. M.Gell-Mann and M.Levy, Nuovo Cimento **16**,705 (1958).

78. P.G.O.Freund and R.J.Rivers, Phys.Lett. **29B**, 510 (1969);
R.Carlitz, M.B.Green and A.Zee, Phys.Rev.Lett. **26**,1515 (1971); Phys.Rev. **D4**, 3439 (1971); Phys.Rev. **D4**, 3501 (1971).

79. A.W.Reid and D.G.Sutherland, Nucl.Phys. **B75**, 426 (1974).

80. J.Wess and B.Zumino, Phys.Lett. **37B**, 95 (1971).

81. M.Jacob and G.C.Wick, Ann.Phys. **7**, 404 (1959).

82. M.D.Scadron, Advanced Quantum Theory (Springer-Verlag, New York, 1979).

83. E.M.Lifshitz and L.P.Pitaevskii, Relativistic Quantum Theory (Pergamon, Oxford, 1973).

84. A.O.Barut, The Theory of the Scattering Matrix (Collier-Macmillan, London, 1967) p.119.

85. E.T.Whittaker and G.N.Watson, Modern Analysis 4th ed.(Cambridge University Press, Cambridge, 1962).

86. S.Mandelstam, Phys.Rev. **115**, 1741 (1959).

Graph Captions

Graph 3.1 Comparison of cross sections on the $\gamma\gamma\rightarrow\rho^0\rho^0$ no-tag data. Also shown are the upper limits of $\gamma\gamma\rightarrow\rho^+\rho^-$ from JADE [30]. Taken from reference [29].

Graph 3.2 Cross section for $\gamma\gamma\rightarrow\omega\rho^0$. The error bars are purely statistical. Also shown is the expected $a_2(1320)$ contribution (full line), a 4-quark state prediction [48]-[50] (dotted) with m=1.65 GeV and a_0=0.5 and the prediction by a t-channel factorization model [53] (hatched region). Taken from reference [38].

Graph 3.3 Cross section for $\gamma\gamma\rightarrow\omega\omega$ vs. $W_{\gamma\gamma}$ (=$\sqrt{s}$ in thesis notation). The error bars shown are statistical. The systematic uncertainty is 20%. Taken from reference [39].

Graph 3.4 Cross sections for the reactions a) $\gamma\gamma\rightarrow k^{*o}\overline{k^{*o}}$; b) $\gamma\gamma\rightarrow k^{*o}k^-\pi^+$+ c.c and c) $\gamma\gamma\rightarrow k^+k^-\pi^+\pi^-$ (non-resonant). Taken from reference [40].

Graph 3.5 Cross sections vs. $W_{\gamma\gamma}$. Systematical errors are not included.
a) $\gamma\gamma\rightarrow k^{*+}k^{*-}$ (crosses) compared with $\gamma\gamma\rightarrow k^{*o}\overline{k^{*o}}$ (dots) from[40]
b) Topological $\gamma\gamma\rightarrow k_s^o k_s^o\pi^+\pi^-$.
c) Topological $\gamma\gamma\rightarrow k_s^o k^{\mp}\pi^0\pi^{\pm}$ (crosses) together with non-resonant $\gamma\gamma\rightarrow k_s^o k^{\mp}\pi^0\pi^{\pm}$ (dots). Taken from reference [41].

Graph 4.1 The HLS model tree-level cross-section (in nb) for $\gamma\gamma\rightarrow\rho^+\rho^-$, equation (4.14), as function of W=$\sqrt{s}$ in GeV.

Graph 4.2 The HLS model tree-level cross section (in nb) for $\gamma\gamma\rightarrow\rho^+\rho^-$, equation (4.17),as a function of x where $s=xm^2$. σ_0 (dashed line), $5\sigma_2$ (dot-dashed line) and $\sigma=\sigma_0+5\sigma_2$ (full line).

Graph 5.1 Equation (5.25), showing the region of integration for the double-dispersion relation representation of $\Psi(s,t)$.

Graph 7.1 Unitarity test for the T_0^{++++} scattering amplitude, where x is defined by $s=xm^2$.

Case (a) $|T_0^{++++}|$ (dashed line) to be compared with $|(\Sigma MM^*)_0|$ (one dot-dashed line).

Case (b) $|T_0^{++++}|$ (two dots-dashed line) to be compared with $|(\Sigma MM^*)_0|$ (three dots-dashed line).

Graph 7.2 Decomposition of $(\Sigma MM^*)_0$, equation (7.23), into component parts for case (b) ie only the Born amplitudes. T_0^{++++} (dashed line), T_0^{++--} (dot-dashed line), T_0^{++00} (two dots-dashed line), T_0^{+++-} (three dots-dashed line) and just visible above the x-axis is $T_0^{+++0} = -T_0^{++-0}$ (for case b) (four dots-dashed line) and the resultant total $(\Sigma MM^*)_0$ (full line).

Graph 7.3 Unitarity test for $\pi^+\pi^-$ scattering. s-wave amplitude (dashed line), p-wave amplitude (dot-dashed line) and unitarity limit (full line).

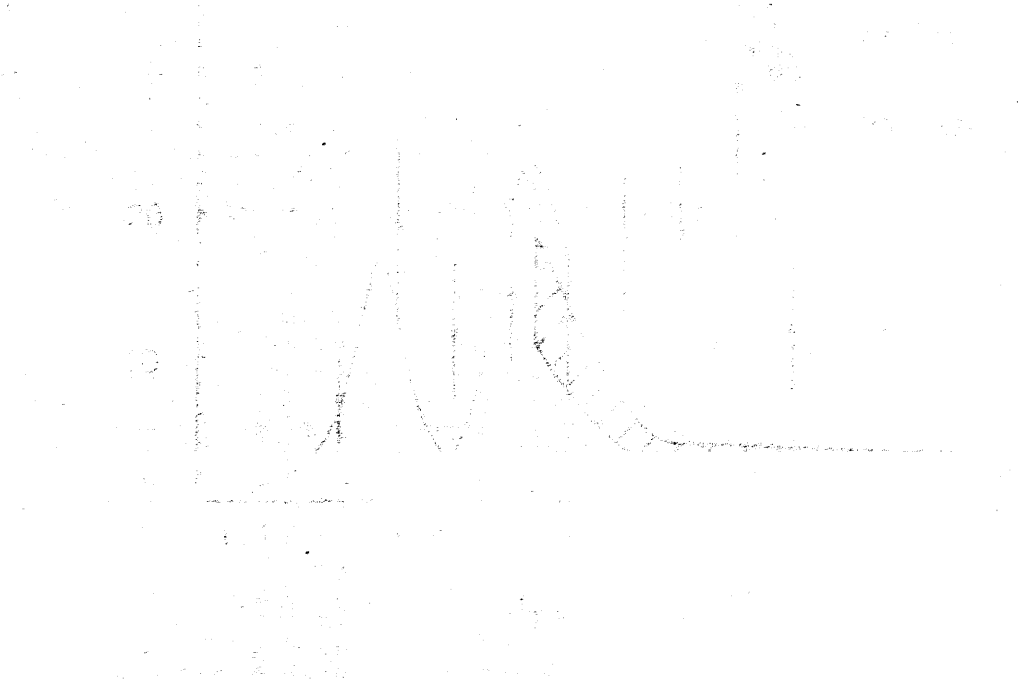

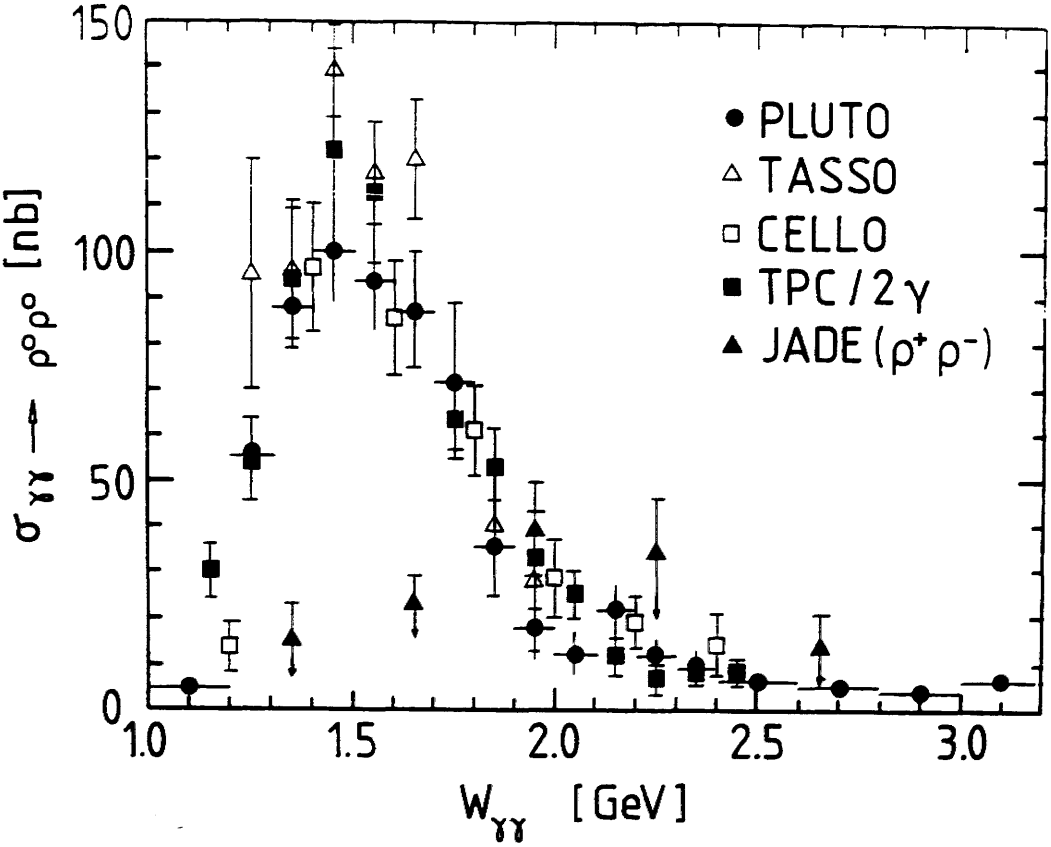

Graph 3.1

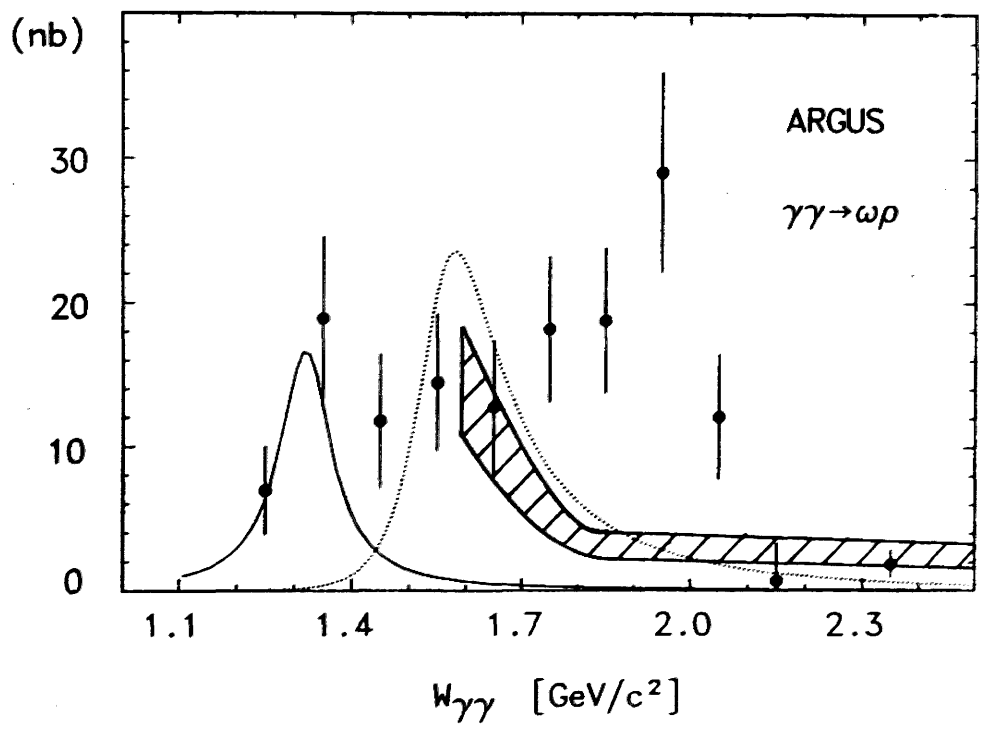

Graph 3.2

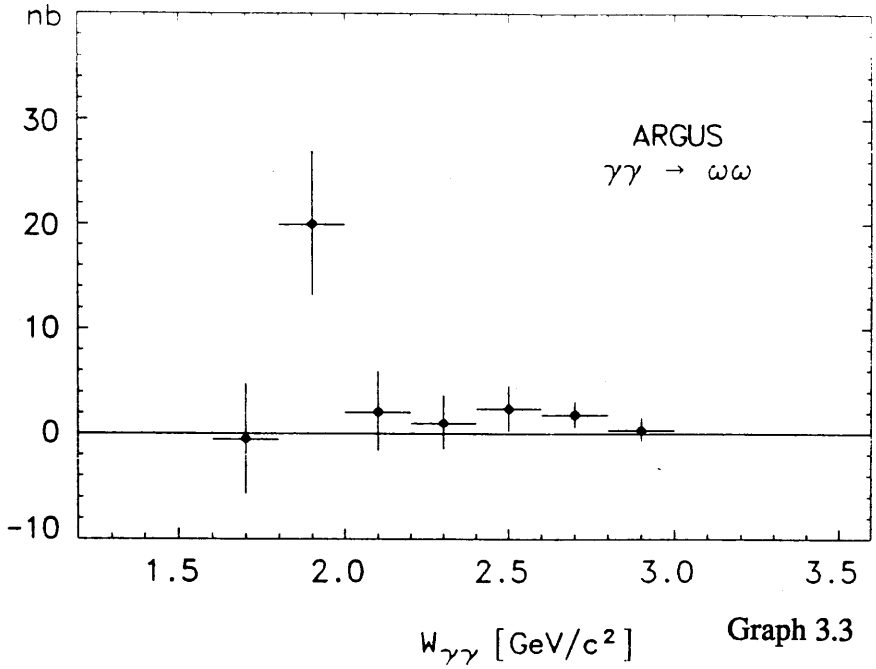

Graph 3.3

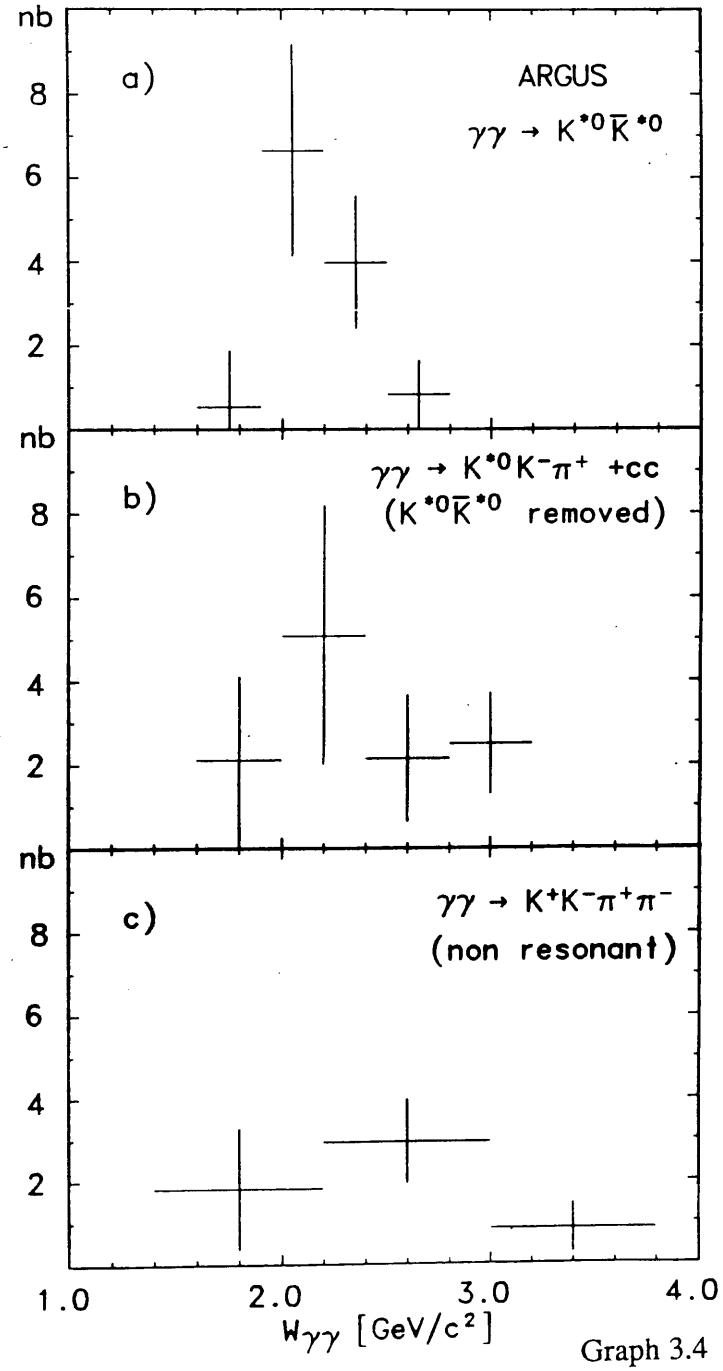

Graph 3.4

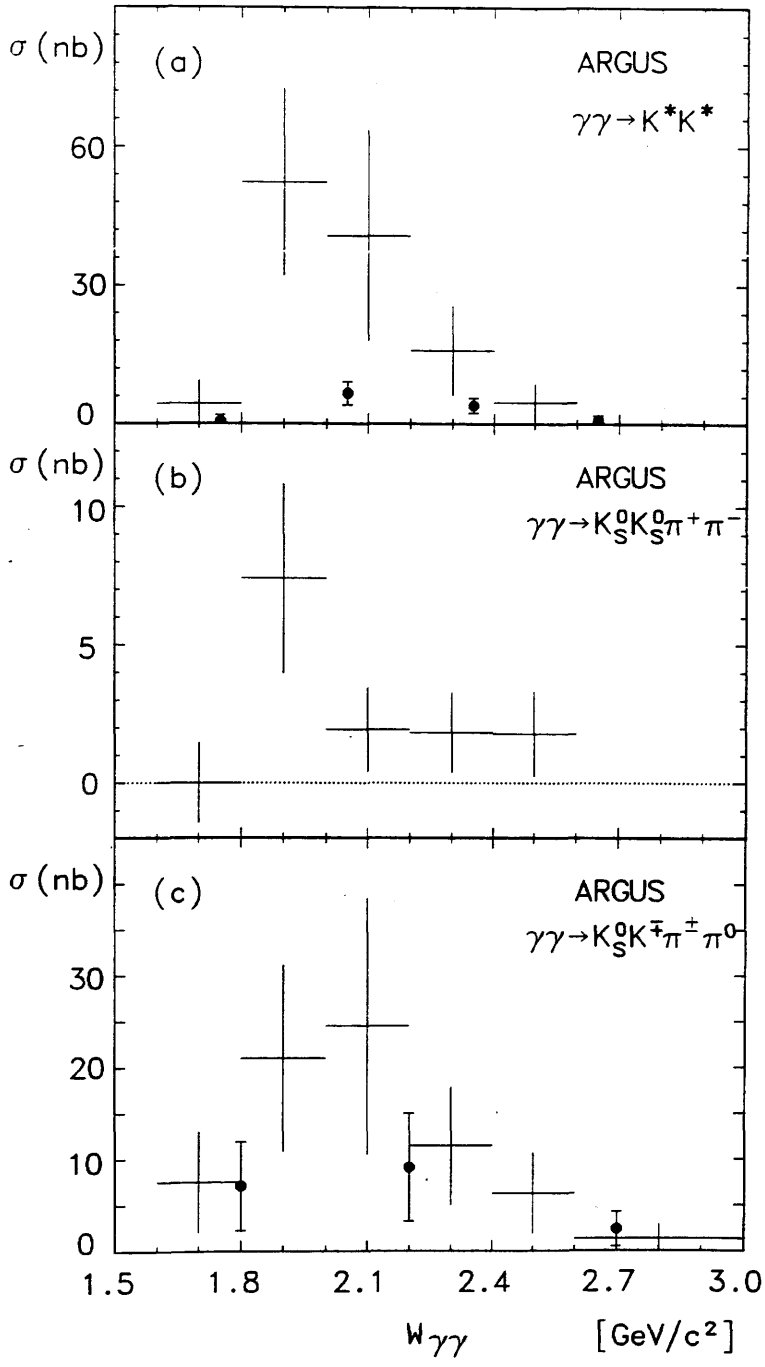
σ (nb)
(a)
ARGUS
γγ→K*K*
60
30
0
σ (nb)
(b)
ARGUS
γγ→K⁰SK⁰Sπ⁺π⁻
10
5
0
σ (nb)
(c)
ARGUS
γγ→K⁰SK∓π±π⁰
30
20
10
0
1.5
1.8
2.1
2.4
2.7
3.0
Wγγ
[GeV/c²]

Graph 3.5

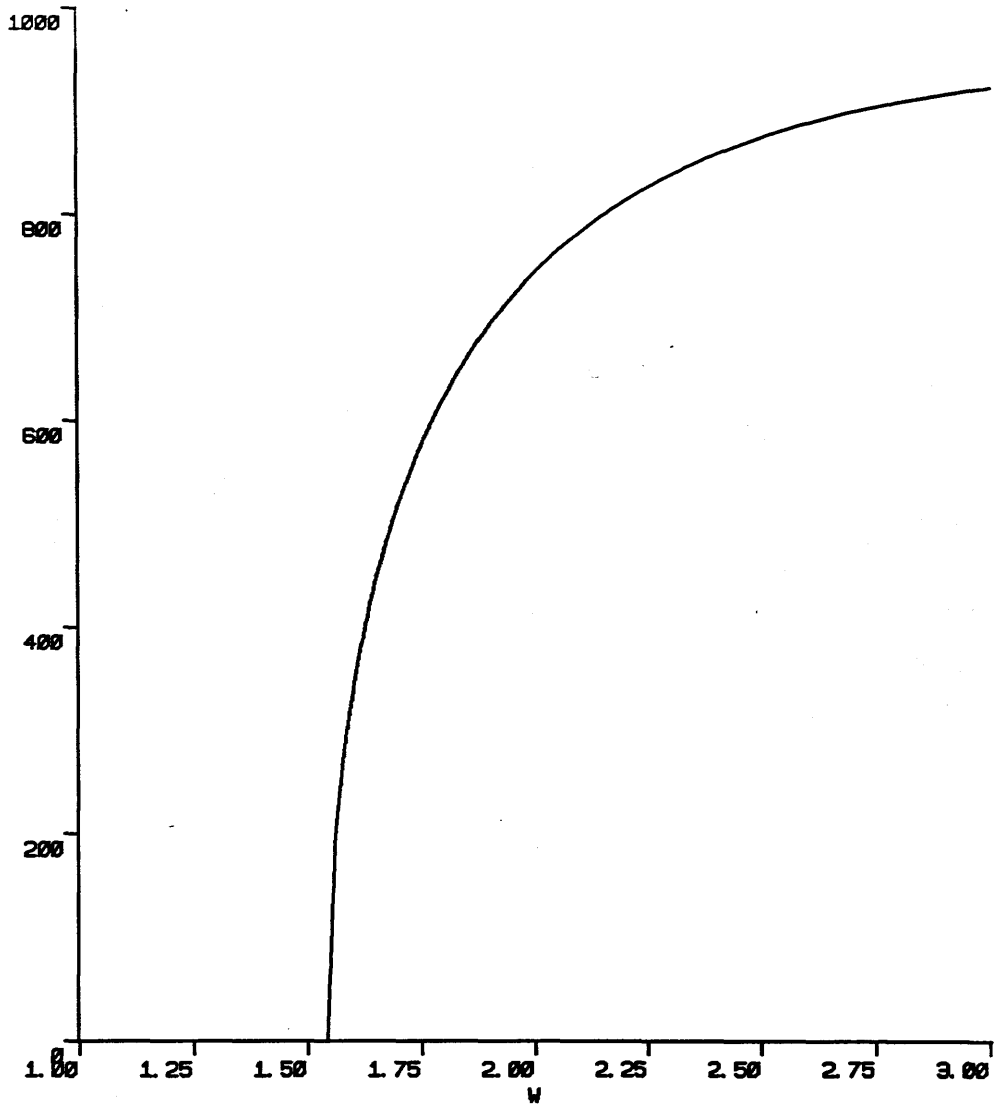

Graph 4.1

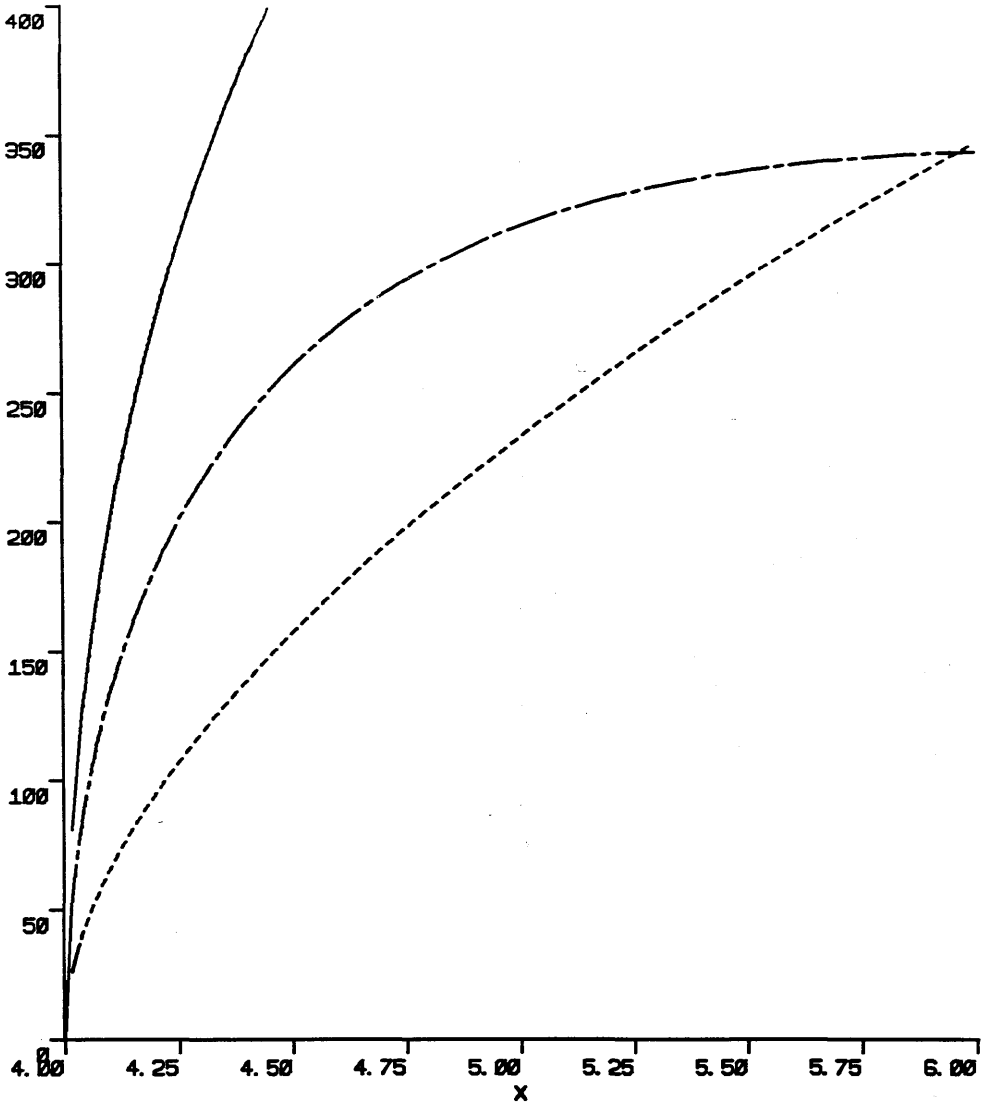
400
350
300
250
200
150
100
50
0
4.00
4.25
4.50
4.75
5.00
5.25
5.50
5.75
6.00
X

Graph 4.2

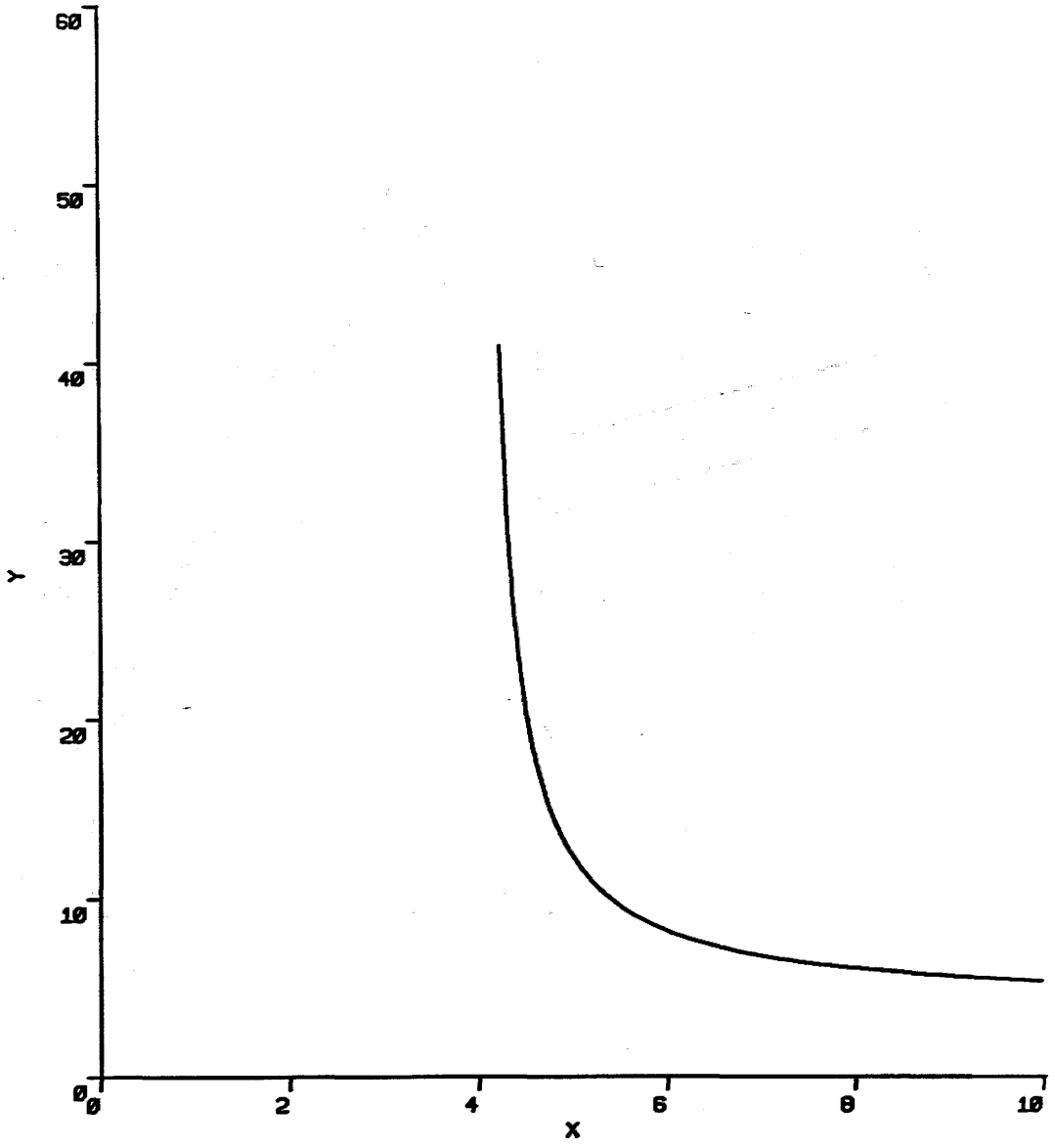

Graph 5.1

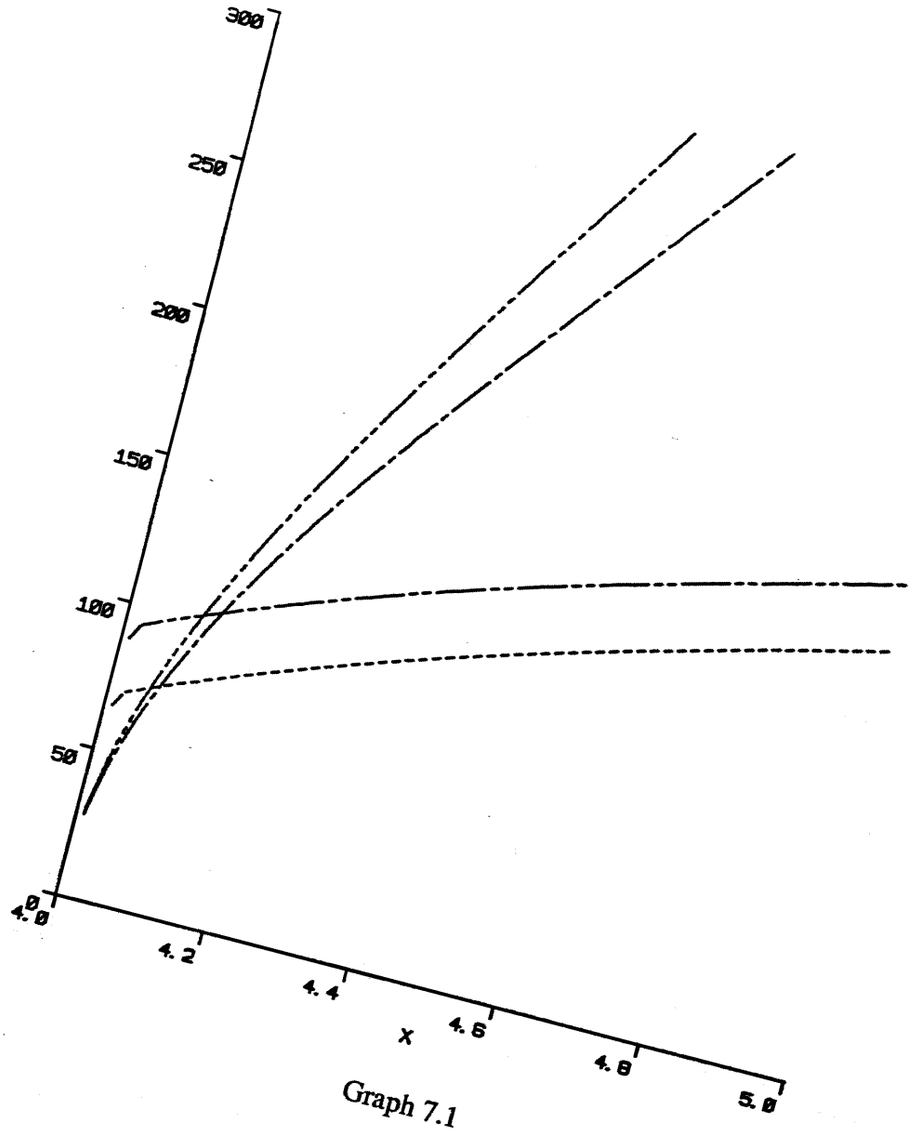

Graph 7.1

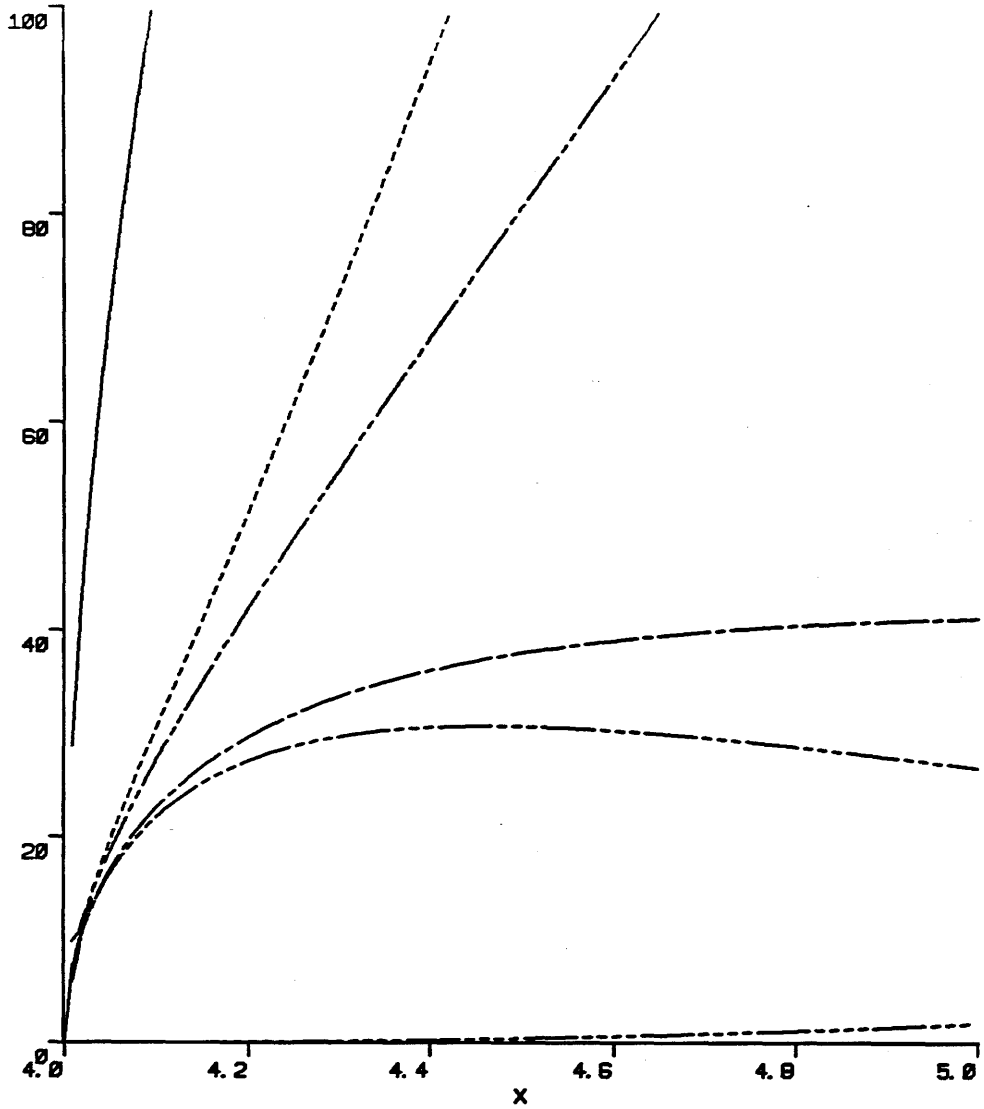

Graph 7.2

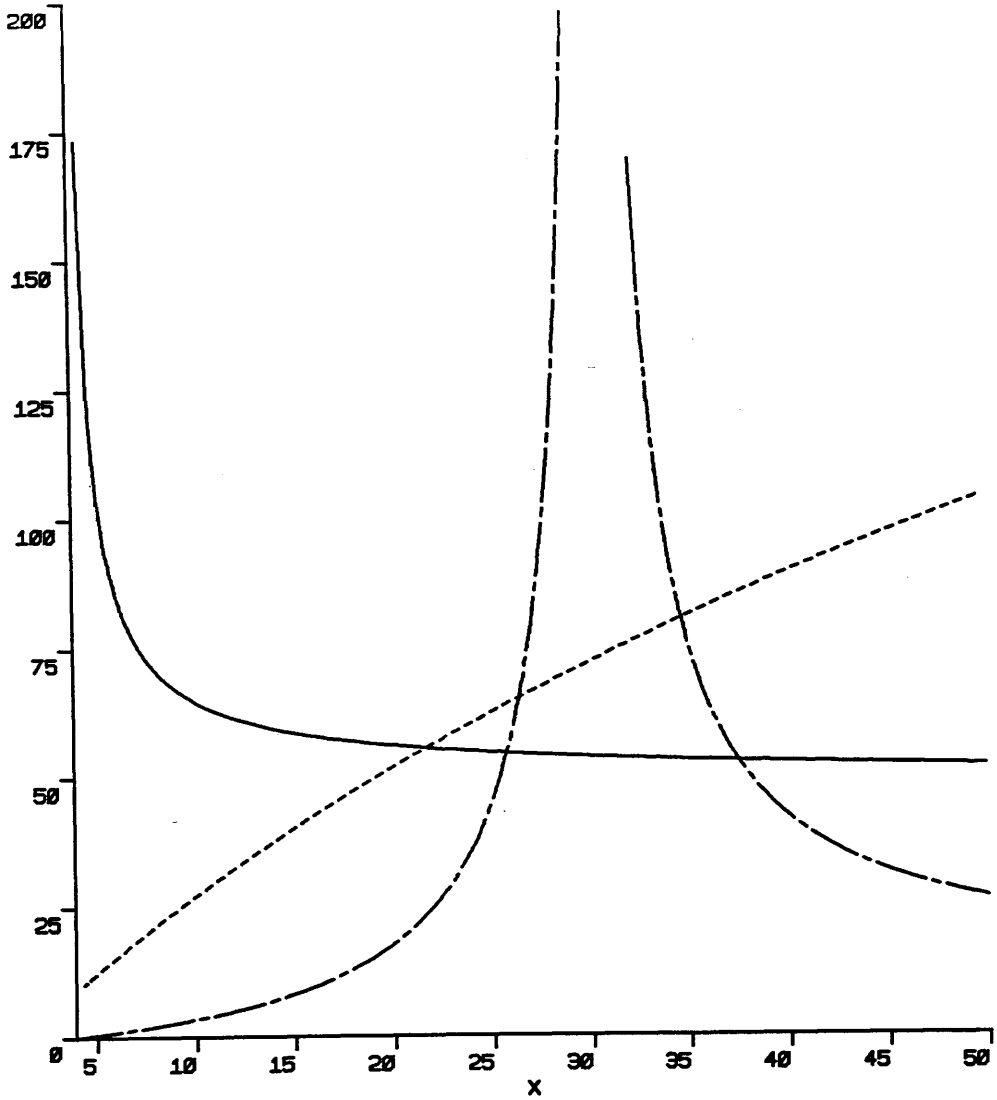

Graph 7.3